

Professorship for Polymer Engineering

Polymer Mixing in a Single Screw Extruder

Part III: Experimental Validation



University of
Applied Sciences

Windesheim



Colophon

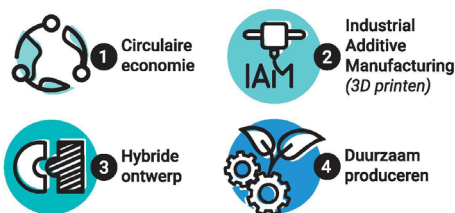
Title: Polymer Mixing in a Single Screw Extruder (Part III: Experimental Validation)

Publication number: LKT-DP-108633-2309

Publication date: September 2023

Authors: T.J. Mateboer MSc
Dr. Ir. J. Buist
Dr. Ir. D.J. van Dijk

Line of research:



Funded by: TechForFuture

In collaboration with: Wavin T&I

This is a publication of Windesheim University of Applied Sciences and is part of Attribution 4.0 International (CC BY 4.0). This means that the content (knowledge) of this publication may be used as a base for new developments, provided that the name of the author and/or Windesheim University of Applied Sciences is stated. Company- specific data from consortium members may be omitted.

The Professorship for Polymer Engineering of University of Applied Sciences Windesheim was founded in 2009; the group's objective is to improve the knowledge base on sustainable processing of plastics and composites within and through the higher education system. Its primary function is as a research group in Polymer Engineering, delivering output in the field of applied science. Befitting research groups at University of Applied Sciences, their research spans from TRL 4 to a maximum of 7: demonstration system prototype in an operational environment.

The team operates within market based projects and comprises lecturers from Civil Engineering, Industrial Product Design and Mechanical Engineering. The output of the projects is integrated into the curriculum of these study programs.



Contents

1. Introduction	4
1.1. General preface	4
1.2. Introduction into experimental validation.....	5
2. Extrusion experiments	6
2.1. Extruder.....	6
2.2. Mix experiments with the pin mixer.....	8
2.3. Residence time distribution (RTD)	9
2.4. Shannon entropy of the extrudate cross section.....	42
3. Extrusion simulations and comparisons to experiments.....	51
3.1. Extrusion simulation setup.....	51
3.2. Methods for quantifying mix quality in extrusion simulations.....	53
3.3. RTD in extrusion simulations and a comparison to experiments.....	57
3.4. Mix quality in the cross section of the simulated extrudate.....	58
4. Conclusion.....	62
5. Future research in simulating extrusion mix quality.....	63
6. Acknowledgements	64
Appendix 1. Simulation setup and mesh study.....	66



1. Introduction

This document is part of a series. This introduction contains a general preface for all documents and a specific outline of the subjects in this document.

1.1. General preface

Plastic pipes are commonly used for the transport of fluids. The properties of the pipe depend (amongst others) on the plastic used in production. The properties of the plastic in their turn, can be modified with additives. For example, the color of a pipe can be adjusted by the addition of a colorant to a polymer compound. The colorants are often mixed through the polymer using specialized equipment, such as a twin screw extruder. In general polymer pipes are manufactured using a single screw extruder with a pre-compounded (pre-mixed) polymer. A basic single screw extruder has poor mixing characteristics. To improve mixing, different mixing elements can be added after the compression zone of the extruder, like a spiral Maddock or a pin mixer, with different mixing characteristics. Using a combination of these mixing elements, it could be more energy- and cost efficient to both extrude a pipe and to mix the polymers with a single screw extruder.

This document is part of a series of documents reporting the outcome of a four years research program, executed by the Professorship for Polymer Engineering of Windesheim University of Applied Sciences and Wavin Technology and Innovation department of the Orbia's community of companies. The project was funded by the center of expertise 'Tech for Future' in two successive projects, namely 'Sustainable extrusion processes in the production of pipes (TFF1703)' and 'Mixing in a single Screw extruder' (TFF1920). The general objective of the program was to gain detailed knowledge of the extrusion process by modern analysis tools like computational fluid dynamics (CFD). One of the benefits of this tool could be a shorter development time of extrusion processes. To prove the strengths of these modern tools, the optimization and selection of mixing elements in single screw extrusion was chosen as these provide a challenging case.

Based on this general objective and the specified case, the following research questions were drafted:

1. What is a proper simulation method for polymer extrusion with respect to mixing?
2. How to quantify mixing quality in an extrusion simulation?
3. How to validate the simulation results and to validate the quantification of mixing?

The basis of the study is a literature search into mixing processes in extrusion, simulation of velocity, temperature, pressure and stresses in extrusion, quantification of mixing based on flow fields in extrusion and validation of mixing in extrusion experiments. Each document contains a specific part of this literature search, which is relevant for the subject in the document.

The first document 'Simulation Method': In this paper we did not limit ourselves to single screw extrusion because in the future we might also want to simulate double screw extrusion. Preferably, a simulation method has to be selected, which is applicable for both single screw as well as double screw extrusion. Different simulation techniques, with respect to discretization method and meshing method for the rotating barrel, are analyzed and demonstrated for different mixing elements.

The second document: 'Mixing Quantification': Several methods to quantify mixing quality were studied. A method has to be selected, which is suitable for the numerical simulations as well as for the experimental validation, in order to compare the results.



The third document: 'Experimental Validation': For the study described in this paper, a single screw extruder on lab scale was acquired with multiple monitoring points in the barrel for temperature and pressure. The screw of this extruder has a simple basic configuration with three zones and only one mixing element. Several screws with different mixing elements are available, to be able to make a clear distinction between the various effects. The screw is easy to change, which makes it possible to study different type of mixing elements. The barrel contains holes that can also be used to inject a second polymer or a colorant, for example between the compression zone and the mixing element.

Upon the completion of these research steps it should be possible to select, using numerical simulations, a combination of mixing elements to optimize mixing quality.

1.2. Introduction into experimental validation

This report is focused on experimental validation of simulated distributive mix quality. Therefore, extrusion experiments were performed, and methods were developed to determine the mix quality experimentally. The experimentally found mix quality was compared to the simulated mix quality in order to verify the simulations.

The main research question: Is the simulated mix quality valid? This question can be broken down into several sub-questions:

- How to measure the distributive mix quality in the extrusion direction?
- How to measure the distributive mix quality in the extrudate cross section?
- Is the simulated distributive mix quality, in the extrusion direction, in agreement with the measured extrudate mix quality?
- Is the simulated distributive mix quality, in the extrudate cross section, in agreement with the measured extrudate mix quality?

Single screw extrusion experiments were performed with a mixing zone included in the screw geometry. Many single screws consist of a feed zone, compression zone and a metering zone and sometimes one or several mix zones. With respect to mixing, the relevant differences between screws takes place in the mixing zones and therefore the scope of this study is limited to these zones. Specialized tools were developed to exclusively determine mix quality after the metering zone, i.e. in the mixing zone and die. The mix quality in the extrusion direction was determined with the residence time distribution (RTD), both by experiments and simulations. Furthermore the extrudate cross section mix quality was determined with microscope imaging and compared to simulations.

This document is not structured with a single chapter with 'materials and methods', a chapter with 'results', instead the document is divided into several subjects. For each subject there are paragraphs with: an explanation of the used methods, a chapter with the results, and a conclusion. The extrusion experiments are very visual and straightforward, therefore those are the first subjects (section 2). It starts with the general extrusion setup (paragraphs 2.1 and 2.2), followed by the RTD measurement methods and results in paragraph 2.3. Paragraph 2.4 shows a method to determine cross section mix quality. Section 3 shows the simulations and a comparison to the experiments. Methods to determine mix quality are shown in paragraph 3.2, the next paragraphs show simulated RTD (paragraph 3.3) and simulation cross section mix quality are shown in (paragraph 3.4) with comparison to the experiments. The last sections (4 and 5) contain conclusions and recommendations for future work.



2. Extrusion experiments

The greater goal of this project is to optimize extrusion mix quality with simulations. In the simulations many parameters can be chosen for an optimization, for example material properties or screw geometry. The simulation procedure is shown in section 3. The simulation procedure was verified with extrusion experiments. The experimental setup and the results are shown in this section. The extruder setup is shown in paragraph 2.1.

The mixing section of a screw seems particularly interesting for a comparison between extruder screws. The relevance of the screw mixing section, when comparing several screws, is discussed in paragraph 2.2. A dosing device that injects straight into the mixing section is discussed in paragraph 2.2. Mix quality was determined in the extrusion direction with the residence time distribution (RTD), see paragraph 2.3. The mix quality of the extrudate cross section was determined as well, see paragraph 2.4.

2.1. Extruder

The extruder and the screw geometry are presented in this section. All experiments were performed on a single screw extruder (C3030, Conextru GmbH) with a barrel diameter of 30 mm.

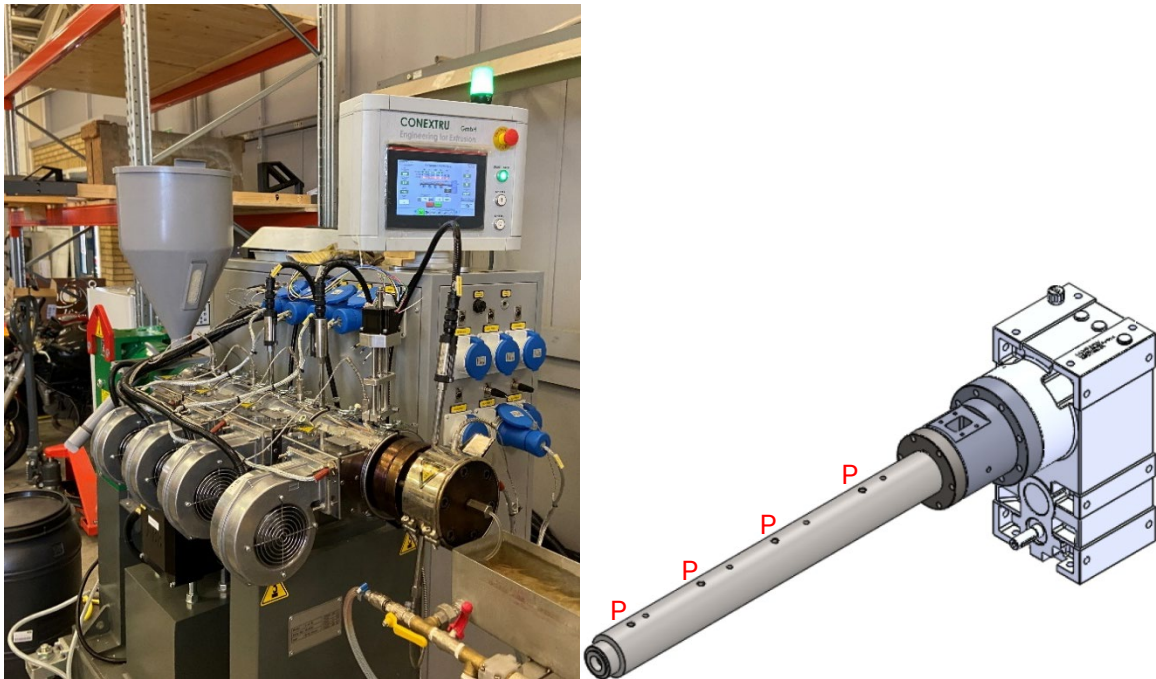


Figure 1. Single screw extruder (C3030 Conextru GmbH) with a barrel diameter of 30 mm. Left: a photo. Right: a schematic of the extruder barrel, the red P's indicate where pressure sensor can be mounted.

The barrel consists of 4 heating /cooling zones and one heating zone for the extruder head. The extruder barrel is somewhat unique since it has 4 positions to mount where a pressure sensor. A capillary die with a diameter of 4 mm and 50 mm length was used for all the experiments. The die melt temperature and pressure were measured on the inside, see Figure 2.

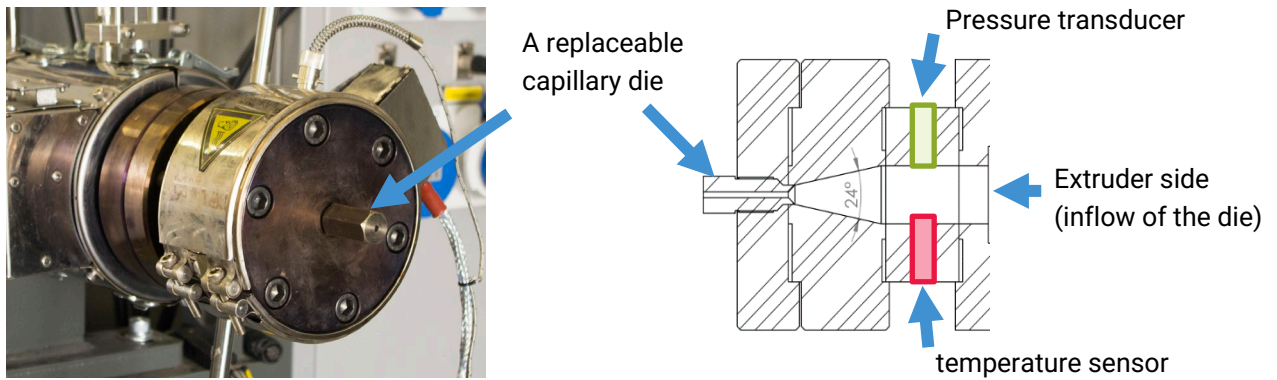


Figure 2. The capillary die with a pressure and melt temperature sensor.

A screw with a pin mixer was used for all experiments, see Figure 3.

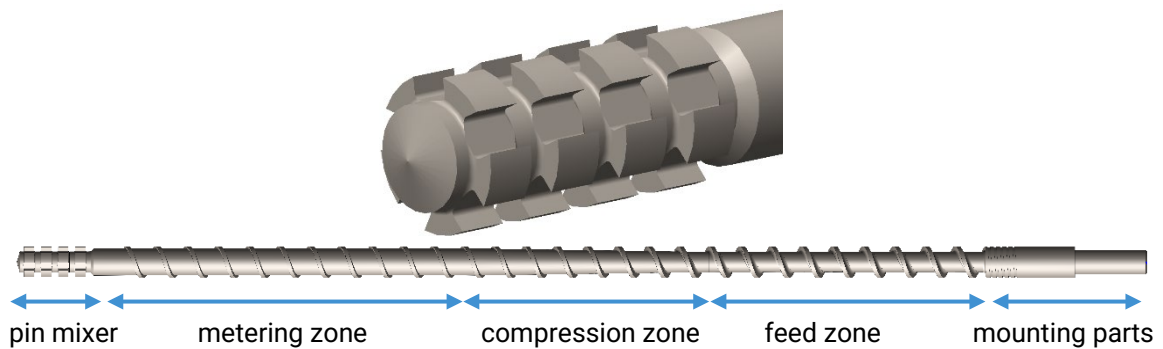


Figure 3. Screw with a pin mixer.

Extrusion experiments were performed with three different material combinations based on HDPE, PP, carbon black masterbatch, chalk and a grey masterbatch. A masterbatch pellet is a unit with polymer matrix and a high additive loading. All the mixing experiments were run at a screw rotational velocity of 30 rpm.

2.1.1. HDPE with a carbon black masterbatch

Experiments were conducted with various materials and colorants. Experts from Wavin T&I selected these materials due to their frequent use by industry. Among these materials was a HDPE (Marlex® TRB-432 Polyethylene, Chevron Phillips Chemical Company LP), see Figure 4 [1]. This was processed at a barrel and die temperature of 190 °C. To color the extrudate a PE masterbatch with 35% carbon black (Marlex® M368 Polyethylene, Chevron Phillips Chemical Company LP) was used [2]. The experiments with HDPE mixed with the carbon black masterbatch are also referred to as ‘the carbon black experiment(s)’ in this document.



Figure 4. Left: HDPE pellets (before mix experiments). Middle left: Carbon black (35%) masterbatch pellets. Right: PE pellets with 82% chalk.

2.1.2. PP with a grey masterbatch

A second set of extrusion experiments was carried out with a PP (Hostalen PP XN112-I, LyondellBasell) and a grey masterbatch (Colour MB PP 7420, Polyplast Müller GmbH) [3, 4]. The grey masterbatch has PP as a matrix material, therefore it is miscible with PP. The exact pigment in the masterbatch is proprietary information and therefore not available for this study, it is most likely a combination of carbon black (black) and titanium dioxide (white). The PP experiments were performed at 220 °C barrel and die temperature (all temperature zones).

2.1.3. PP with a chalk filler

The same PP (as in 2.1.2) was also used to mix in a PE with 82% chalk. The PE with chalk is referred to as 'chalk' in the rest of this document. The experiments were performed with a barrel and die temperature of 220 °C.

2.2. Mix experiments with the pin mixer.

The interesting difference between screws is the mixing zone, for example there are screws with a Maddock section, a Twente mixing ring, a pineapple mixer, etc. The other zones (feed zone, compression zone and metering zone) are not specifically meant for mixing and are quite similar between different screws. Therefore, in this study the focus is on mix quality of the mixing section, and not the mixing behavior of the other zones.

Usually mixing of additives into a polymer starts by adding masterbatch pellets to the polymer pellets and then the premix is fed into the hopper. The additive is already somewhat mixed in the compression zone and the metering zone before it reaches the specialized mixing section.

For this study any mixing before the specialized mixing section is considered an error in mix quality measurements of a specific mixing section. Therefore, it would be best to preclude any mixing in the extruder before the specialized mixing sections. This was achieved by injecting the masterbatch just before the pin mixer, and not in the hopper. A specialized tool to inject additives into the barrel, named AIT (additives injection tool), was developed with PBS Machinery, see Figure 5. The AIT is a very small ram extruder, it has a cylinder filled with a masterbatch, the masterbatch is injected into the barrel with a plunger.

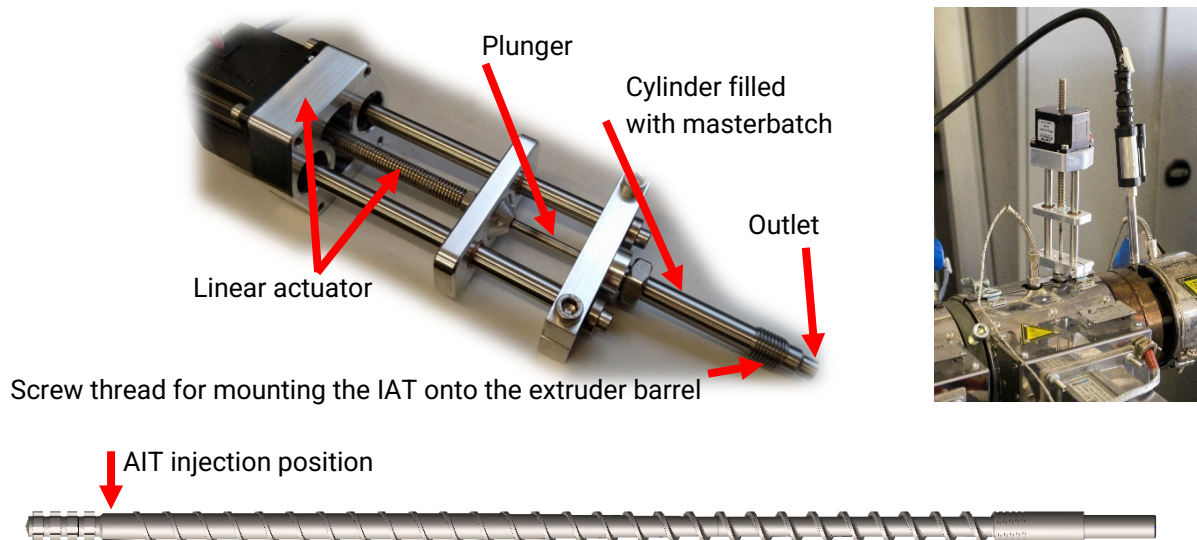


Figure 5. The AIT (additives injection tool) used for introducing additives into the extruder barrel. Upper left: the completely assembled tool. Upper right: tool installed onto the extruder barrel. Lower: the injection position of the AIT relative to the screw (just before the pin mixer).

The plunger contains a stepper motor, this allows for steady state injection of masterbatch, or a single shot of masterbatch. The AIT cylinder has an inner diameter of 4 mm, the outlet is 1 mm in diameter. The barrel wall is 25.75 mm thick, the cylinder is firmly screwed into the barrel wall.

The cylinder is heated by the extruder barrel, the masterbatch is melted before it is driven through the outlet. The AIT works well with masterbatches, even at high extruder pressure (~200 bar), but not with chalk filled pellets.

2.3. Residence time distribution (RTD)

With a high distributive mix quality an additive is both distributed homogeneously over the extrudate cross section and distributed along the length of the extrudate. This section is focused on the mix quality along the length of the extrudate.

Figure 6 shows a schematic example of a blue masterbatch distributed only across a small section of the extrudate, therefore the mix quality is low in this example. This in contrast with the example with the high mix quality of the orange masterbatch. The orange masterbatch is distributed more evenly over a very long part of the extrudate.

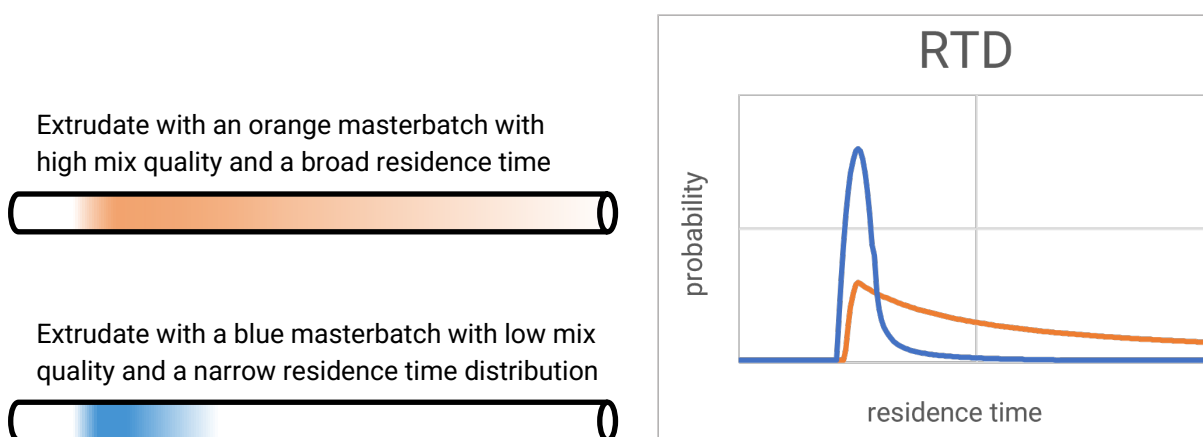


Figure 6. Representation of RTD. Left: schematics of 2 extrudates, upper extrudate with high mix quality, lower extrudate with low mix quality. Right: RTD corresponding with the left two extrudate schematics.

Not only is the masterbatch elongated along the extrudate length, it is also stretched in the time it takes to exit the extruder. Some of the colorant will reach the die exit in a short time (short residence time), while it might take a long time for the rest of the masterbatch pellet to exit the extruder. The RTD is the probability (P_i [-]) of a fraction of the additive mass (m_i [kg]) to arrive at the die exit, as a function time (t [s]), see the graph in Figure 6.

$$P_i(t) = \frac{m_i(t)}{m_{total}} \quad 1$$

In an experiment the total additive mass (m_{total} [kg]) is the mass of the masterbatch pellet. A wider RTD stands for a higher distributive mix quality in the extrusion direction. The orange masterbatch example (Figure 6) shows a broad RTD (high mix quality), the blue masterbatch shows a narrow RTD (low mix quality). The RTD is further explained in part 2: **Mixing Quantification**, this includes references to literature concerning different methods of measuring RTD [5].

Measuring the RTD comes down to measuring the fraction of the additive mass as a function of time ($m_i(t)$ [kg]). In the current study 2 methods were used. An optical method where the $m_i(t)$ was determined by a dependent variable. And a more time consuming method where the additive was separated with burn off experiments and $m_i(t)$ was measured.

The optical method to determine the RTD and the results are explained in detail in paragraph 2.3.1. This method is fairly quick, applicable to any opaque additive in translucent melt, and it uses a relatively small amount of additive. Therefore, potentially many mix experiments can be performed with this method within a short period of time. The wt.% (percentage of weight) of the additive is not measured directly, instead the light attenuation of the additives in the extrudate is measured. The wt.% of the additive distribution can be calculated from light attenuation by applying the Beer-Lambert law. This method was verified with burn off experiments.

The burn off experiment is the second method to determine the RTD. The method and results are shown in paragraph 2.3.2. With this method the wt.% of the additive is measured directly, which makes it a reliable method. A disadvantage is the many work hours (days) needed per mix experiment, furthermore this method is only applicable to non-flammable additives and a high wt.% is preferred. This method is called 'burn off RTD' in the rest of this document.

The optical RTD is preferred since it is quick compared to the burn off RTD. The optical RTD was however verified with the burn off RTD.

2.3.1. RTD optical measurements

RTD is a representation of the distributive mix quality of the extrudate in the extrusion direction. The RTD can be determined by measuring the amount of transmitted light, see Figure 7.

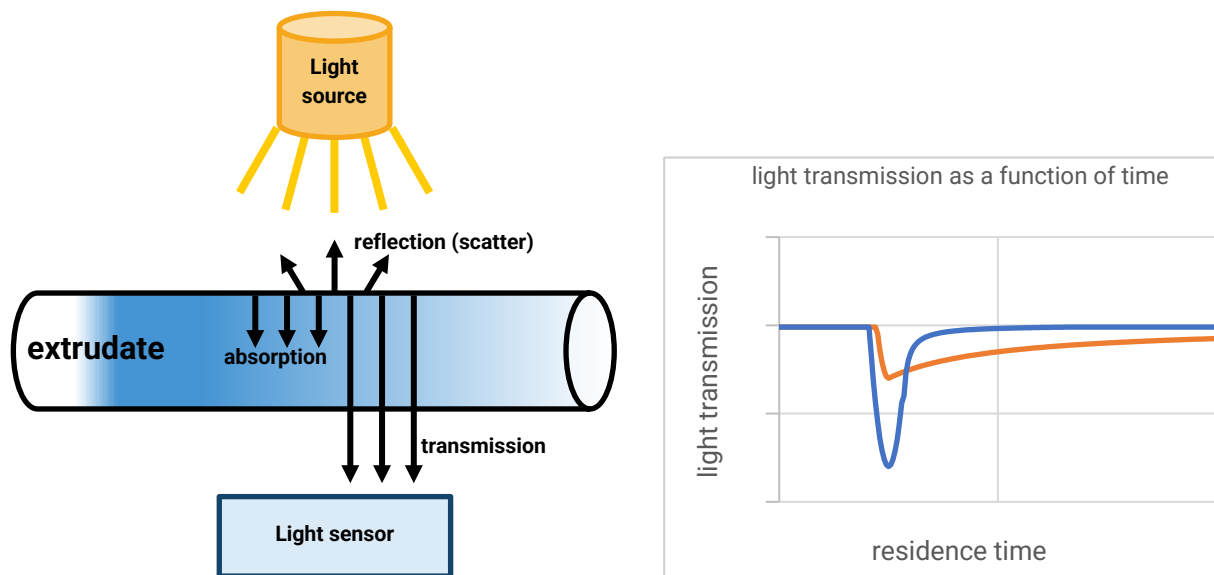


Figure 7. Left: schematic of light transmission measurement of an extrudate. Right: light transmission as a function of time.

As light is emitted to the extrudate, some light is absorbed, some light is scattered, some light is transmitted and measured with a light sensor. Polymers (such as HDPE and PP) are translucent at extrusion temperatures (>190 °C). Therefore, the hot extrudate transmits a lot of light. Many additives, such as carbon black, chalk and titanium dioxide, are opaque, therefore, the higher the additive content, the lower the light transmission.

The Beer-Lambert law is a relation between light attenuation and material properties of the medium through which light travels. The law can be applied to calculate the wt.% of the additive as a function of time from the light attenuation as a function of time.

The derivation of the Beer-Lambert law is briefly discussed in paragraph 2.3.1.1, followed by an explanation of how the RTD relates to the light attenuation of the extrudate (paragraph 2.3.1.1.1). To evaluate the accuracy in terms of systematic error (paragraph 2.3.1.1.4), sensitivity (paragraph 2.3.1.1.3) and consistency (paragraph 2.3.1.1.2) are considered.

The materials and methods are shown in section 2.3.1.3, including relevant details of the used sensors (paragraph 2.3.1.4.1), the light attenuating properties of the additives (paragraph 2.3.1.4.2) and measurement procedures (paragraph 2.3.1.4.3).

Results and conclusions are, respectively, shown in sections 2.3.1.5 and 2.3.1.6.

2.3.1.1. Probabilistic derivation of light attenuation due to particles

When shining light onto extrudate with a low additive concentration, most particles will block some of the light. However, at a high additive concentration, most of the light is blocked by the particles near the light emitter, while other particles are in the shadow and do not contribute to light attenuation. Consequently, we can conclude that the intensity of the transmitted light is not directly proportional to the wt.% of the additive.

In this paragraph the interaction of a beam of light (I_0 [lux]) with many particles is considered to derive the light attenuation as a function of particle concentration, see Figure 8 [6, 7]. The objective of this derivation is to demonstrate the non-linear relation between wt.% of the additive and transmitted light. The outcome of this derivation is similar to the Beer-Lambert law, although with some differences due to simplification made for the purposes of this derivation. These simplifications include a reduction of particle size to a single value without a size distribution and the photon particle interaction was reduced to whether or not a photon was blocked. Additionally, the fluid is considered completely translucent.

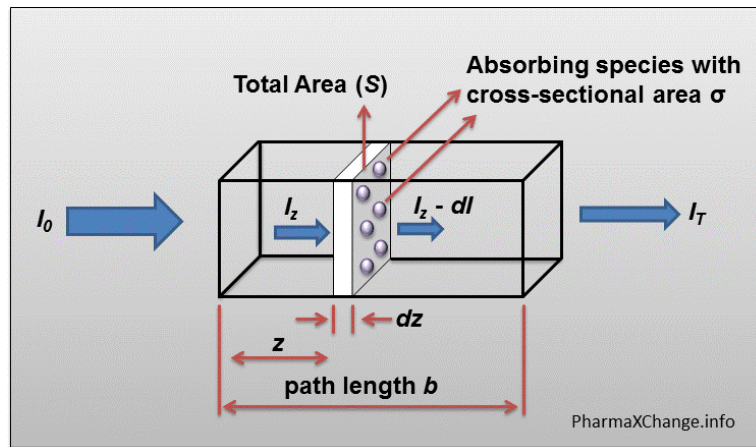


Figure 8. Schematic representation of light absorption by particles (Figure copied from reference [7]).

The particles are distributed in a translucent fluid, light (I_0 [lux]) is emitted to the fluid and some of the light (I_T [lux]) is transmitted by the fluid, see Figure 8.

Considering an infinitesimally thin (dz [m]) volume of the fluid (dV [m^3]), with cross-sectional area S [m^2], the infinitesimally small number of particles (dN) in this thin fluid is:

$$dN = n \cdot S \cdot dz \quad 2$$

Here, n [m^{-3}] is the number of particles per unit of volume ($n = dN/dV$).

The total cross-sectional area of the particles in the thin fluid volume is dN multiplied with the cross-sectional area (σ [m^2]) of a single particle.

$$\sigma \cdot dN = \sigma \cdot n \cdot S \cdot dz \quad 3$$

The infinitesimally small probability (dP_{photon}) of a single photon to be blocked by a particle within the infinitesimal thin fluid volume is equal to the ratio of the total particle cross sectional area ($dN \cdot \sigma$) to the cross-sectional area of the fluid (S).

$$dP_{\text{photon}} = \frac{\sigma \cdot n \cdot S}{S} dz \quad 4$$

The fluid cross section can be omitted from equation 4 because it appears in both the numerator and dominator on the right side of the equation.

A beam of light with intensity I_z [lux], as shown in Figure 8, enters an infinitesimal thin volume of fluid ($S \cdot dz$) perpendicular to the fluid cross section. The beam's intensity decreases by an infinitesimal amount (dI [lux]) proportional to dP_{photon} :

$$dI = -I_z dP_{\text{photon}} \quad 5$$

dI can be expressed as a function of dz by combining equations 4 and 5:

$$dI = -I_z \sigma \cdot n \cdot dz \quad 6$$

When all terms that depend on I_z are relocated to the left side of the equation, and all terms that depend on dz are relocated to the right side:

$$\frac{1}{I_z} dI = -\sigma \cdot n \cdot dz \quad 7$$

The total reduction of light over fluid thickness b , as shown in Figure 8, can be calculated by integrating equation 7 over $z = 0$ to $z = b$.

$$\int_{I_0}^{I_T} \frac{1}{I} dI = \int_0^b -\sigma \cdot n \cdot dz \quad 8$$

Where, I_0 [lux] is the light intensity of the light entering the fluid, I_T [lux], the light intensity of the light transmitted by the fluid. Solving the integral results in:

$$\ln(I_T) - \ln(I_0) = -\sigma \cdot n \cdot (b - 0) \quad 9$$

Which simplifies to:

$$\ln\left(\frac{I_0}{I_T}\right) = \sigma \cdot n \cdot b \quad 10$$

Equation 10 shows the light attenuation (I_T/I_0) of particles in a translucent medium derived with the probability of a photon to be blocked by a particle. The transmitted light intensity is an exponential function of the particle concentration which is shown in equation 11 and depicted Figure 9. Note that the particle density is directly proportional to the wt.%.

$$I_T = e^{-\sigma \cdot n \cdot b} I_0$$

11

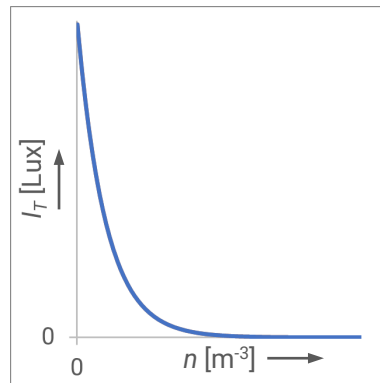


Figure 9. Transmitted light intensity as a function of particle density.

This derivation was for illustrating the non-linear relation between wt.% of the additive and transmitted light intensity. Note that the particle photon interaction was simplified to whether a photon was blocked by a particle. Nonetheless equation 10 is very similar to the definition of absorbance (A [-]) with only a factor of $1/\ln(10)$ difference:

$$A = \log_{10} \left(\frac{I_0}{I_T} \right) = \ln \left(\frac{I_0}{I_T} \right) \cdot \ln^{-1}(10) \quad 12$$

The absorbance is a linear function of the molar attenuation coefficient of the additive (ϵ [$\text{m}^2 \cdot \text{mol}^{-1}$]), the distance that the light travels through the extrudate (b [m]), and the molar concentration of the additive (c [$\text{mol} \cdot \text{m}^{-3}$]).

$$A = \epsilon cb \quad 13$$

Note the similarities between the right side of equations 10 and 13. The concentration I is directly proportional to the number of particles per unit of volume (n). And the particle cross-sectional area (σ) is analogous to the molar attenuation coefficient (ϵ), both are material coefficients on which the light attenuation depends. Although particle cross-sectional area as the only material parameter is a simplification, particle photon interaction was simplified to whether a photon was blocked by particle. Note that the absorbance (A [-]) differs from the absorption of light since the absorbance is a function of attenuation caused by absorption ($I_{\text{absorption}}$ [lux]) as well as scattering (I_{scatter} [lux]) and reflection ($I_{\text{reflection}}$ [lux]), see Figure 7 and equation 14.

$$I_T = I_0 - I_{\text{absorption}} - I_{\text{scatter}} - I_{\text{reflection}} \quad 14$$

In conclusion the transmitted light intensity and the light attenuation are not linear functions of wt.% of the additive. Instead, they are logarithmic and exponential functions of wt.% of the additive. Therefore, the Beer-Lambert law is needed to determine the wt.% of the additive from transmitted light measurements.

2.3.1.1.1. Residence time distribution based on light attenuation

The RTD is the probability (P_i) of an the fraction of the additive mass ($m_i(t)$) to arrive at the die exit, as a function time (t). The previous paragraph showed that the additive mass can be calculated with the Beer-Lambert law, equation 15. In this paragraph the Beer-Lambert law will be used to derive P_i as a function of transmitted light.

During a mix experiment the absorbance as a function of time ($A(t)$) can be determined by measuring the transmitted light intensity as a function of time ($I_T(t)$):

$$A(t) = \log\left(\frac{I_0}{I_T(t)}\right) \quad 15$$

Absorbance is a function of molar concentration (c [$\text{mol}\cdot\text{m}^{-3}$]) as shown in equation 13. Molar concentration is proportional to the wt.% of the additive of the polymer (w [-]). See equation 16, where M [$\text{kg}\cdot\text{mol}^{-1}$] is the molar mass and ρ [$\text{kg}\cdot\text{m}^{-3}$] is the density.

$$w = c \frac{M}{\rho} \quad 16$$

The mass of the additive (m [lux]), in the extrudate, can be calculated from wt.% of the additive in the extrudate mass ($m_{\text{extrudate}}$ [lux]).

$$m = w \cdot m_{\text{extrudate}} \quad 17$$

The additive mass as a function of time ($m(t)$) can be calculated by substituting equation 17 with W and $A(t)$ from equations 16 and 15. In this new equation, c can be substituted by c isolated from equation 13.

$$m(t) = m_{\text{extrudate}} \frac{M}{\rho \epsilon b} A(t) \quad 18$$

The total additive mass (m_{total}) is the sum of all the additive mass samples.

$$m_{\text{total}} = \sum_{j=s}^N m_{\text{extrudate}} \frac{M}{\rho \epsilon b} A_j \quad 19$$

Where A_j is the absorbance at residence time t_j [s], with s the first sample with additive and N the total number of samples/measurements.

The RTD ($P_i(t)$) probability can be calculated with the additive mass and the total by combining equations 1, 18, 19.

$$P_i(t) = \frac{m_{\text{extrudate}} \frac{M}{\rho \epsilon b} A_i(t)}{\sum_{j=s}^N m_{\text{extrudate}} \frac{M}{\rho \epsilon b} A_j} \quad 20$$

A_i is the absorbance at residence time t_i . The extrudate diameter (b), mass ($m_{\text{extrudate}}$) and the additive material properties (ϵ , M and ρ) are assumed to be constant during an extrusion experiment. Therefore equation 20 reduces to:

$$P_i(t) = \frac{A_i(t)}{\sum_{j=s}^N A_j} \quad 21$$

$\sum_{j=s}^N A_j$ is independent of time, therefore $A_i(t)$ is linear proportional to the residence time distribution ($A_i(t) \sim P_i(t)$).



The absorbance depends on the emitted and transmitted light intensity (equation 15), therefore $P_i(t)$ can be written as a function of light intensity:

$$P_{i_optical} = \frac{\log\left(\frac{I_0}{I_{i_T}}\right)}{\sum_{j=s}^N \log\left(\frac{I_0}{I_{j_T}}\right)} \quad 22$$

Where I_{i_T} and I_{j_T} representing the transmitted light intensity at respectively residence time (RT_i and RT_j), with s the first sample with additive and N the total number of samples/measurements.

In conclusion the RTD can be calculated with only the emitted light intensity and the transmitted light intensity as a function of time. Furthermore, the absorbance as a function of time and $P(t)$ are proportional to each other ($A(t) \sim P(t)$).

2.3.1.1.2. Consistency

The accuracy of the optical RTD method can partly be verified through a consistency check using varying amounts of additive mass (m). The mix behavior is not expected to change if the total additive fraction is low, and the method of adding the additive does not change. Consequently, two mix experiments with $m_{1total} \neq m_{2total}$ should still result in the same probability distribution.

$$P_1(t) = P_2(t) \quad 23$$

The relation between m_1 and m_2 can be determined by combining equations 1 and 27.

$$\frac{m_1(t)}{m_{1total}} = \frac{m_2(t)}{m_{2total}} \quad 24$$

The additive mass can be expressed as a linear function of the absorbance, see equation 18. By combining equations 1 and 27 we can find the relation between A_1 and A_2 :

$$m_{extrudate} \frac{M}{\rho \epsilon b} \frac{A_1(t)}{m_{1total}} = m_{extrudate} \frac{M}{\rho \epsilon b} \frac{A_2(t)}{m_{2total}} \quad 25$$

Several parameters (ϵ , M , ρ , $m_{extrudate}$) remain constant across experiments and can consequently be omitted, leading to a simplified equation.

$$\frac{A_1(t)}{m_{1total}} = \frac{A_2(t)}{m_{2total}} \quad 26$$

In this study, the ratio A/m_{total} is defined as the relative absorbance [kg^{-1}]. The total additive mass is controlled, and the absorbance is measured during the experiment. As a result, experiments with varying total additive mass can be compared with the relative absorbance. Consistency across experiments is shown if the relative absorbance is the same across experiments with varying amounts of total additive mass.



2.3.1.1.3. Sensitivity at a high wt.% of the additive

To get the RTD the wt.% of the additive is determined by measuring the light transmission. With a high additive fraction most of the light will be absorbed, see Figure 9, an increase in wt.% will result in only a small decrease of transmitted light. This behavior can also be illustrated with the derivative dl_T/dn , the derivative of equation 11.

$$\frac{dl_T}{dn} = -I_0 \cdot \sigma \cdot b \cdot e^{-\sigma \cdot n \cdot b} \quad 27$$

As the transmitted light increases, dl_T/dn approaches nearly 0 lux as is shown in Figure 10.

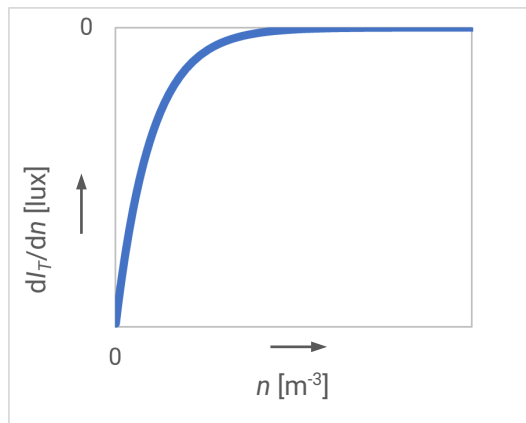


Figure 10. dl_T/dn as a function of particles per unit of volume. Note the top of the vertical axis is at 0 lux.

Note that n is proportional to the wt.% of the additive, therefore the sensitivity in change in wt.% (dl_T/dm) also becomes nearly 0 lux/kg.

A low light transmitted intensity and sensitivity at a high wt.% of the additive means that uncertainty contributions and light scatter will have more effect on the measurements. Therefore, it is preferred to mainly experiment with a low wt.% of the additive.

2.3.1.1.4. Background illumination bias and emitted light intensity

Thus far, the emitted and transmitted light intensity have been discussed as if they are directly measurable quantities. However the polymer also attenuates the light, and some background light is expected. This paragraph describes how the transmitted light intensity, the emitted light intensity, and the background illumination bias (BIB) can be determined with measurements.

Background illumination bias

The BIB is a systematic error in the measured light intensity. Therefore, the measurements were corrected for the BIB. The transmitted light intensity (I_T) can be calculated with the measured light intensity ($I_{measured}$) and the BIB (I_{BIB}).

$$I_T = I_{measured} - I_{BIB} \quad 28$$

The BIB can be determined from the measured light when $I_T = 0$ lux. At this point, as shown in Figure 9, the BIB can be found with equation $I_{BIB} = I_{measured}$. During experiments, a high wt.% of the additive can be identified by a low measured light intensity combined with a light intensity plateau ($dl/dt \approx 0$ [lux/s]), as referenced in paragraph 2.3.1.1.3.

This behavior is depicted in Figure 11; the red dashed circles in the right graph indicate the highest additive mass, and the lowest light intensity is marked in the left graph. Furthermore, the light intensity is at a plateau ($dI/dt \approx 0$ [lux/s]) while at the same time the additive mass reduces quickly $dm/dt \ll 0$ [s⁻¹]. The light intensity at this plateau is nearly all BIB (represented by the green dashed line in Figure 11 at the left). Therefore, the BIB can be determined at this plateau during a mix experiment.

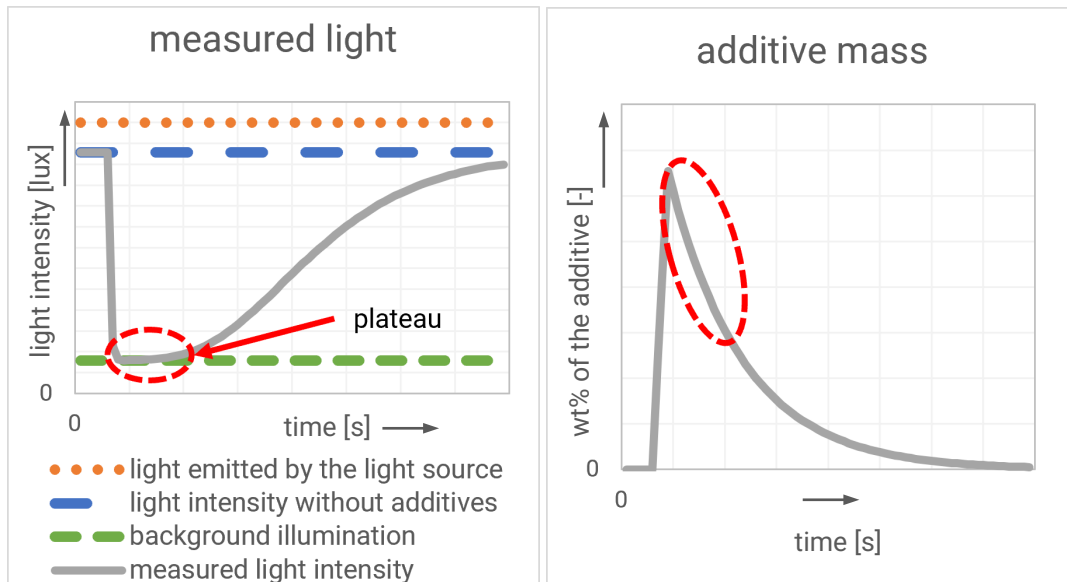


Figure 11. Illustrations of a hypothetical measurement. Left: Light intensity as a function of time. Right: wt. % of the additive as a function of time.

This method assumes a very high additive mass at some time during the experiments. This assumption can be verified using the burn off RTD. The assumption is correct if the burn off RTD shows a high wt.% of the additive while the measured light intensity shows a plateau.

An alternative method to determine the BIB might involve increasing the wt.% of the additive until the light intensity no longer increases, even though the wt.% of the additive continues to increase. At this point all measured light is BIB. The downside of such method is that it requires a lot of time and might interfere with following experiments. The AIT is not suitable for continuous injection of a masterbatch; therefore, the additive has to be added in the hopper. This masterbatch must be completely flushed out of the extruder before experiments can continue, since a tiny amount of masterbatch can cause a measurement error. It takes a very long time for all of the masterbatch to be flushed out of the whole extruder. Therefore, the first method is the preferred method to determine the BIB.

The BIB may be composed of environmental lighting, including sunlight scattering from the windows, and light reflections on the extrudate. Therefore, the BIB was determined for each series of measurements and for each material.

Emitted light

The light is attenuated both by the additive and the polymer. For the RTD only the light attenuation by the additive is relevant. Therefore, to eliminate the effect of the polymer on attenuation in the calculations, the emitted light (I_0), is not defined as 'light emitted by the light source' (the orange dotted line in Figure 11 at the left). Instead, it is defined as the measured light intensity, when no additives are present in the extrudate ($I_{\text{measured without additives in the extrudate}}$, the blue dashed line in Figure 11 at the left), with the BIB subtracted.

$$I_0 = I_{\text{measured without additives in the extrudate}} - I_{BIB}$$

29

The emitted light intensity can be determined with a light intensity measurement without any additives.

2.3.1.2. Noise reduction

To reduce noise the measured light intensity was filtered with a moving average.

The RTD is anticipated to exhibit a smooth curve, see for example figure 54 in part 2: *Mixing quantification*. Consequently, fluctuation over short periods (< 10 s) are unlikely to represent the mix quality and are more likely attributable to noise [5]. Such noise might originate from radiation affecting the electronics, a random error component in the background illumination, or some instability in the extrudate flow.

The optimal period for a moving average can be determined through a Fourier analysis of the light intensity, with the period being the reciprocal of the frequency at the highest peak in the frequency response. Fourier analysis is a technique that transforms a time dependent signal into a frequency dependent representation.

To summarize the measured light intensity will be filtered with a moving average.

2.3.1.3. Goals of the optical RTD experiments

The primary objective of the optical RTD experiments is to acquire a measured RTD, which can be used to verify the simulations. In addition, several experiments were executed to gauge the accuracy of the optical RTD method. This includes stability (standard deviation, creep) and repeatability during the measurements.

Consistency is partly checked by repeating the mix experiments with different amounts of additive material. The mix behavior is not expected to change as long as the total additive fraction is low, and the method of adding the additive does not change. Therefore, the optical RTD is expected to be independent of the amount of additive material.

The optical RTD method, materials and setup is explained in paragraph 2.3.1.4, the optical RTD results are shown in 2.3.1.5.

2.3.1.4. Materials and methods for the optical RTD measurements

An experimental setup was developed for optical RTD measurements. Photos and a schematic cross section of the setup are shown in Figure 12.

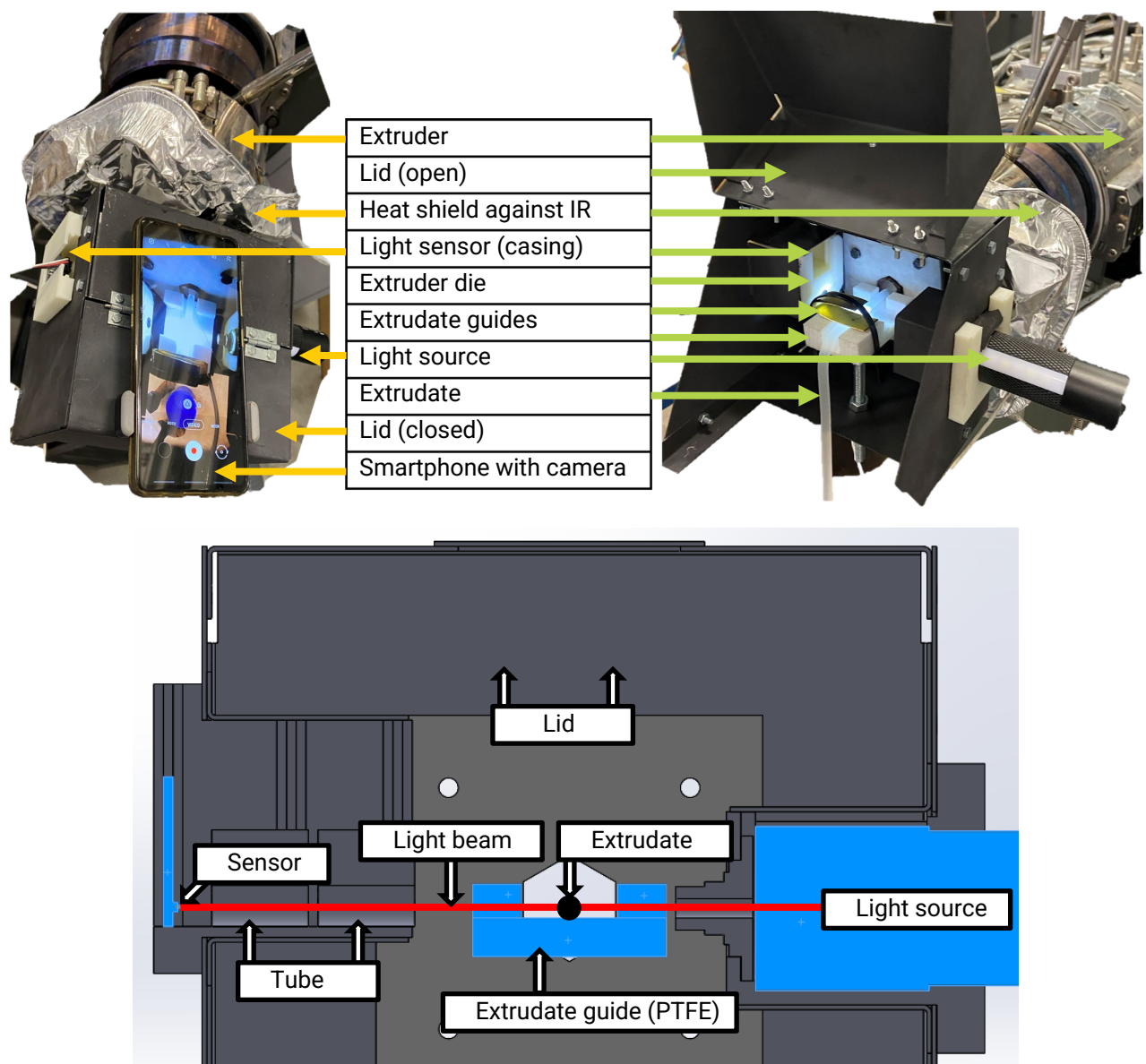


Figure 12. Photos and schematic of the optical RTD measurement setup. Upper left: setup with a closed lid and a smartphone to film the extrudate. Upper right: the setup with an open lid. Lower: Schematic cross section of the RTD measurement setup.

The extrudate runs through the optical RTD measurement setup. HDPE and PP are translucent near the extruder die, but translucency reduces quickly due to the formation of polymer crystals. Therefore, the optical measurement setup was positioned very close to the extruder die. The optical RTD measurement setup uses a guide to fix the extrudate position and align the extrudate with the light source and the light sensor. Extrudate slip is desired in the guide to avoid stick-slip or extrudate buildup. As a result, the guide is primarily constructed from PTFE for its non-adhesive properties. While the upper section is constructed from brass, its minimal force on the extrudate ensures that it minimizes drag.

The light sensor should measure only light transmitted through the extrudate. Any other light on the sensor is BIB or noise. Therefore, the light sensor is completely covered, except for a tube aligned with the sensor, extrudate and light source. Furthermore, the lid can be closed to minimize scatter light. The remaining scatter light comes from the light source and reflected/scattered between the extrudate and the extrudate guide.

The extrudate position and shape is dependent on the extruder die and extrudate guides (see Figure 12) and on the speed/force of pulling on the extrudate. Pulling using gravity is a very steady process and results in a consistent extrudate shape and position and was therefore used for all experiments except for the PP + chalk experiment. The extrudate of the PP +chalk was pulled, by hand, through a water at room temperature bath to collect it for the burn off experiments, see paragraph 2.3.2. Unfortunately, the lid could not be closed when the water bath was used, and therefore less background light was blocked in this experiment.

A smartphone can be mounted on top of the optical RTD measurement setup. The smartphone was used to film the extrudate during the RTD experiment. Filming was started manually when the masterbatch was injected. The film timestamp is the residence time.

The outside of the optical RTD measurement setup was actively cooled with air (fan) to prevent overheating of the electronics (in particular the light sensor with an operating temperature between -30 °C to 85 °C). Furthermore a heat shield was positioned between the extruder head and the optical RTD setup.

2.3.1.4.1. Light sensor, light emitter and datalogger

The light sensor, the light source, and additives all operate within a light spectrum that's visible to humans. As a result, during an experiment, the measurement setup—including the alignment of the light source with the extrudate and a qualitative assessment of the colorant wt.% (e.g., the shade of black/grey of the extrudate)—can be checked visually.

The white light source is a LED flashlight (Ansmann Future Multi 3in1). The light intensity can be adjusted using a D.C. variable power supply.

The light sensor is an AMS104 light sensor with a light-sensitive area of 0.51 mm by 0.68 mm. The sensor has a build in filter for a spectral response like that of a human eye, with a peak sensitivity at 580 nm, as shown in Figure 13.

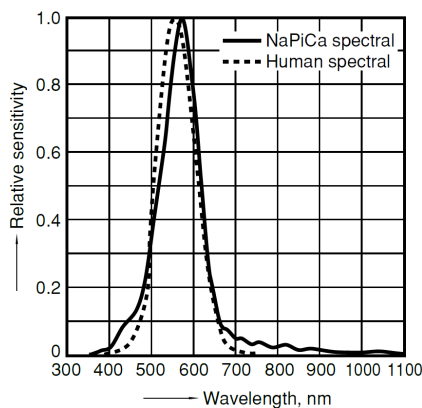


Figure 13. Sensitivity of AMS104 light sensor (NaPiCa) compared to a human eye sensitivity [8].

The sensor is mounted on a P/N1127 PCB (Printed Circuit Board), the board sends an analogue signal to an Arduino UNO [8]. The Arduino has a 10 bit ADC (Analog to Digital Converter) resulting in a combined range of 1-1000 lux with a resolution of 1 lux. The Arduino operates at a sampling rate of 9600 Hz and stores a moving average (with a period of 0.1 s) every 0.1 s. Calculating the moving average and storing the measured value takes some CPU power, leading to an actual sampling rate less than 9600 Hz. A sampling rate of 10 Hz might seem excessive but can be beneficial when some filtering (such as a moving average) is needed afterwards. The data was processed with MS Excel and GNU Octave.

The Arduino was also used to control the stepper motor of the AIT device, see section 2.2. Therefore, the residence time is synchronized with the injection of the additive.

2.3.1.4.2. Light attenuating properties of the additives

Chalk, carbon black and a grey masterbatch were used as additives with the mix experiments, see paragraph 2.1. In this paragraph the light attenuating properties of these additives are considered.

Light attenuating properties of Calcium carbonate

Calcium carbonate (CaCO_3) can be transparent, but light scatters in chalk since it consists of small particles ($0.5 \mu\text{m} - 100 \mu\text{m}$) and CaCO_3 has a high refractive index (1.55) [9, 10]. PP and HDPE have an almost identical refractive index (both 1.5) therefore one might expect a translucent polymer-chalk composite [11]. In contrary the chalk does not mix very well with PP and HDPE because chalk is hydrophilic while PP and HDPE are hydrophobic [12]. The chalk forms agglomerates in the polymer matrix and the compound is opaque.

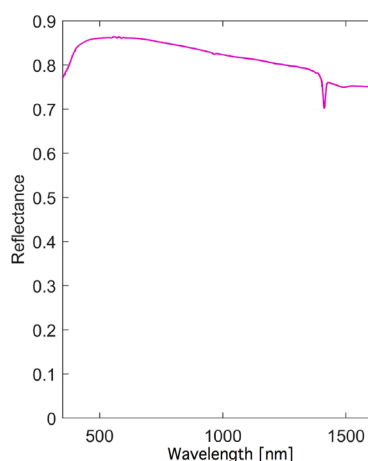


Figure 14. Reflectance of chalk [13].

Figure 14 shows a high chalk reflectance at the same wavelengths ($\sim 500 \text{ nm}$ to 650 nm) as the sensitivity of the light sensor and the human eye sensitivity.

Light attenuating properties of carbon black and the grey masterbatch

Carbon black also absorbs light in the visible spectrum, see Figure 15, and at the same wavelength ($\sim 500 \text{ nm}$ to 650 nm) as the light sensor sensitivity.

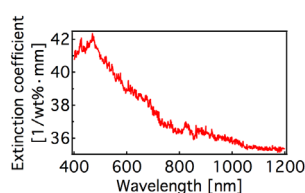


Figure 15. Absorption spectrum of carbon black [14].

It was unknown, in this study, what the pigments in the grey PP masterbatch are. It might be a combination of carbon black and titanium dioxide. Both masterbatches and the PE with chalk are shown in Figure 4, all of them are visibly opaque and therefore suitable for an optical RTD experiment in the visual light spectrum.

2.3.1.4.3. Overview of optical RTD experiments

Several experiments were carried out to evaluate the accuracy and for a comparison of “burn off RTD” and “simulated RTD”. A short overview of the conducted experiments is shown in this paragraph.

Visual evaluation of the RTD

To gain an understanding of the experiments, a qualitative assessment of the RTD was performed by visually examining the extrudate from a carbon black experiment.

Light source adjustment

The setup has a range of 1-1000 lux with a resolution of 1 lux. The resolution in RTD ($P(t)$) depends, among others, on how much of the light sensor range is used. To aim for optimal results the light source is adjusted until I_0 is between 800 lux and 1000 lux.

Light sensor and light emitter stability

The stability of the light sensor and light emitter was determined by performing a 400 s measurement without any extrudate. The stability was expressed with a standard deviation in the measured light intensity and with the linear slope (dI/dt).

Noise

Some random error in the measured light intensity may originate from radiation affecting the electronics, a random error component in the background illumination, or some instability in the extrudate flow. To reduce noise the measured light intensity was filtered with a moving average. The optimal period, for the moving average, was determined through a Fourier analysis of the light intensity of a HDPE + CB masterbatch experiment. This filter was applied to all measurements.

Repeatability and stability

The repeatability was checked through a visual comparison $I_T(t)$ of 3 repeating mix experiments with PP + 241 mg grey MB (masterbatch) and 3 repeating experiments with HDPE + 30 mg carbon black MB. Furthermore, the random error and drift were analyzed.

Background illumination bias

The BIB was determined for each polymer + additive combination. If the additive quantity is high enough, then most of the light is absorbed/scattered and background light is dominant. This results in a plateau with a very low light intensity. At this plateau the BIB can be determined.

Consistency

To check for consistency the optical RTD ($A_{relative}(t)$) was determined with different amounts of additive (m_{total}). These experiments were performed both with PP + grey MB (60 mg up to 241 mg) and HDPE + carbon black MB (30 mg up to 121 mg).

Experiments for a comparison to a burn off RTD

Extrusion experiments with PP and chalk were performed for a comparison of the optical RTD and burn off RTD. This experiment was performed in duplicate. During the first experiment the extrudate was subjected to gravitational pull, resulting in a more stable extrudate cross section and therefore a more stable optical RTD. But for the burn off RTD the extrudate has to be collected, and pulled, manually. With this second experiment the optical RTD and burn off RTD were determined simultaneously.

For each of the burn off experiments, 1.8 g of chalk was used to achieve a high additive concentration.

These experiments were carried out to verify the optical RTD, not to study the mixing behavior of the mixing section of the screw. Therefore, using the AIT was not relevant for this experiment, furthermore the AIT was not suitable for injecting the chalk filled PE. The PE was fed into the hopper instead of using the AIT. The hopper was emptied before the chalk was added.

The burn off experiments are shown in section 2.3.2 and the comparison of optical RTD with burn off RTD is shown in section 2.3.3.

Experiments for a comparison to the simulated RTD

The optical RTD measurement with HDPE + carbon black MB were used for verification of the simulations. The simulated RTD and a comparison to the optical RTD is shown in paragraph 3.3.



2.3.1.5. Optical RTD results

Several optical RTD experiments were performed, this paragraph shows a visual assessment of the RTD. The following paragraphs show the quantitative results of the RTD, stability, repeatability, and consistency.

Several extrudate samples, of a carbon black experiment, were collected for visual inspection, see Figure 16.

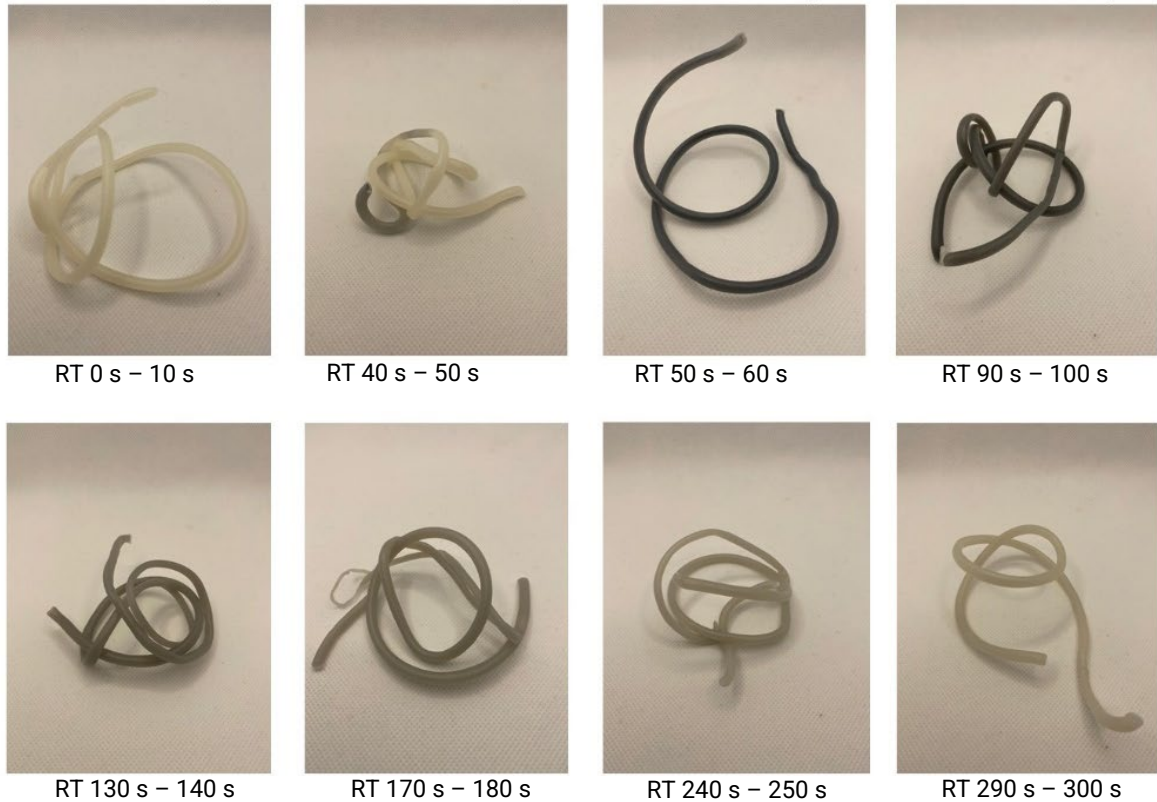


Figure 16. Extrudate samples at different residence times (RT) after the carbon black masterbatch was added.

The sample at RT (residence time) = 0 s is white since it only contains HDPE without carbon black. At RT = 40 - 50 s the extrudate is a bit darker, and at RT = 50 - 60 s the extrudate is black due to the carbon black. Therefore the shortest residence time seems to be slightly below 50 s. The extrudate becomes gradually lighter with an increase in residence time.

Extrudate photos were made during a carbon black experiment, see Figure 17.

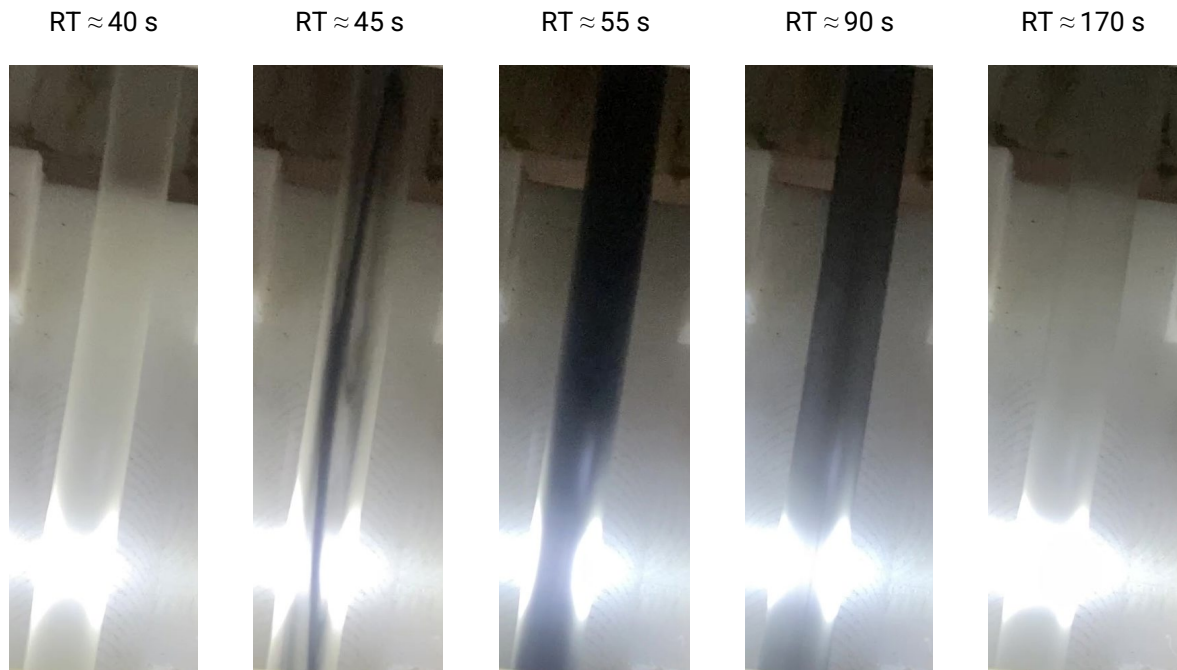


Figure 17. Extrudate photos made inside the optical RTD measurement setup at different residence times.

The photos also show light scatter at the incoming side (right side) of the extrudate and some light scatter where the light exits the extrudate (left side). The extrudate is translucent at $RT \approx 40$ s, the first streaks of carbon black are shown at $RT \approx 45$ s. The extrudate is black at ≈ 55 s, interestingly at this time there still is some light scatter at the side where light exits the extrudate (left side). At $RT \approx 90$ s the extrudate is more grey than black and at $RT \approx 170$ s the extrudate is almost as translucent as it was at $RT \approx 40$ s.

2.3.1.5.1. Light sensor and emitter stability

In the previous paragraph extrudate photos were shown to gain understanding of the experiment. The current paragraph is focused on the quantitative data of the stability RTD measurement setup.

Light intensity without any extrudate was measured to determine the stability of the light sensor and emitter combination, see Figure 18.

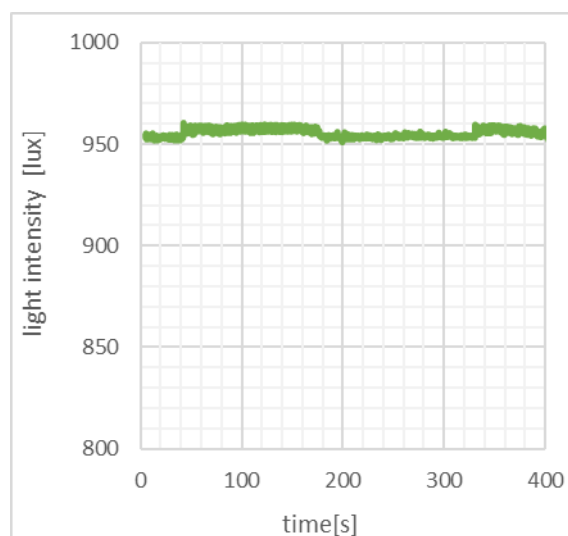


Figure 18. Light intensity as a function of time, without extrudate. Note: the light intensity scale starts at 800 lux.

The light sensor and light emitter combination is stable, the linear slope ($dl_{transmitted}/dt$) is only -2 mLux/s. This decay is less than the resolution (1 lux) during the whole 400 s measured. There is some scatter, the standard deviation is 2 lux. Every couple of minutes the measured light intensity takes a step of ~4 lux. It is unclear whether this is due to the light sensor or the light emitter. The steps are for a large part responsible for the standard deviation, in between the steps the standard deviation is only 1 lux.

The transmitted light showed some decay after several measurements (each lasting more than 400 s). The most likely explanation for the decay is a reduction of light intensity from the flash light. The flashlight might have become hot, but this is not attributable to heat from the extrudate but rather due to its own energy consumption and lack of effective heat dissipation. The flashlight was encased in a thick polymer mounting bracket, which is not optimal for heat transport. Furthermore, a significant amount of light is trapped within the same casing and converted to heat.

The creep in light transmission was prevented by letting the flashlight cool down between experiments. Unfortunately, the experiments involving HDPE + 8 mg CB MB were an exception; these measurements were conducted before the light transmission creep was observed.

2.3.1.5.2. Repeatability and noise reduction

To evaluate the accuracy of the repeatability, random error and drift were considered. Furthermore, the frequency of the noise was determined and used to smooth the results with a moving average.

Noise reduction

To improve the interpretation of the data, the random error (noise) was analyzed and filtered with a moving average. The noise can originate from radiation affecting the electronics, a random error component in the background illumination, or some instability in the extrudate flow. The noise was most prevalent with the HDPE with carbon black experiments; therefore, these were used for Fourier analysis. The optical RTD was determined by measuring the light intensity (transmitted light) as a function of residence time, see Figure 19.



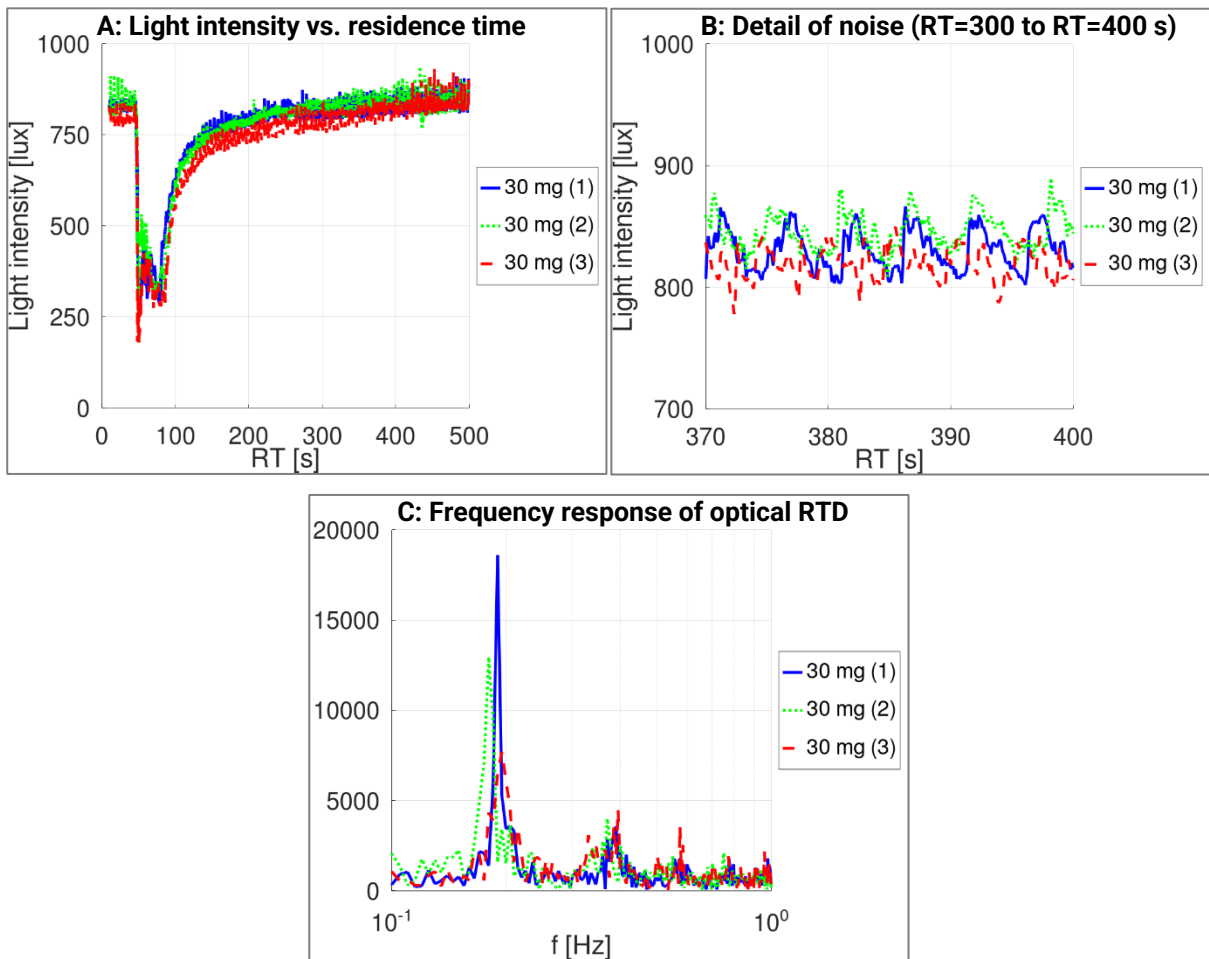


Figure 19. 3 HDPE experiments with 30 mg CB masterbatch and 3 PP experiments with 241 mg grey masterbatch. A: Light intensity as function of residence time. B: Light intensity as function of residence time zoomed in on noise from RT = 300 to 400 s. C: Frequency response of the optical RTD.

As can be seen from Figure 19 B, the measurements do show some noise, which is a zoom to the noise. A Fourier analysis, see Figure 19 C, shows a peak in the frequency response, at 0.2 Hz. It is not clear what the origin is of this 0.2 Hz noise, it seems unlikely that it originates from the extruder since the screw flight passings is at a different frequency (0.5 Hz). The light sensor and emitter also do not show such high noise levels, see paragraph 2.3.1.5.1. It might be from extrudate handling or some minor flow instability, although this was not observed during the experiments. Normally after the optical RTD setup the extrudate flowed down in a spiraling motion, it might be that the period of the spiral is 5 s and that this motion is the origin of the 0.2 Hz noise. This noise was filtered by using a moving average with a period of 5.1 s. The PP experiments showed less noise compared to the HDPE experiments. To maintain uniformity, all graphs representing absorbance and probability are shown with a moving average of 5.1s.

Repeatability, random error and drift

Experiments were repeated 3 times for HDPE + 30mg masterbatch and PP + 241 mg masterbatch, see Figure 20.

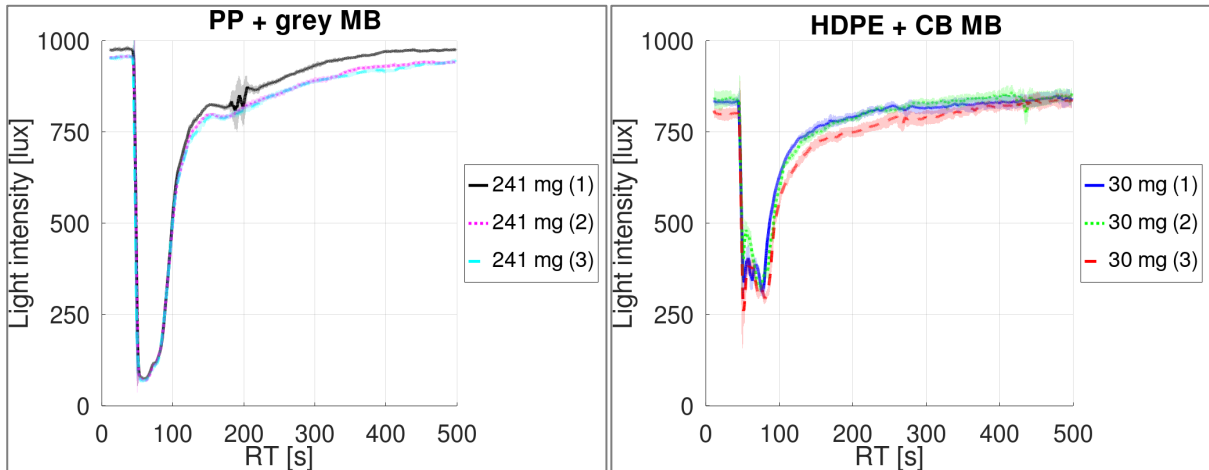


Figure 20. Moving average of the light intensity with a period size of 5.1 s, the light-colored bands show the standard deviation within the 5.1 s period. Left: 3 PP experiments with 241 mg grey masterbatch. Right: 3 HDPE experiments with 30 mg CB masterbatch.

Before each experiment, the light source was adjusted so that the initial light intensity (I_0) falls between 800 lux and 1000 lux. This adjustment aims to utilize most of the sensor's range (1-1000 lux), see I_0 in Table 1.

The 3 HDPE experiments show a very similar curve, the same was found for the 3 PP experiments. Several regions can be identified. The first was from $RT = 0$ to 47 s with a very high light intensity, indicating absence of carbon black. Between $RT = 47$ s and $RT = 49$ s there is a very sharp decrease in light intensity, indicating an increase in masterbatch. Therefore, the shortest observed residence time is 47.5 s. The light intensity is low in the range of $RT = 47.5 - 86$ s indicating a high masterbatch content. After $RT = 86$ s the light intensity starts to increase, indicating a decrease of masterbatch content. After 170 s the light intensity closely resembles its initial value recorded before $RT = 40$ s, suggesting that most of the masterbatch has passed through. In the range of $RT = 470 - 500$ s the light intensity is stable (slope is < 0.5 lux/s) and is nearly the same value as it was at the start of the experiment, see also Table 1. This suggests that (almost) all masterbatch has passed, furthermore that drift in the light emitter is minimal.

These regions with high and low masterbatch content agree with the observations shown in Figure 16 and Figure 17. The regions with a low masterbatch content, at the beginning from 10 - 40 s and at the end from 470 - 500 s, were used to determine the random error and drift, see Table 1. In general, the random error is higher with the HDPE measurements compared to the PP measurements.

Table 1. Average light intensity of carbon black experiments at the start and at the end. These values are calculated with the raw data without a moving average.

Material	I_0 (average and standard deviation of the light intensity at the start of each experiment between 10 s and 40 s)	Average and standard deviation of the light intensity at the end (between 470 s and 500 s)	Drift between the start and the end	Slope at the end (between 470 s and 500 s)
HDPE (1)	832 ± 10 lux	844 ± 20 lux	1.5 %	-0.23 lux/s
HDPE (2)	840 ± 22 lux	850 ± 18 lux	1.2 %	0.02 lux/s
HDPE (3)	800 ± 15 lux	836 ± 19 lux	4.5 %	0.12 lux/s
PP (1)	977 ± 6 lux	964 ± 6 lux	-1.3 %	0.45 lux/s
PP (2)	956 ± 4 lux	929 ± 5 lux	-2.9 %	0.16 lux/s
PP (3)	955 ± 7 lux	919 ± 6 lux	-3.8 %	0.04 lux/s

In two areas there is some deviation between measurements. Experiment 1 with PP (Figure 20 left, black continuous line), the standard deviation (grey band) is high between RT = 180 s and 205 s, this is due to a one time bumping into the extrudate. Furthermore, with the HDPE experiments in the range of RT = 47.5 - 86 s there are some peaks and valleys which are not in agreement between the different experiments. This range is further investigated, in paragraph 2.3.1.5.4, together with the carbon black experiments with 60 mg and 120 mg carbon black.

In summary, the experimental data for both HDPE and PP types are highly repeatable, evidenced by low drift rates (< 5% over 500s) and low standard deviations (< 2.6% in low masterbatch content areas). However, an offset between experiments exists, attributed to the initial adjustment of the light emitter. These findings confirm the reliability of the measurement techniques used and indicate consistent quality in the plastic extrusion process.

2.3.1.5.3. Background illumination bias

The light incident on the sensor is partly due to transmission through the extrudate, but also originates from background illumination. The BIB (background illumination) is a systematic error for the optical RTD measurements and is discussed in paragraph 2.3.1.1.4. The BIB may be composed of environmental lighting (including sunlight scatter from the windows) and light reflections on the extrudate. Therefore, the BIB was determined for each series of measurements and for each material. In this paragraph the BIB is determined for the PP + grey MB, HDPE + carbon black MB and PP with chalk measurements.

PP + grey MB background illumination

The PP measurements, with 241 mg grey masterbatch, show a quick transition from a high slope to a stable value, see Figure 20 left. This area is the previously discussed plateau (paragraph 2.3.1.1.4) where the background illumination dominates the measured light intensity. This is further confirmed by the offset (in light intensity) of PP measurement 1 compared to measurements 2 and 3. The offset is visible at the start and end of the measurements, but has disappeared at the plateau. The plateau is between RT ≈ 52 - 62 s, zoomed in on this range in Figure 21. The minimum value, at this plateau, is 67 lux, this was used as the BIB for the transmitted light calculations for PP.

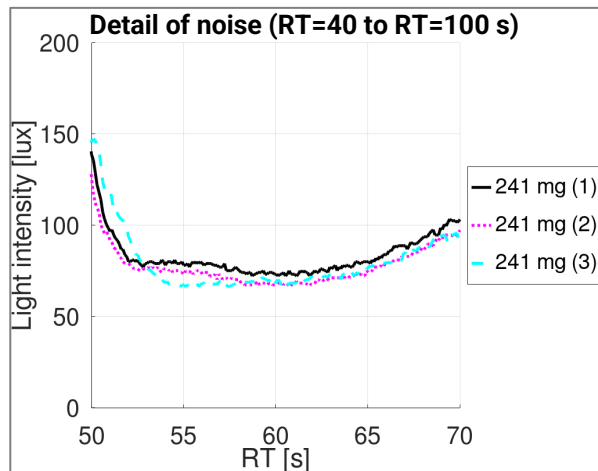


Figure 21. PP with grey masterbatch: light intensity as function of residence time, focused on the valley from RT = 50 to = 70 s.

HPDE + CB MB background illumination

HDPE extrusion experiments with 30 to 121 mg carbon black MB were performed, the measured light intensity is shown in Figure 22.

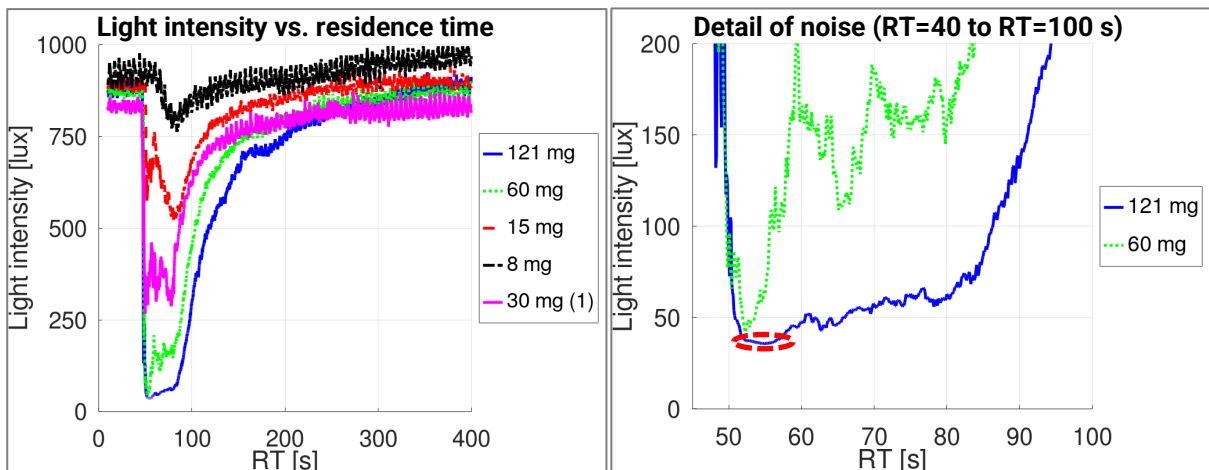


Figure 22. Left: light intensity as a function of time for carbon black experiments with different amounts of masterbatch. Right: the same graph but zoomed in at the peak with an RT between 45 s and 100 s and with a light intensity scale between 0 lux and 200 lux. The minimum light intensity plateau is marked with striped, red line.

The HDPE + 121 mg CB measurement shows a plateau between RT = 52.5 s and RT = 56.5 s, see Figure 22 at the right. This is the lowest measured light intensity of all HPDE measurements. At this plateau, the standard deviation is only 0.5 lux, while it is at least 20 lux in the same range with all the other carbon black measurements. 0.5 lux is similar to the BIB determined with the light emitter and sensor combination. This plateau is most likely the BIB for the carbon black measurements. The minimum value, at this plateau, is 37 lux, this was used as the noise level for the relative absorbance calculations.

Light intensity with varying amounts of carbon black is further discussed in paragraph 2.3.1.5.4.

PP + chalk background illumination

The PP + chalk experiment occurred in two conditions: one with gravity pulling and another with manual pulling through a cooling bath, see Figure 23 at the left. Gravity pull was the standard for all optical RTD experiments, this PP + chalk experiment was the exception. The extrudate was pulled manually in order to collect the extrudate for burn off experiments, which are shown in section 2.3.2.

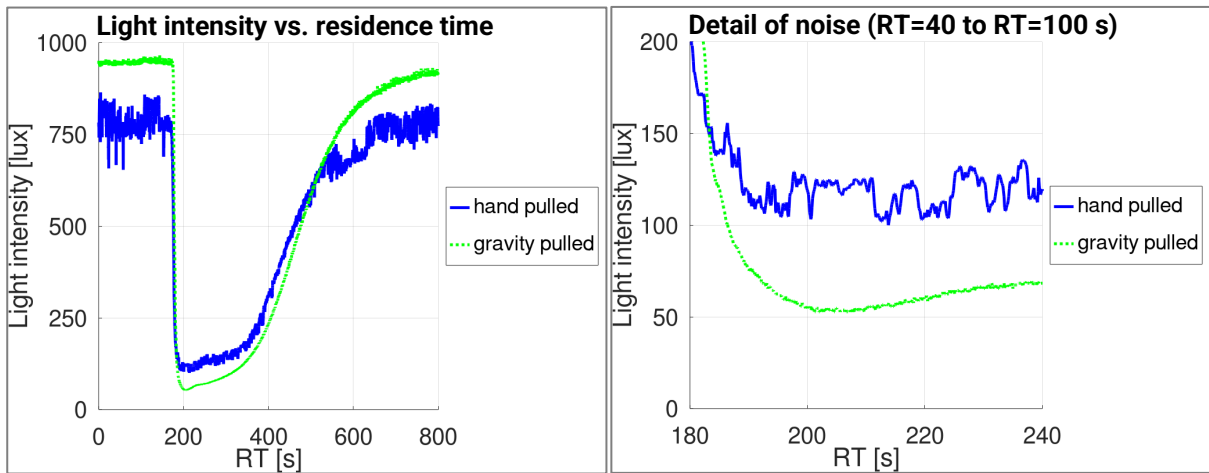


Figure 23. Left: light intensity as a function of time for PP with chalk. Right: the same graph but zoomed in at the peak with an RT between 180 s and 260 s and with a light intensity scale between 0 lux and 200 lux.

The manually pulled experiment exhibits greater scatter, attributable to two factors. Firstly, the lid could not be closed, and therefore allowing more background light to enter the setup. Secondly pulling the extrudate manually is less consistent compared to pulling by gravity. This results in slight differences in extrudate diameter, and possibly alignment of the extrudate between the light sensor and light emitter. A background illumination plateau is less clear for the chalk experiments (see Figure 23 at the right) when compared to the masterbatch experiments. The light intensity does stabilize ($dl/dt \approx 0$) for more than 20 s, therefore the minimum light intensity at this plateau is assumed to be the BIB. The background light intensity is higher for the hand pulled experiment, therefore the BIB is higher with the hand pulled experiment (99 lux) compared to the gravity pulled experiment (52 lux).

In summary, all three material combinations exhibit the expected plateau, utilized to determine the BIB. This BIB was used to calculate the transmitted light intensity, the absorbance and probability as shown in the next paragraphs.

2.3.1.5.4. Consistency

The experiments were performed with varying amounts of additive to verify the consistency of the measurements. First the measured light intensity is considered, then the relative absorbance.

Light intensity with a varying amounts of additive

The measured light intensity of HDPE with varying amounts of carbon black is shown in Figure 22 and the PP with varying amounts of grey masterbatch is shown in Figure 24.

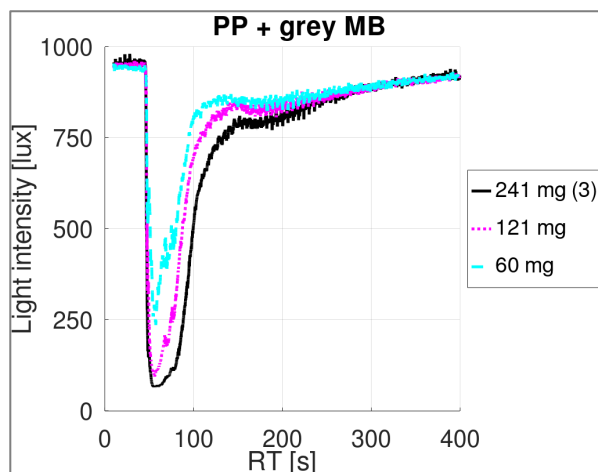


Figure 24. Light intensity as a function of time for PP with varying amounts of grey masterbatch.

The curve of light intensity as a function of residence time is somewhat similar between the experiments. Most show a sharp decrease in light intensity between RT = 47 s and RT = 49 s, indicating an increase in colorant from the masterbatches. The light intensity is lower at larger amounts of additive. For example the HDPE with 121 mg CB descends to 37 lux, at RT = 55 s, while with 15 mg CB the light intensity is never less than 523 lux. The exception is the light intensity at the start, this light intensity was set before each experiment.

To summarize, the light absorption varies depending on the total amount of additive.

Relative absorbance with a varying amounts of additive with the PP + grey MB experiments

Figure 25 shows the calculated relative absorbance for the PP + grey masterbatch experiments.

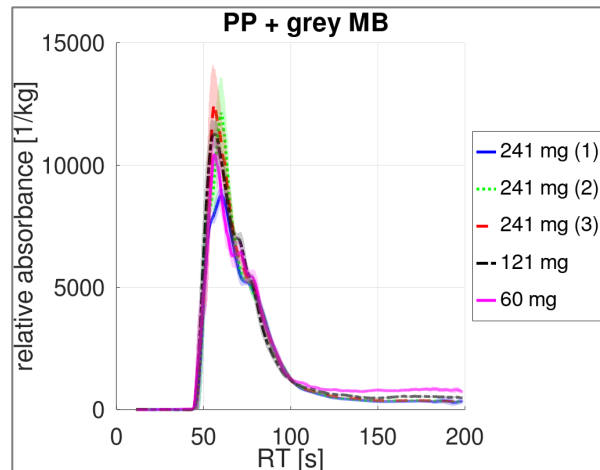


Figure 25. Relative absorbance as a function of residence time for PP with varying amounts of grey masterbatch. Note the relative absorbance is a moving average with a period of 5.1 s; the standard deviation in the moving average is shown as a light-colored band.

The relative absorbance is in agreement with the experiments with varying total amounts of added grey MB. There is scatter at the peak (RT \approx 60 s), this is partly due to a low sensitivity at a low transmitted light intensity, see 2.3.1.1.3.

The different curves are nearly identical and thereby the consistency is verified for the PP + grey MB experiments.

Relative absorbance with a varying amount of additive mass with the HDPE + CB MB experiments

Figure 26 shows the calculated relative absorbance for the HDPE with varying amounts of CB masterbatch.

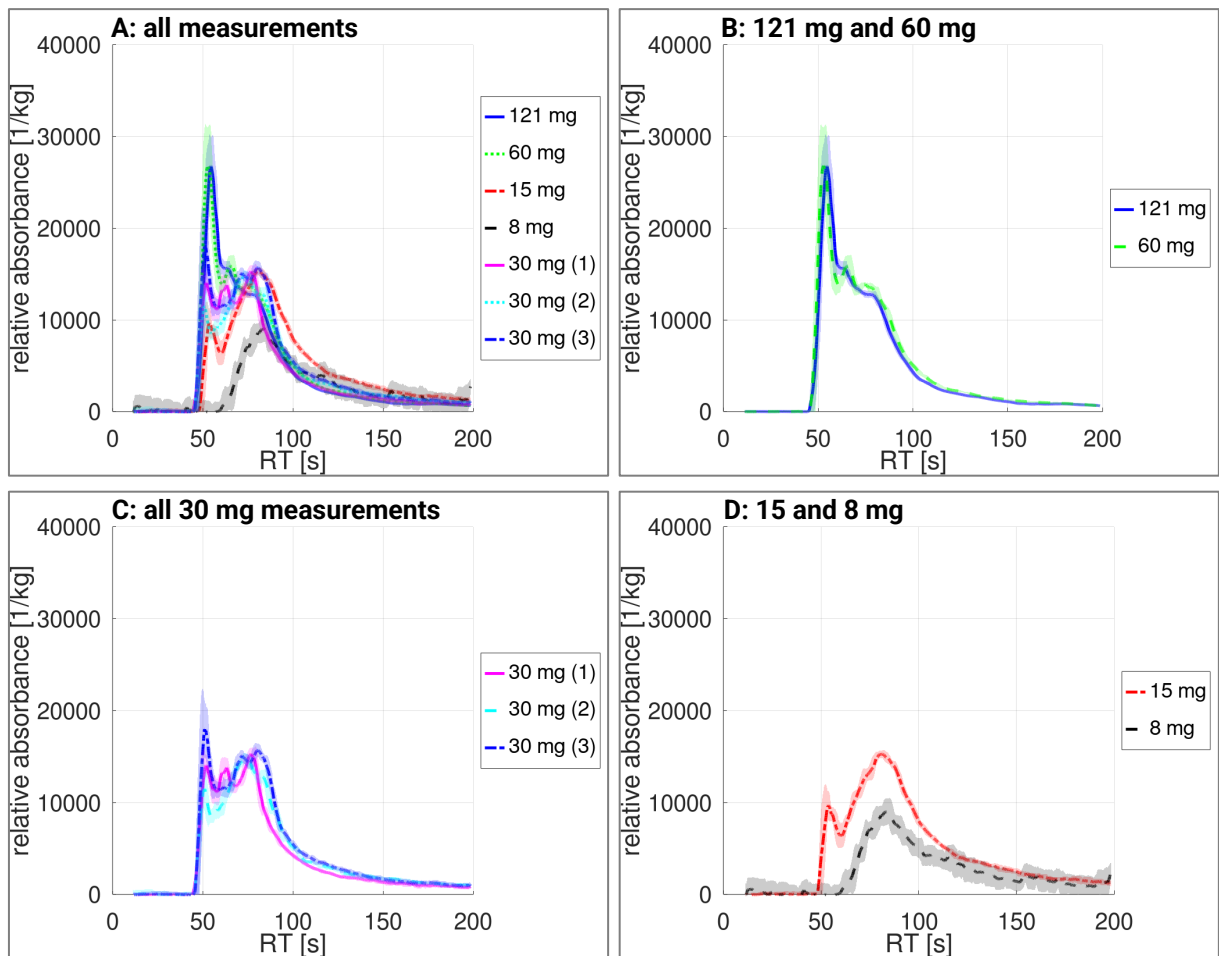


Figure 26. Relative absorbance as a function of residence time for HDPE with varying amounts of carbon black masterbatch. Note the relative absorbance is a moving average with a period of 5.1 s, the standard deviation, in the moving average, is shown as a light colored band. A: curves of all varying amounts of carbon black shown together. B, C and D: the same curves are repeated but than in separate graphs for clarity.

The experiments with HDPE and carbon black generally align when residence time exceeds 86 s. However, discrepancies are shown in two areas: the relative absorbance when the residence time is less than 86 s, and throughout the experiment with 15 mg CB MB. Both deviations are discussed below.

At $RT < 86$ s the relative absorbance seems to be a function of the total mass of the additive, this is also shown by the average relative absorbance over time, see Figure 27.

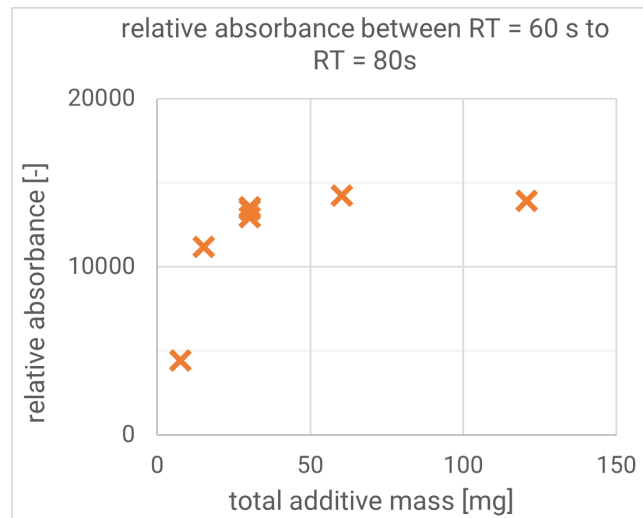


Figure 27. The relative absorbance as a function of total additive mass. In this graph the time average relative absorbance between RT = 60 s to RT = 80 s is shown.

At RT < 86 the relative absorbance is low with a low total mass of additive and increases with higher mass of the additive until it stabilizes at ≥ 60 mg. This might be due to start and stop effects of the AIT, which have a greater effect at a low total mass of additive. The masterbatch is forced into the extruder using the AIT by a piston which is driven with a stepper motor. The stepper motor uses 0.125 s to get up to speed, while injecting 2 mg masterbatch. Therefore, the first part of the masterbatch injection is at a low inflow rate. Furthermore, there might be some trapped air which may compress during injection of the masterbatch and which expands after injection was stopped. This air may function as a sort of spring, with a more gradual increase in flow rate and gradual decrease of flow rate adding to the lowered velocity at the startup. At a low inflow velocity, the masterbatch stays more close to the barrel wall with a low velocity, and therefore a higher residence time. The impact of this startup effect is more pronounced with a low (8 mg up to 30 mg) total amount of masterbatch compared to a high amount (60 mg and 121 mg). This might also be why this effect is not visible with PP with grey MB (see Figure 26), those experiments were all performed with a higher amount of MB (60 mg up to 241 mg).

The second deviation is with the 15 mg experiment at RT > 86 s. Here no obvious error could be identified. In general errors become more dominant when the signal (measured light intensity) is lower and therefore be more noticeable with 15 mg CB compared to > 30 mg CB. But no new errors were identified.

Summarizing the relative absorbance is consistent if the total amount of additive is at least 60 mg or more, see also Figure 26B. With less additive the relative absorbance shows some deviation at RT < 86 s. This might be due to startup effects of the masterbatch inflow with the AIT. These effects are less with a higher total duration of the masterbatch injection of 2 s or more. The HDPE experiments with 60 mg and 121 mg CB masterbatch were most reliable and successful and are therefore used to calculate the probability and to verify the simulated RTD.

2.3.1.5.5. Probability

In this study the optical RTD is the probability of a wt.% of the additive to arrive at the die exit after a specific amount of residence time. This can be calculated with the transmitted light intensity, see equation 22. The BIB (background illumination bias) was determined in paragraph 2.3.1.5.3 and will be applied for the probability calculations. Furthermore, the previous paragraph showed that the light measurements are stable (paragraph 2.3.1.5.1) and that the mix experiments are repeatable (paragraph 2.3.1.5.2). Some noise was found at a frequency of 0.2 Hz, therefore the probability calculations were performed with a moving average. Paragraph 2.3.1.5.4 showed that the experiments are consistent with at least 60 mg of additive, therefore the probability is only calculated for experiments with at least 60 mg of additive and is depicted in Figure 28.

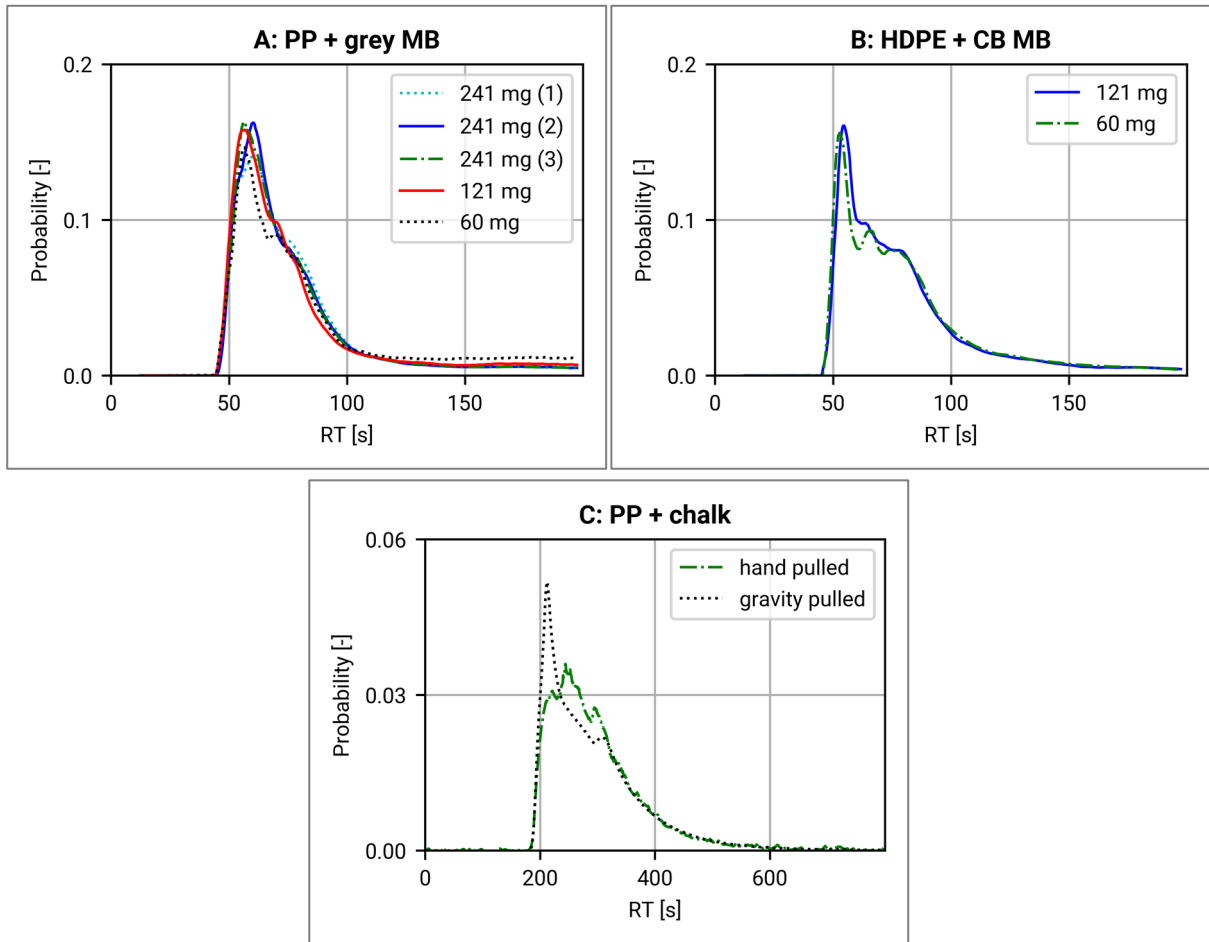


Figure 28. Probability as a function of residence time. A: PP with grey masterbatch. B: HDPE with carbon black masterbatch. C: PP with chalk. Note: both vertical and horizontal axis of graph C are on a different scale compared to the other graphs.

The PP with grey masterbatch and the HDPE with carbon black show a similar RTD. This seems reasonable since both experiments were performed with very similar settings although with a different polymer and additive.

Both these experiments were performed using the Additive Injection Technology (AIT), while the PP with chalk experiment was conducted by adding the additive directly into the hopper. The latter approach resulted in higher residence times and broader RTDs.

The chalk experiments were performed twice, once with manually pulling the extrudate, and once with gravitational pull on the extrudate. The difference in probability is most likely due to the difference in pulling, not a representation of a difference in mix quality since the optical RDT method is both repeatable and consistent. Manual pulling is less steady and results in more noise in the measurements. Consequently, the optical RTD with gravity pulled extrudate was used for a comparison to the burn off RTD.

2.3.1.6. Conclusions and recommendations for optical RTD

The RTD can be determined with the optical method. By applying the Beer-Lambert law the wt.% of the additive distribution (RTD) can be calculated with the measured light intensity.

Stability of the light emitter and light sensor

The light emitter and sensor combination was very stable with only a deviation of 2 lux during a 400 s measurements. And less decay than the resolution (1 lux) of the sensor.

There was some decay of the light emitter after the duration of several experiments. This was most likely due to an increase in temperature. The creep in light transmission was prevented by letting the flashlight cool down in between experiments. For future research it is recommended to use a thermally more stable light source or a setup with better heat dissipation.

Repeatability and stability

Both the experiments with HDPE + CB and PP + grey MB were repeatable, with less than 5 % drift and a standard deviation of less than 2.6 %. The random error was found to be most prominent at 0.2 Hz, this was filtered with a moving average with a period of 5.1 s.

Background illumination bias

The BIB (background illumination bias) was determined at the low light intensity plateau. This background illumination plateau was present in all measurements although some were short and therefore less distinct. Therefore, it is recommended for future research to include measurements with very high additive loadings in order to determine the background noise level.

Consistency

A higher additive loading results in less transmitted light, nonetheless the relative absorbance is independent of the additive loading, thereby confirming the consistency of the optical RTD.

There were some exceptions, specifically the RTD was different with a total amount of additive of 30 mg or less. This is most likely due to start up effects of injecting masterbatch into the barrel. It is recommended to do future experiments with at least 60 mg additive.

A comparison to burn off RTD and simulated RTD

The optical RTD can be verified with a comparison between the optical RTD, with PP + chalk, and the burn off RTD with PP + chalk (section 2.3.3). Furthermore, the optical RTD experiments with HDPE + 60 mg CB and HDPE + 121 mg CB are very suitable for validation of the extrusion simulations.

2.3.2. RTD with burn off experiments

Wt.% of the additive as a function of residence time can be measured with burn off experiments of the chalk experiments. In short, the procedure is:

1. chalk was fed into the hopper at the start of the mixing experiment
2. every 5 s an extrudate sample was collected and the residence time (time after the chalk was fed into the hopper) was logged
3. The polymer of each sample was burned off in an oven, and the left over chalk was weighed

The residence time distribution (RTD) is a description of the probability ($P_{i_burnoff}$) of an additive unit to arrive, at the die exit, after a specific residence time.

$$P_{i_burnoff} = \frac{m_{i_chalk}}{\sum_{j=s}^N m_{j_chalk}} \quad 30$$

Where m_i and m_j the additive mass of respectively sample i and j at a specific residence time interval (RT_i and RT_j), with s the first sample with additive and N the total number of samples.

The advantage of this method is that the wt.% of the additive is measured directly. Therefore, the burn off RTD can be used to verify the optical RTD. A disadvantage of the burn off RTD is that it is time consuming.

The methods (paragraph 2.3.2.1), results (paragraph 2.3.2.2) and conclusions (paragraph 2.3.2.3) are shown in this section.



2.3.2.1. Burn off RTD method and materials

The burn off RTD was determined by collecting a series of extrudate samples with chalk as the additive. Each sample is in a specific range of residence times, for example sample 1: RT is 200 s - 205 s, sample 2: RT is 205 s - 210 s, etc. Each extrudate sample was put in a cup, the mass of the sample with cup was weighed ($m_{cup+pol+chalk}$). The polymer was burned off for 1800 s in an oven (Nabertherm Muffle Furnace) at 625 °C. The cup and the chalk did not burn and were cooled down (at least 3600 s) to room temperature (23.5 °C). The mass of the chalk with cup ($m_{cup+chalk}$), and the cup mass (m_{cup}) were measured, and the chalk wt.% (w) calculated. Before each mass measurement the cups temperature was measured with an infrared thermometer (Ridgid micro IR-100). The cup temperature was always 23.5 ± 0.5 °C during the mass measurements. Each sample has a specific residence time, therefore the burn off RTD could be determined.



Figure 29. Left: oven for burn off experiments. Middle: temperature measurement of the sample cup. Right: measuring the mass of a sample.

The samples were collected from the extrudate of the optical RTD experiment with PP + chalk (manually pulled). The screw rotational velocity was 30 rpm, the barrel and die temperature zones were all set at 220 °C. 1.8 g chalk filled PE was added into the hopper, the hopper was emptied before adding the chalk. Each sample is collected 5 s of extrusion. The optical RTD does not show much chalk before RT 180 s, therefore collecting samples started at RT = 145 s. For the burn off experiments multiple cups were used (a typical mass of the cups is 65 g). The mass measurements were performed with a Sartorius 1702 balance [15].

Method for uncertainty calculation for the burn off RTD and the buoyancy effect

Given the small chalk mass relative to the measuring cup and polymer sample mass, a minor uncertainty in the cup mass measurement can lead to a significant uncertainty in the chalk mass. Therefore, the uncertainty in the chalk wt.% was analyzed.

The chalk wt.% (w) was calculated with equation 31.

$$w = \frac{m_{cup+chalk} - m_{cup}}{m_{cup+pol+chalk} - m_{cup}} - W_{pol_residue} \quad 31$$

Non-flammable components in PP, such as polymerization catalysts, are not included in RTD measurements. Thus, the wt.% of PP residue ($W_{pol_residue}$) has been separately measured and subtracted from the total residue fraction. $W_{pol_residue}$ was determined with PP (without chalk) burn off experiments as described in previous paragraphs.

The cup is about 65 g, the extrudate sample is about 3.6 g, and the chalk is only a fraction of this mass. In other words the majority of each mass measurement is the mass of the cup. Therefore, even a small uncertainty in the mass measurement can translate to a quite large uncertainty in the chalk wt.%. Several parameters contribute to the mass measurement, the most prominent contributors are shown in equation 32. This equation applies to all mass measurements.

$$m = m_{meas} - m_{res} - m_{lin} - m_{cal} - m_{buoy} \quad 32$$

The measured mass (m_{meas}) is the average of several consecutive measurements, the uncertainty is the standard deviation. The uncertainty of the balance indication (m_{res}) is the resolution (0.1 mg). Any object in a gas experiences some buoyancy (m_{buoy}). The buoyancy depends on the gas density and the density of the object. The density changes due to temperature, therefore the buoyancy changes. The uncertainty due to buoyancy was determined by measuring the cup mass at several temperatures from 23 °C to 50 °C. The uncertainty due to calibration (m_{cal}) is canceled out since it is a relative mass measurement within one range of the balance. The balance linearity (m_{lin}) applies to the linearity between measurements. The balance linearity (m_{lin}) is 0.2 mg with a range of 200 g. Assuming that linearity errors are uniformly distributed across the range, the resulting uncertainty is 1 µg/g. For convenience the linearity uncertainty was not calculated for each measurement, instead a maximum value was calculated. The mass measurements are relative measurements, the maximum expected difference between the measurements is the roundup of the expected extrudate mass (9 g). Therefore, the linearity uncertainty is a mere 9 µg. All uncertainty contribution have a normal distribution, except the resolution which has a uniform distribution.

The total uncertainty was calculated with the Monte Carlo method. With this method the chalk wt.% is calculated with random values within the uncertainty distribution of the variables. This calculation is repeated multiple times (10^6). The distribution of the calculated chalk wt.% is the total uncertainty.

The results of this methodology are discussed in paragraph 2.3.2.2.

Probability distribution of the burn off RTD

A residence time distribution is a description of the probability (P_i) of an additive unit to arrive, at the die exit, after a specific residence time, see equation 30.

The additive mass (m_{i_chalk}) can be calculated from the wt.% of the additive (w_{i_chalk}), the mass of the sample with cup measured ($m_{i_cup+pol+chalk}$) and the mass of the chalk with cup ($m_{i_cup+chalk}$) of sample i .

$$m_{i_chalk} = (m_{i_cup+pol+chalk} - m_{i_cup+chalk}) w_{i_chalk} \quad 33$$

The probability ($P_{i_burnoff}$) of an additive unit to arrive at RT_i , according to the burn off experiment, can be calculated by substituting m_{i_chalk} and m_{j_chalk} in equation 30 with equation 33.

$$P_{i_burnoff} = \frac{(m_{i_cup+pol+chalk} - m_{i_cup+chalk}) w_{i_chalk}}{\sum_{j=s}^N (m_{j_cup+pol+chalk} - m_{j_cup+chalk}) w_{j_chalk}} \quad 34$$

Burn off duration

A chalk filled PE was used for the RTD experiments. An experiment was performed to determine the chalk wt.% in the pellets and to verify whether 900 s at 625 °C is sufficient for the burn off experiments. The chalk filled PE was burned off for 720 s, 1440 s and 2160 s, the chalk fraction was determined with the method shown in the above paragraphs.



Experiments summarized

4 experiments were performed:

1. Burn off duration was determined by determining the PE + chalk wt.% as a function of burn off duration.
2. After burn off of the PP (without chalk) some residue is left behind. The wt.% of this residue was determined.
3. Extrusion mix experiment with chalk, extrudate samples collected every 5 s. The polymer was burned off, the chalk mass measured. The chalk mass as a function of residence time was determined.
4. The buoyancy of the cup and sample has an effect on the uncertainty in measured mass. Therefore, the measured mass as a function of temperature was determined.
5. The burn off RTD was calculated.

2.3.2.2. Results of the burn off experiments

The results of the burn off experiments are shown in this section.

Burn off duration

Chalk filled PE pellets were weighed as a function of burn off duration, see Figure 30.

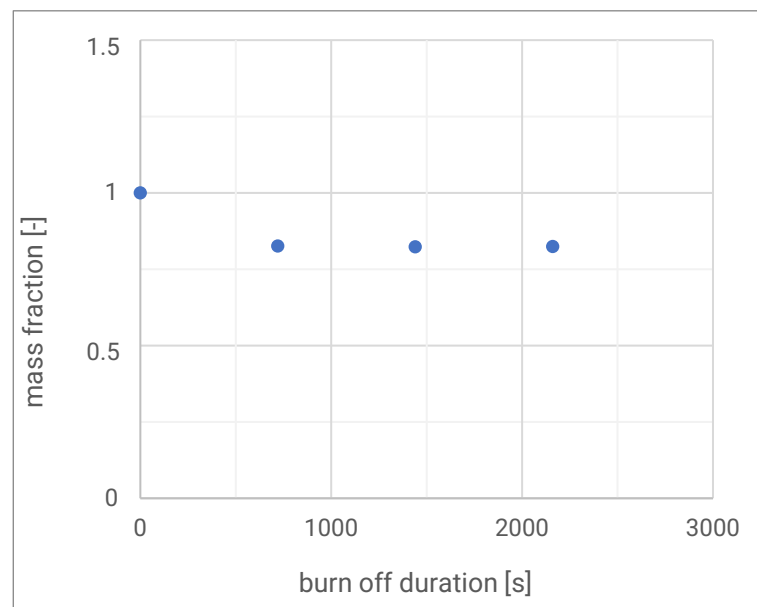


Figure 30. Chalk filled PE pellets mass fraction as a function of burn off time.

The mass fraction reduces to 82 % at 720 s, and is constant at a longer burn off duration. All the volatile and combustible components (such as PE) were burned off before 720 s burn off time. Therefore the 900 s burn off at 625 °C is a suitable burn off time and temperature for the burn off experiments.

Polymer residue after burn off

7 samples of 3.6 g PP, without chalk, were burned off as well. On average 8.3 mg residue (0.23 % of the sample) was left after the burn off, the standard deviation was 2.8 mg. The standard deviation was dominated by one measurement with only 2.0 mg residue. Without this measurement the average residue was 9.4 mg with a standard deviation of 0.6 mg. The residue wt.% of the 7 PP samples ($W_{pol_residue}$) is 0.23 ± 0.08 %.

Buoyancy effect and uncertainty in the burn off RDT

The mass of a burn off cup was measured at several temperatures to determine the extent of the buoyancy effect, see Figure 31.

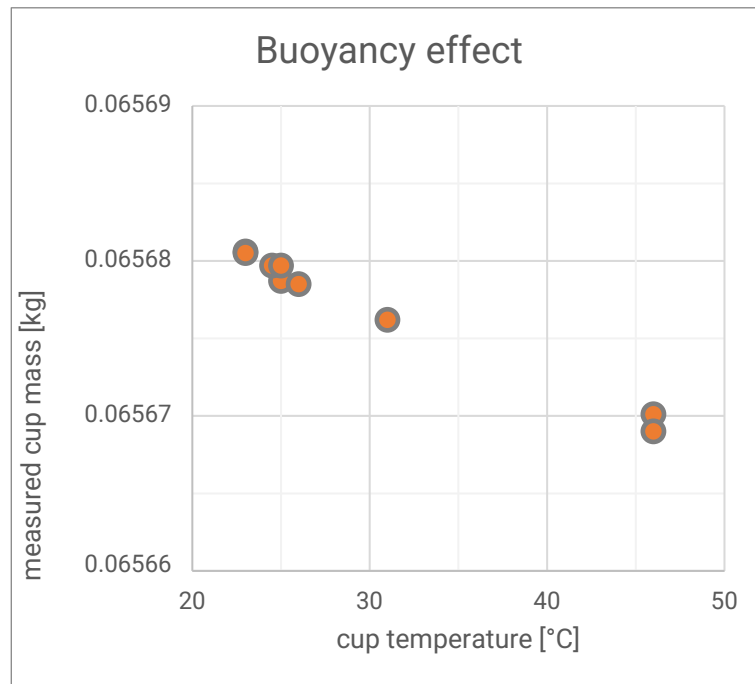


Figure 31. Buoyancy effect, the measured cup mass as function of cup temperature.

The measured mass reduces with 0.47 mg/K ($5 \cdot 10^{-7}$ kg/K). That is an uncertainty contribution of 0.23 mg due to the buoyancy effect for each mass measurement at 23.5 ± 0.5 °C. The standard deviation for a typical cup mass measurement was 0.08 mg. Figure 32 show all the uncertainty contributions for a single mass measurement (32).

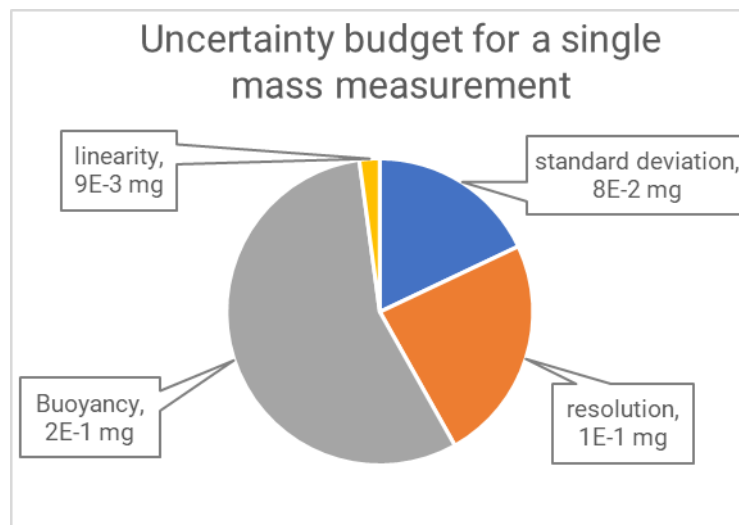


Figure 32. The uncertainty budget for a single mass measurement.

Buoyancy is the largest uncertainty contributor for the mass measurements. For future work the uncertainty, in the mass measurements, can be reduced by reducing the temperature uncertainty and reducing the cup mass.

To account for the presence of non-flammable components in the PP, corrections were applied to the measured burn-off mass of the extrudate samples. Subsequently, the uncertainty in wt.% stands at 0.08%. This uncertainty is largely driven by the variation in the PP residue wt.% (without chalk), which itself is predominantly influenced by a single outlier measurement amounting to 2.8 mg. Elimination of this outlier yields a significantly lower wt.% uncertainty of 0.002%. Variations may exist in the non-flammable wt.% within the PP. Such differences tend to normalize during the extrusion process due to distributive mixing, as evidenced by the absence of a high standard deviation in extruded samples.

For instance, the first four extrudate samples (with RT < 160 s) are unlikely to contain any chalk, yet the standard deviation across these samples is only 0.01%. In future research, it is advisable to replicate these non-flammable wt.% tests not with PP pellets, but with extruded PP.

Chalk as a function of residence time

The burn off residue mass (without correction for the non-flammable parts in the PP) and the burn off RTD are shown in Figure 33.

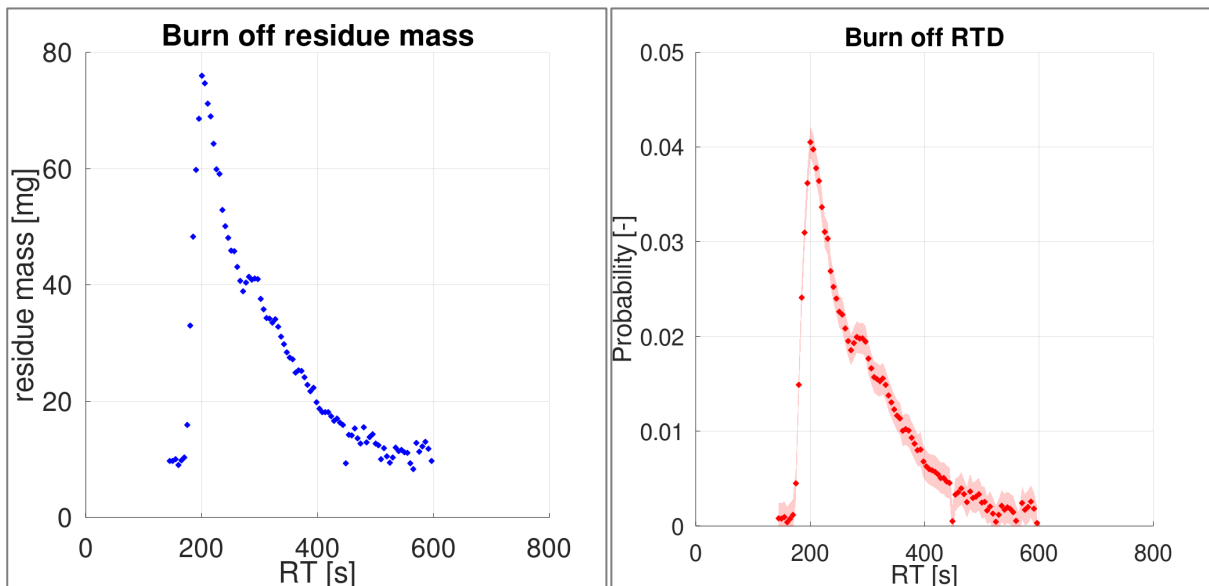


Figure 33. Left: burn off residue mass, this is both chalk and other non-flammable residue from the PP. Right: Burn off RTD, the light red band shows the uncertainty.

The RTD shows several regions, there is no chalk mass before RT = 160 s. The chalk wt.% increases from RT = 175 s to 200 s. The highest measured chalk mass is at RT = 200 s with 66 mg, that is 1.8 wt.% of the extrudate sample. In the next region the wt.% decreases from RT > 200 s. The chalk wt.% is almost gone after RT = 570 s. Most of the curve is quite smooth, for example the standard deviation is only 0.01 % from RT = 145 s up to RT = 160 s.

2.3.2.3. Conclusion burn off RTD

The burn off experiments show clearly a distribution in residence time. Up to RT = 160 s, no chalk was found. The wt.% of chalk increases rapidly between RT = 175 s and 200 s, reaching a maximum of 1.83 ± 0.08 wt.%. The chalk wt.% decreases after RT = 200 s, at RT = 600 s the chalk wt.% is almost back to zero.

There are non-flammable components in the PP. The measured burn-off mass of the extrudate samples underwent corrections to account for these non-flammable components in the PP. There is a large random error in the measured residue wt.% of the PP. This PP residue was determined with burn off experiment of PP pellets, there might be large differences in the non-flammable wt.% between PP pellets. Such differences will smooth out in the extruder due to distributive mixing. For future work it is recommended to determine the residue wt.% of the PP after it is extruded.

The burn off method proves effective in determining the RTD. And the burn off RTD can be used to verify the optical RTD. The chalk mass per sample is quite small (< 80 mg), while a relatively heavy cup (~65 g) is needed for the burn off experiment. Therefore, the measurements are highly sensitive for temperature influences, which was actively monitored with an infrared thermometer. However, the experiments are labor-intensive and time-consuming. A total of 50 working hours were allocated solely for the burn-off experiments, excluding preparations, extrusion experiments, and data processing.

2.3.3. Comparison between burn off RTD and optical RTD

The RTD was determined both with an optical method (section 2.3.1) and a burn off method (section 2.3.2) for the chalk experiments. With the burn off measurements the wt.% of the additive is measured directly, which makes it a reliable method, while with optical RTD the wt.% is determined indirectly with light attenuation. Therefore, the optical RTD method was verified by comparing it to the burn off RTD using their respective probability distribution functions.

To ensure a fair comparison, the measurement range of the optical RTD is shortened to the same length as the burn off RTD. Consequently, $s=142.5$ s and $N = 602.5$ s.

With the optical RTD method the background illumination bias (BIB) was determined using the assumption that the highest wt.% is at a peak and not at a plateau, paragraph 2.3.1.1.4. This 'peak' feature of the RTD can easily be verified with the burn off RTD.

2.3.3.1. Results

The probability distributions of the optical RTD of PP + chalk and the burn off RTD are shown in Figure 34.

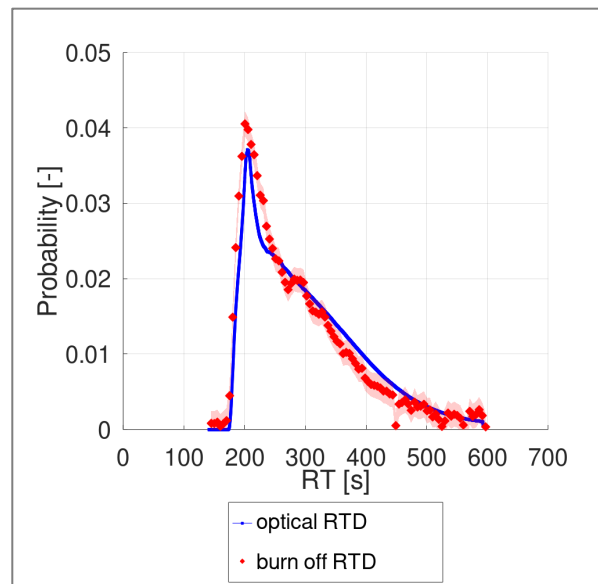


Figure 34. Optical RTD compared to burn off RTD.

The optical RTD and burn off RTD are virtually identical, which validates the optical RTD method.

The burn off RTD shows a clear peak at 200 s, thereby verifying the assumption that there is no high wt.% of the additive plateau. This also validating the technique to identify the BIB with the optical RTD, see also paragraph 2.3.1.1.4.

2.3.3.2. conclusion

The optical RTD and the burn off RTD are very much in agreement with each other. Furthermore, the optical RTD method presumes a RTD peak, which is clearly present in the burn off RTD. This validates the optical RTD method. Both methods are suitable to determine the RTD. But the optical method is fairly quick, suitable for flammable additives (such as carbon black) and only a small amount of additives are needed and is therefore the preferred method.

2.3.4. Conclusion and recommendations for the RTD experiments

Mix experiments were performed with a screw with a pin mixer. An optical and a burn off method were developed to determine the RTD.

Light attenuation as a function of time was measured with the optical method. Absorbance was calculated from light attenuation by applying the Beer-Lambert law. The absorbance is linear to the wt.%, therefore absorbance as a function of residence (optical RTD) is linear to the wt.% as a function of residence time. The optical RTD measurement method is stable, repeatable and consistent.

The optical RTD was verified with the burn off RTD. For this verification an extrusion experiment with PP and chalk was performed. The optical RTD was measured during extrusion, while the extrudate was collected for the burn off RTD. The extrudate was divided into samples, each sample with a specific residence time. The PP was burned in an oven at 625 °C, leaving chalk residue. The chalk mass as a function of residence time (in the extruder) was determined. The burn off RTD and the optical RTD are very much in agreement with each other, which validates the optical RTD method.

The optical RTD method holds several advantages over the burn off method, which is limited to non-flammable additives. The optical approach is not only quicker but also requires a smaller amount of colorant, and is suitable for both flammable and non-flammable additives. For these reasons, the optical RTD method is recommended for future RTD measurements.

The optical RTD (HDPE with carbon black) will be used for verification of the simulations.

2.4. Shannon entropy of the extrudate cross section

The extruder's mixing process distributes additives through the molten plastic in 3 directions of the 3 dimensional extrudate. While the mixing in the extrusion direction can be quantified with the RTD, see paragraph 2.3, the remaining 2 directions are in the cross section of the extrudate, which is called 'cross section mix quality' in this report.

This section consists of 2 parts. First, paragraph 2.4.1 provides a briefly overview of the experimental setup and a visual evaluation of these images. Next, paragraph 2.4.2 presents a method for quantifying the cross section mix quality and this method is applied to the microscope images.

2.4.1. Visual evaluation of mix quality in the cross section via microscopic images

After conducting extrusion mix experiments, microscopic images of the extrudate at specific residence times (RT) were captured. The method is shown in paragraph 2.4.1.1. Paragraph 2.4.1.2 shows a visual evaluation of the microscopic images.

2.4.1.1. Materials and methods for microscopic images of the extrudate cross section

The experiments were performed with a screw rotation speed of 30 rpm and a barrel temperature of 185 °C. A carbon black masterbatch was added in a 2 s shot of 159 ml. The extrusion flow rate (Q [kg/s]) was determined by collecting extrudate during 120 s and measuring the extrudate mass. This experiment has the same settings as the mix experiment with HDPE and carbon black for the RTD measurements (see paragraph 2.3).

Collecting extrudate samples at specific residence times

The masterbatch was added with the AIT positioned between the screw and pin mixer, see paragraph 2.2. The extrudate was cut, at the extruder die, at the time of injecting the masterbatch. A large extrudate sample was collected from $RT = 0$ s, when the masterbatch was injected, up to $RT = 110$ s. One side of this sample is defined as ERT (Early Residence Time) with $RT = 0$ s, the other side as LRT (Late Residence Time).



The following steps were repeated several times to collect samples for microscopy:

1. The sample was weighed (m_i) and the residence time at LRT was determined with $RT_i = m_i/Q$.
2. At the LRT a 0.5 mm thick sample was cut with a microtome for microscopy at RT_i .
3. The large sample was cut at the LRT side in order to shorten it with ~ 10 s.

The steps of cutting, weighing and cutting were repeated until a series of samples were collected with specific residence times, see Figure 35. Note that the samples were collected from a high residence time to a low residence time, but the results are presented in a sequence of increasing residence time.

Microscopy

The samples were examined with a microscope (Optem) , see Figure 35. The microscope uses backlight, so the light shines through the sample into the lens. All images were taken at the same backlight intensity and camera settings. With this procedure several microscopic images were collected at specific residence times.

2.4.1.2. Visual evaluation of the extrudate cross section

An extrudate sample was collected, cut and visually inspected with the microscope, see Figure 35.

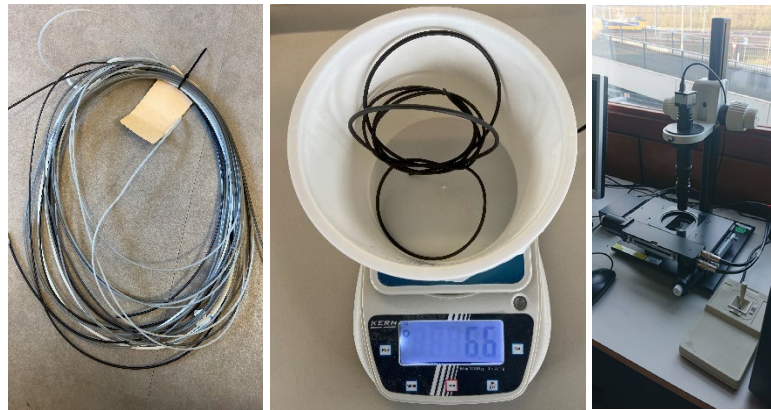


Figure 35. Left: the extrudate sample of the whole experiment. Middle: sample is weighed. Right: microscope imaging.

The carbon black can easily be distinguished from the white HDPE. The example, shown in Figure 36, shows circular streaks of carbon black, a somewhat higher concentration of carbon black in the middle and a thick carbon black circle near the outside of the extrudate sample.

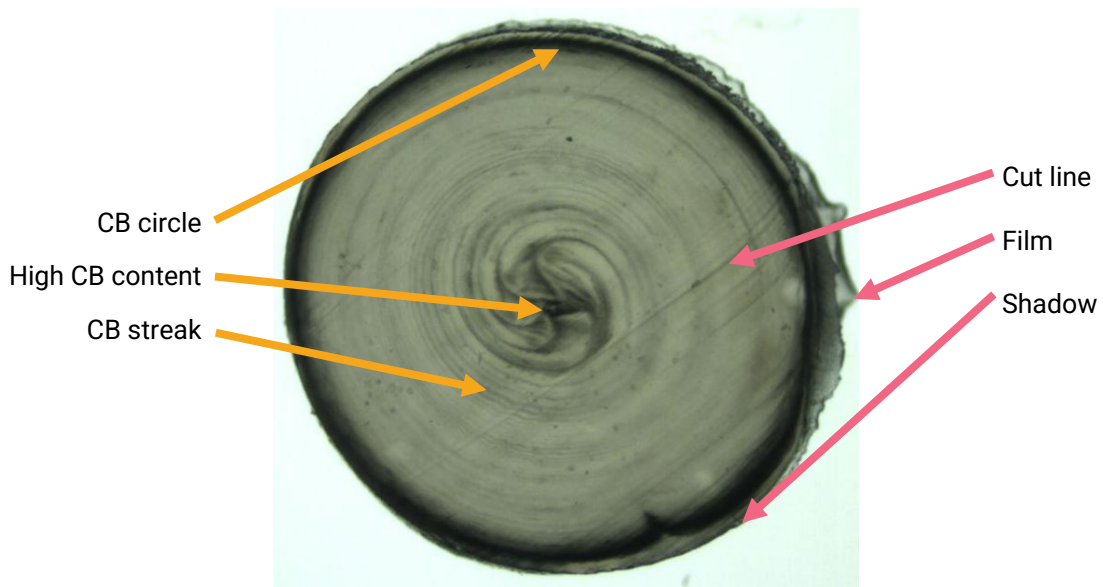


Figure 36. An example of a microscopic image of the extrudate cross section. Several depositions of CB (carbon black) are indicated with orange arrows. Some artifacts of extrudate cutting and imaging are indicated with red arrows.

The extrudate samples also show some artifacts of the cutting process, specifically a cutting line and a film at the outside. Furthermore, there is shadow around the images and some of the samples are not perfectly round. These are minor inconveniences for a visual evaluation but are somewhat of an annoyance when quantifying mix quality, see paragraph 2.4.2. The microscopic image does show the carbon black depositions, but the local carbon black density is difficult to estimate. Grey likely represents less carbon black compared to black. Furthermore, it seems likely that there is a threshold carbon black density above which the image pixels are black even if the density is much higher than the threshold. This is similar to the plateau found in the optical RTD, see paragraph 2.3.1.

Extrudate cross sections at varying residence times

An extrudate sample was collected during 120 s, the sample was weighed, the calculated mass flow rate was 0.81 g/s. The residence time was determined using the mass of each sample and the mass flow rate. The microscopic image and the corresponding residence time are shown in Figure 37.

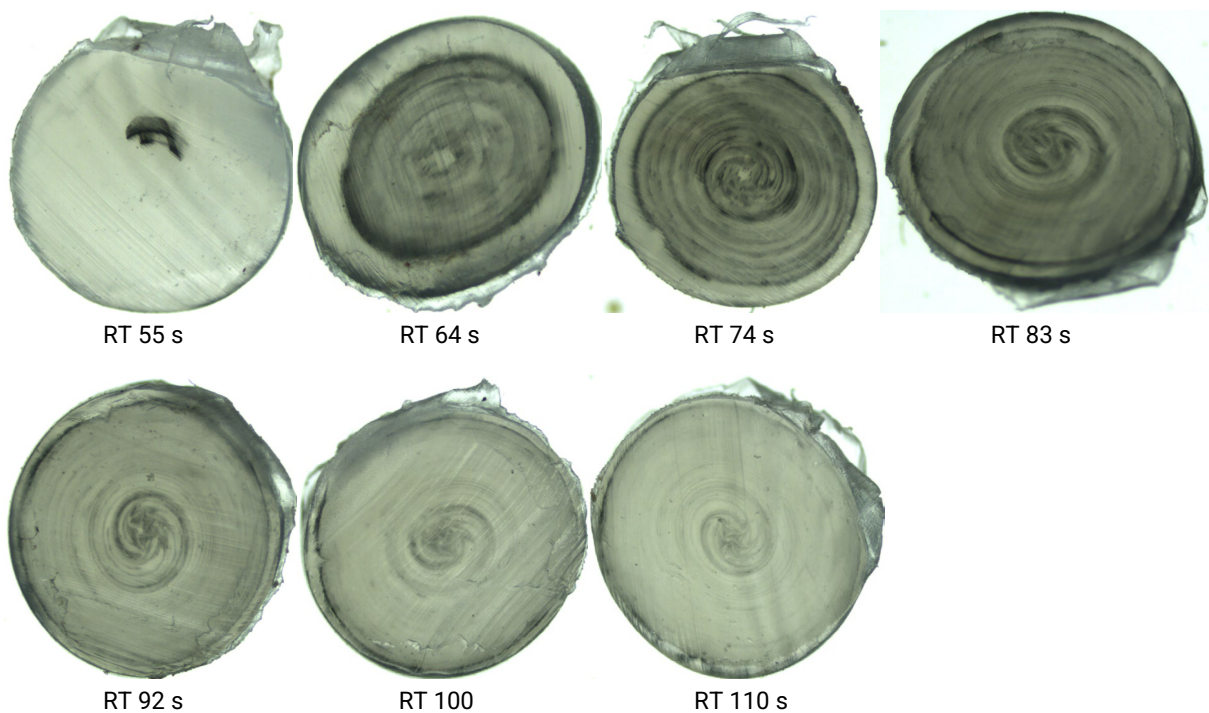


Figure 37. Microscopic images at several residence times (RT) of the carbon black masterbatch.

A small amount of carbon black first appears in the middle of the extrudate (RT = 55 s). With increasing residence time the carbon black deposition covers a larger area. The outer border of this carbon black deposition area is marked with a dark circle of carbon black. This distribution seems reasonable; high velocity in the center, leading to a low residence time and first appearance of the carbon black. The carbon black gradually reduces and has mostly disappeared at RT = 110 s. A decrease of carbon black content is in agreement with the optical RTD, see paragraph 2.3.1.

It seems that the carbon black is mostly in the middle at a low residence time (RT = 55 s) and mostly at the outside at a high residence time (RT = 110 s) and distributed relatively homogeneously somewhere in the middle (RT = 83 s). Therefore the mix quality present in the cross section is low with a low or high residence time, while the mix quality is high at RT = 83 s.

2.4.1.3. Conclusion microscopy

Cross sectional mixing is very well visible with microscopic images of the extrudate. The cross section mix quality is low with a low or a high residence time, while the mix quality is high somewhere in between (RT = 83 s). These images are suitable for a comparison to mix simulations (see section 3).

2.4.2. Quantification of the mixing quality with the microscopic images

The mix quality in the cross section can be quantified with the Shannon entropy. How Shannon entropy was applied in other studies and in extrusion simulations is discussed in part 2: **Mixing Quantification** [5].

The method for processing microscopic images and quantifying mix quality is shown in paragraph 2.4.2.1, the results are presented in paragraph 2.4.2.2.

2.4.2.1. Method to quantify cross section mix quality

The distribution of carbon black, in the extrudate cross section, is presented as a distribution of black pixels in the microscopy images, see 2.4.1. The level of homogeneity of the distribution of these black pixels can be quantified with the Shannon entropy.

Relative Shannon entropy (S) is calculated with the probability (p_i) that a black pixel (carbon black) is in bin i , of M bins in total, and will be referred to from here on as the Shannon entropy.

$$S = \frac{-\sum_{i=1}^M p_i \ln p_i}{\ln M} \quad 35$$

p_i is equal to the number of black pixels (c_i) in bin i divided by the total number of black pixels (N). Figure 38 shows several hypothetical examples of extrudate cross section with varying mix quality. The figure also shows a bin division and the calculated Shannon entropy.

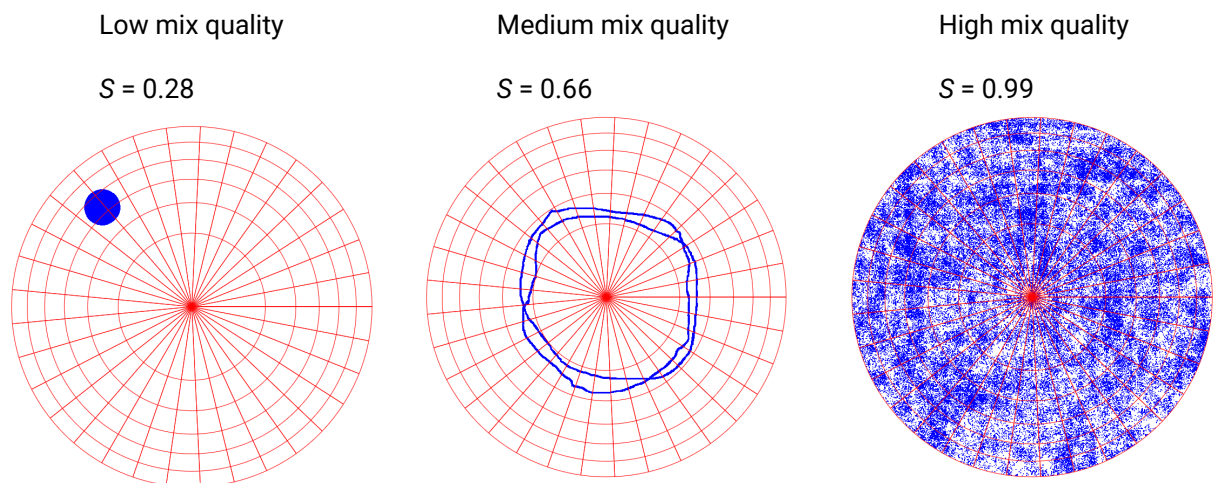


Figure 38. Hypothetical examples of mix quality. The additive is shown in blue, the polymer in white, and the borders of the bins are shown in red. Left: low mix quality. Middle: medium mix quality. Right: high mix quality.

The mixing quality is low with an inhomogeneous probability distribution, see particle distribution at the left in Figure 38. The mixing quality is high with a homogeneous probability distribution, see particle distribution at the right in Figure 38. The Shannon entropy is a measure of probability distribution, therefore the Shannon entropy can be applied as a measure of mixing quality.

A low Shannon entropy corresponds to a low mixing quality. The maximum Shannon entropy and maximum mixing quality is reached when $S = 1$. The Relative Shannon entropy is in the range $0 < S \leq 1$, which makes it possible to estimate the mixing quality with Shannon entropy.

Image processing and Shannon entropy calculations with GNU Octave

All Shannon entropy calculations were performed with GNU Octave. GNU Octave is a programming language for scientific computing. Scripts were made for image processing and Shannon entropy calculations. The mix quality calculation procedure consists of the following steps:

1. Make microscopic images. This step is shown in paragraph 2.4.1.
2. Mark the extrudate border in the images (MS Paint)
3. Sharpen the image (GNU Octave scripts)
4. Convert RGB microscopic image to a monochromatic image (GNU Octave scripts)
5. Create a bin distribution within the extrudate border (GNU Octave scripts)
6. Calculate the number of black pixels in each bin (GNU Octave scripts)
7. Calculate the Shannon entropy (GNU Octave scripts)

Several procedure steps are briefly discussed in this paragraph.

Marking the extrudate border (step 2)

The extrudate does not cover the whole microscopic image therefore the GNU Octave script needs to be told which parts have to be included in the Shannon entropy calculations. A red circle was used to mark (in MS Paint) the round border of the extrudate sample (step 2), see Figure 39.

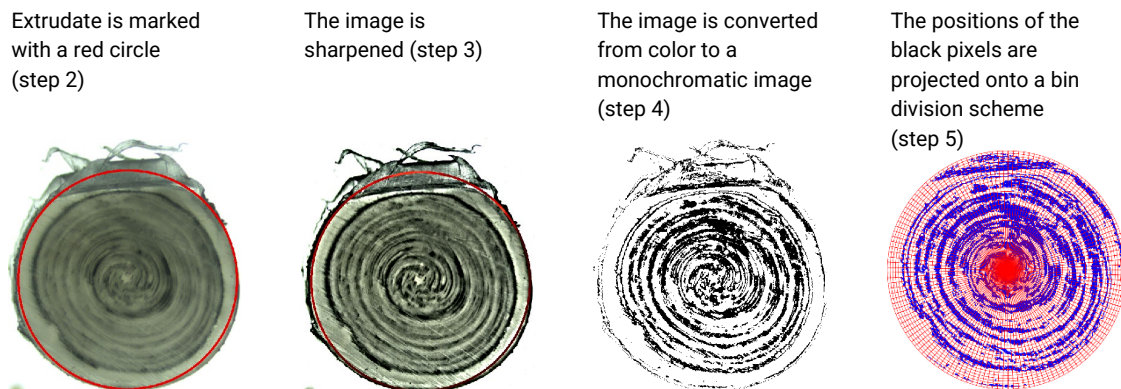


Figure 39. Several steps with a microscopic image (RT = 74 s) to calculate the Shannon entropy in GNU Octave.

A dark shadow is visible around the extrudate image. The GNU Octave scripts cannot differentiate between the shadow pixels and the carbon black pixels. Therefore, the red circle is positioned in such a way that minimal amount of shadow is inside the circle (and included in the Shannon entropy calculations), while (almost) all of the extrudate is inside the circle.

Image sharpening (step 3)

The extrudate images clearly show carbon black streaks and carbon black depositions. These are visually noticeable since there is a clear color transition from a carbon black streak to natural HDPE. The images show a low darkness contrast between carbon black and HDPE.

A sharpening tool was used to amplify the color transitions in the image. This is step 3. The unsharp masking (USM) is an image sharpening technique, which was applied to the images [16]. With this technique a Gaussian blur is applied to a copy of the image. Then the original image and the blurred copy are compared, and the pixels that differ between the images are subtracted from the image. The USM technique sharpens the color transitions. Parameters are available for both the Gaussian blur and the subtraction threshold. The parameters were determined with visual evaluation, they were equal for each image.

Image conversion to monochromatic (step 4)

The GNU Octave calculates Shannon entropy with the distribution of black pixels, while the microscopic image is in color. Therefore, the image was converted to a monochromatic image.

A threshold is set for each pixel, the pixel is converted to black if the pixel is darker (all RGB colors) than a certain threshold, and white if the pixel is above the threshold. This is step 4. The threshold was determined by visual evaluation whether the black pixel distribution was a good representation of the carbon black distribution. This threshold was set once, and kept constant for all pixels and for all images.

Dividing the image into bins (step 5)

The area within the red circle is divided up into several bins (step 5).

All steps in GNU Octave were applied with the same parameters for each image of the extrusion experiment, including the sharpening and the conversion to a monochromatic image.

Number of bins for Shannon entropy calculations

The extrudate is circular, hence a circular bin division scheme was adopted, as shown in Figure 38 and Figure 39. Given that mixing in the extrudate cross-section occurs in two dimensions, both angular and radial mixing are expected to contribute equally to the Shannon entropy calculations. A comprehensive discussion on the impact of bin shape and size is provided in part 2: *Mixing quantification* [5]. Accordingly, bins were designed to have roughly equal length and width, although they are not square in shape. All bins share the same surface area, leading to variations in their shapes; some bins appear elongated compared to others.

The bin size defines the scale of observation [17]. Mixing quality at a macroscopic level can be determined with a low number of bins. Mixing quality on a microscopic level needs to be determined with a high number of bins.

The bins should not be too small, the microscopic image has $1280 \cdot 1024 = 1310720$ pixels. The image area covered by a pixel might be on the border of 2 bins, and therefore partly occupies both bins. The Shannon entropy is however not calculated with the area covered by a pixel, but by a point position. Therefore, a single pixel never occupies more than 1 bin. The error in Shannon entropy is relatively small with large bins compared to the area covered by one pixel. But this systematic error increases with a decrease of bin size. Shannon entropy calculations of a hypothetical distribution of black pixels is shown in Figure 40.

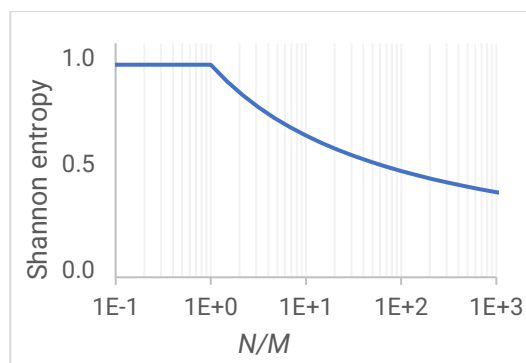


Figure 40. Shannon entropy calculations of a hypothetical distribution of black pixels. Note the horizontal axis is on a logarithmic scale.

In this example the black pixels are homogeneously distributed across the image, in other words a very high mix quality. The example Shannon entropy also shows a high mix quality with $S = 1$ as long as the number of black pixels is more than the number of bins ($N > M$). But the Shannon entropy decreases with more bins than black pixels ($N < M$), the low Shannon entropy incorrectly indicates a low mix quality. This might be the case with very few black pixels in a large image (small amount of carbon black), or if the bins are relatively small compared to the pixel size. Notice that this error in Shannon entropy only becomes large with $N \ll M$ in the example shown in Figure 40.

The extrusion die has a 2 mm radius, so a bin width of 0.09 mm is comparatively small, resulting in 3243 bins. The specific bin size is not highly critical for this study. However, for better accuracy, it is essential that minor variations in bin size do not substantially impact the Shannon entropy value. To confirm this, the Shannon entropy was evaluated as a function of bins size to ensure it is independent of bin size near 3234 bins.

2.4.2.2. Results extrudate cross mix quality as function of residence time

Extrusion mix experiments were performed with a carbon black masterbatch. Microscopic images were made of the extrudate cross section at specific residence times. A method was developed for quantifying the mix quality in the extrudate cross section. This paragraph shows the Shannon entropy of the microscopic images.

Evaluation of image processing

The microscopic images were processed with GNU Octave scripts, as illustrated in Figure 39. The process involves several steps: marking the extrudate with a red circle, which is challenging due to its irregular shape; sharpening the image; and then converting it to a monochrome version. This monochrome version effectively highlights carbon black depositions and allows for accurate bin projection (step 5 of the process). However, this conversion does incur some loss of information. Specifically, nuances like the density of carbon black, which may be indicated by pixel darkness, are lost. Additionally, unwanted artifacts like the cutting line and film residues are still visible and can erroneously contribute to Shannon entropy calculations. See Figure 36 and paragraph 2.4.1.2 concerning these cutting artifacts. In summary, while effective, the image processing method has limitations affecting Shannon entropy calculations.

Evaluation of the number of Shannon entropy bins

It is preferred that the Shannon entropy is relatively insensitive with respect to the number of bins. Therefore, the Shannon entropy as function of number of bins was calculated for each image, see Figure 41. This figure is not meant for evaluating the Shannon entropy itself, only the sensitivity of the Shannon entropy to the number of bins.

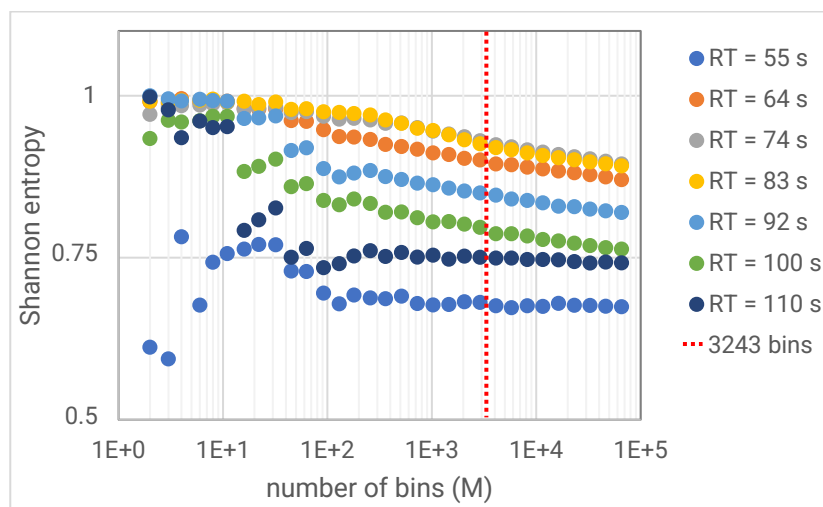


Figure 41. Shannon entropy as function of number of bins (M). Note this figure is not meant for evaluating the Shannon entropy itself, only the sensitivity of the Shannon entropy to the number of bins. Note the horizontal axis is on a logarithmic scale.

There is some scatter of the Shannon entropy for $M < 10^2$, while the Shannon entropy is relatively insensitive at a higher number of bins. Therefore, a typical bin width of 0.09 mm (3243 bins) seems fine for the Shannon entropy calculations.

The images with a higher Shannon entropy (such as RT = 83 s) show a small and gradual decrease with increase of number of bins. This might be a systematic error as was discussed in paragraph 2.4.2.1.

Results of the Shannon entropy as function of residence time

The Shannon entropy as function of residence time was calculated using 3243 bins and is shown in Figure 42.

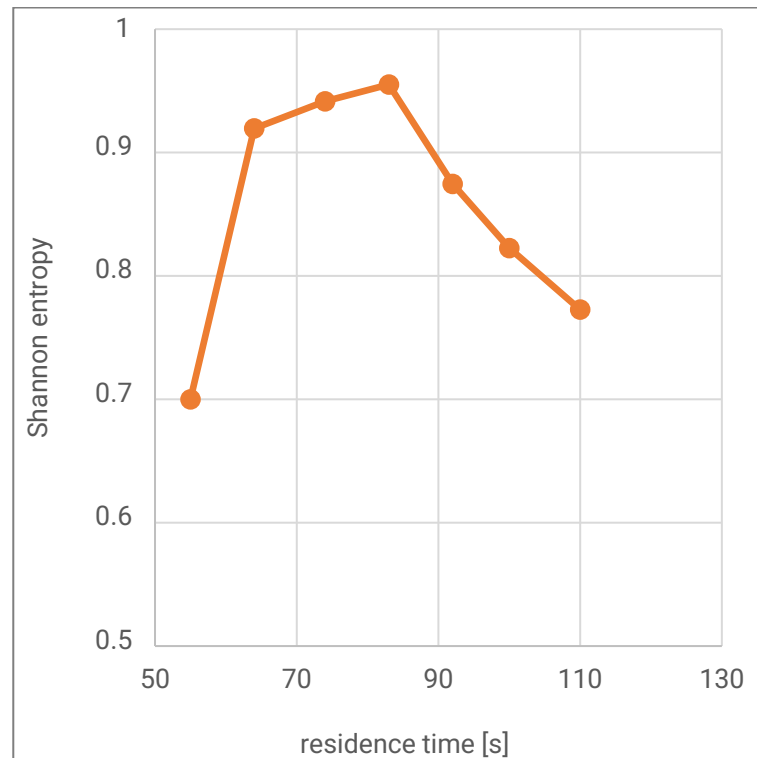


Figure 42. Shannon entropy as function of residence time with 3243 bins.

A higher Shannon entropy stands for a better distributive mix quality. The Shannon entropy start with a relatively low value of 0.7 at RT = 55 s. The Shannon entropy rapidly increases to $S > 0.9$ for a residence time of 64 s up to 83 s. The Shannon entropy gradually decreases at RT = 83 s and higher. This means that the mix quality is highest at a residence time from 64 s up to 83 s. While the mix quality is worse at a very short residence time (55 s) or long residence time (~110 s).

2.4.2.3. Conclusion quantifying cross section mix quality

A method to quantify mix quality of the extrudate cross section was developed. Microscopic images of the extrudate were used for this method. Some image processing was performed in GNU Octave and Shannon entropy calculations were performed to quantify mix quality. Shannon entropy as function of residence time was calculated. There is a clear distinction in mix quality at different residence times. The mix quality is low at a high residence time (~110 s) and at a low residence time (55 s), while the quality is high somewhere in between (64 s to 83 s).

The extrudate cross section is not perfectly round, while the Shannon entropy bin distribution scheme is circular. For future studies it is recommended to increase the roundness of the extrudate with a more steady extrudate pulling speed during extrusion, instead of pulling by hand. Another option might be in changing the bin distribution scheme. The GNU Octave scripts may be modified to work with non-circular samples.

2.4.3. Conclusion and recommendation

Experiments on extrusion mixing were conducted by injecting 1.6 ml carbon black masterbatch in the barrel between the screw and the pin mixer, focusing exclusively on the pin mixer's mixing quality.

Microscopic images of the extrudate cross section at various residence times revealed distinctive carbon black deposits: centered at lower residence times and more towards the outside at higher times. Both visual evaluation and Shannon entropy calculations show a low mix quality at shorter (55 s) and longer (110 s) residence times, with higher mix quality around $RT = 83$ s. However, artifacts from sample cutting and the deviation from a perfect circular shape of the extrudate samples suggest a need for refinement in the sample collection and preparation process.

This method is suitable as a tool for a quantitative comparison of mix quality and is recommended when comparing different mixers and for validating the simulated mix quality. Although the optical RTD might be preferable when comparing many mix experiments since the optical RTD is less time consuming.



3. Extrusion simulations and comparisons to experiments

The overall goal of this study is to develop tools to model the mixing quality inside a single screw extruder. These tools can be applied to optimize the extrusion mix process, specifically the geometry of the screw mix zone.

The lab extruder was simulated with the same settings and parameters as with the experiments as are shown in section 2. The simulated mix quality in the extrusion direction was determined with the residence time distribution (RTD), the simulated mix quality in the cross section was determined with the Shannon entropy.

CFD simulation procedures for extrusion were developed, see part 1: *Simulation method*. [18]. The experiments and simulations, reported in this document, were performed with a laboratory extruder (30 mm barrel diameter) instead of the pilot extruder (75 mm barrel diameter) shown in part 1 and part 2 [5, 18]. A new mesh study was performed to find a proper mesh size for this extruder screw with pin mixer. The mesh study is available in Appendix 1. A brief simulation setup will be shown in paragraph 3.1.

Procedures to determine the mix quality (RTD and Shannon entropy) using simulations were developed, see part 2: *Mixing quantification* [5]. Some modifications were needed to conform the simulated mix quality to the experimental setup (section 2), most notably a Shannon entropy calculation as function of particle residence time. The modified method will be explained in paragraph 3.2.

A comparison between the simulated RTD and the optical RTD is shown paragraph 3.3. A comparison between the simulated Shannon entropy and the experimentally found Shannon entropy will be presented in paragraph 3.4.

3.1. Extrusion simulation setup

The simulations use the extruder and screw geometries illustrated in Figure 43, these geometries match those used in the experiments, see Figure 2 and Figure 3.



Figure 43. Extruder, in blue a cross section of the fluid domain, in gray the immersed solid (the screw). The red arrow points to the location of the AIT inflow position. The red line depicts a tracer particle path.



The optimal simulation settings, derived from a mesh study, are summarized in Table 2 and further details can be found in Appendix 1.

Table 2. Summary of extrusion simulation parameters.

Parameter	Value
Barrel diameter.	30 mm
Die diameter.	4 mm
AIT inflow diameter as depicted in Figure 44.	1 mm
The typical mesh element size is informed by the mesh study in Appendix 1.	0.31 mm
Element size used for the extrusion die.	0.15 mm
Element size used for the AIT inflow and the surrounding area as depicted in Figure 44.	0.05 mm
Mass flow rate set at the AIT inflow opening, identical to the extrusion experiments.	30 mg/s
The screw rotational velocity matches that of the extrusion experiments.	30 RPM
The fluid model used is detailed in equation 36.	Bird-Carreau
Power law index (n) within the Bird-Carreau model.	0.24
Relaxation time (λ) specified in the Bird-Carreau model.	100 s
Zero shear viscosity (η_0) for the Bird-Carreau model.	1.4 MPa·s
Infinite shear viscosity (η_∞) as defined in the Bird-Carreau model.	10 Pa·s

In the simulations a circular inflow opening was included to simulate the masterbatch inflow from the AIT. This AIT inflow was used for the inflow of tracer particles, thus a good description of the velocity field is relevant. Therefore, the AIT inflow is surrounded by a cylindrical volume, of 4 mm in diameter and 2.5 mm deep, with a very small typical element size, see Figure 44.

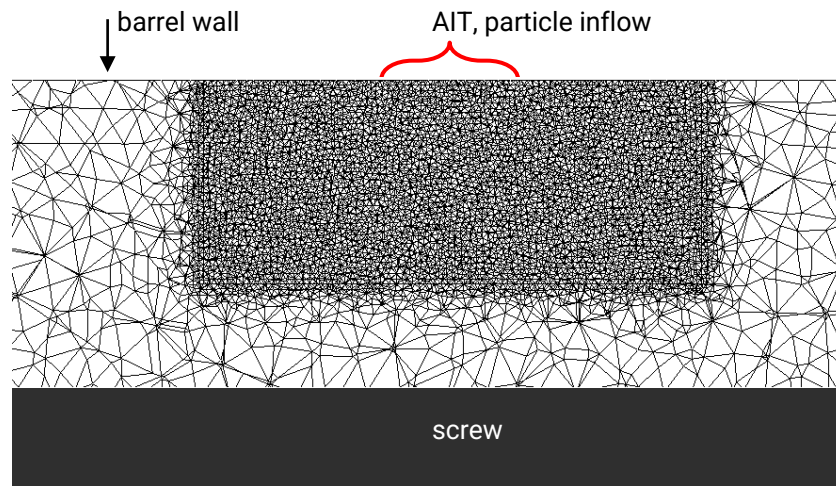


Figure 44. Local mesh cross section near the AIT particle inflow. Notice a very fine mesh, 0.05 mm element size, surrounding the AIT inflow and less, 0.31 mm element size, fine mesh in the rest of the fluid domain.

In these simulations, the focus was on fluid flow, therefore, the melting of HDPE pellets wasn't incorporated. Consequently, the feed zone was omitted from the simulations. The fluid flow was modelled with the Bird-Carreau model, see equation 36.

$$\eta(\dot{\gamma}) = \eta_{\infty} + (\eta_0 - \eta_{\infty}) \left(1 + (\lambda \dot{\gamma})^2 \right)^{\frac{n-1}{2}} \quad 36$$

The screw rotational velocity was 30 RPM, identical to the extrusion experiments. A 0 Pa pressure condition was set at the inflow and at the die exit.

3.2. Methods for quantifying mix quality in extrusion simulations

The goal of this study is to model mix quality with CFD. The flow paths of small units of fluid or additive units describes distributive mixing. The flow paths can be revealed through the use of tracer particles, see Figure 45 for an example. The flow paths are very different from each other with good distributive mixing. Therefore, these flow paths have to be studied in order to determine distributive mixing quality.

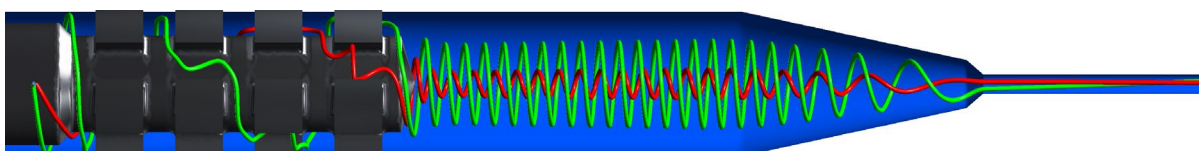


Figure 45. Example of 2 tracer particles in the extrusion simulation. Not the whole extruder is shown, only the pin mixer and the extrusion die. The particles start at the same position as where the AIT was mounted, i.e. the same position as where the additive flows into the extruder in the experiments. Note: the particle paths seem to be spiraling, this is due to the rotating frame of reference, i.e. the observer rotates around the extruder.

Previously, in part 2: *Mixing Quantification* [5], the procedures for determining mixing quality with RTD and Shannon entropy in the simulation have been presented. In that section, Shannon entropy was determined once, using 100 k particles. This quantity was sufficient as particle residence time was not a consideration. However, a deviation from this method arises in experiments detailed in section 2.4.2, where mix quality was measured using Shannon entropy as a function of residence time. To align with these experiments, the simulation tools from part 2 underwent necessary adjustments. As a consequence, an extensive number of tracer particles (>1 M) became essential to provide an in-depth representation of mix behavior in relation to residence time.

This section consists of 3 segments:

- 3.2.1: Techniques and tools customized for efficient tracer particle generation and processing.
- 3.2.2: Residence time distribution computation methods.
- 3.2.3: Methods for Shannon entropy evaluations as a function of residence time.

3.2.1. Tracer particle generation and processing

This section shows methods and considerations when generating and processing tracer particles.

One and two-way particle interaction

Two types of tracer particle interactions exist: one-way and two-way. While both methods enable tracking of the tracer particles, the two-way interaction allows these particles to locally influence certain fluid parameters in simulations. For the extrusion experiments small amounts of additives with a miscible polymer matrix were used. These additives were not expected to have a significant influence on the flow paths. Therefore, one way interaction is preferred for the extrusion simulations.

Particle tracking in the CFX solver

The path of each particle is determined by calculating the next particle position with the velocity and trajectory of the fluid at the current particle position. This results in undesirable behavior at the immersed boundary wall. With the immersed boundary method an immersed solid can move through a fluid domain. The CFX-Solver applies a source of momentum to the fluid inside the immersed solid domain in order to force the flow to move with the solid, see also part 1: *Simulation method* [18]. Particles do not interact with the walls of an immersed solid domain [19]. Therefore the particle may travel through the immersed solid based on the fluid velocity. The particle velocity is the fluid velocity, which matches the immersed solid velocity inside the immersed domain. Obviously in the experiments the tracer does not travel through the screw. Therefore, the immersed boundary method is not suitable for particle tracking with CFX.

Streamlines in the post processor

Streamlines are an alternative to the tracer particles in the CFX solver. The terms streamline and tracer particle are used as synonyms in the rest of this document. Streamlines can be introduced in the post processor (Ansys CFD Post), and by definition only have a one way interaction with the fluid since the streamlines are calculated after the simulation solver finished. With the default setting the streamlines behave the same as the tracer particles in the CFX-solver and travel through the immersed boundary. But this can be prevented by keeping the immersed boundary (i.e. the screw) stationary (0 m/s). This is attained by using a rotating frame of reference (i.e. a rotating cylindrical coordinate system), the axis of rotation and speed are aligned with the screw. Therefore, the screw is stationary in this rotating frame of reference while the barrel wall is rotating. Within CFD-post the rotating frame of reference or a stationary frame of reference (i.e. cartesian coordinate system), velocity can be viewed and used for calculating streamlines. A comparison between streamlines in a rotating and a stationary frame of reference is shown in Figure 46.

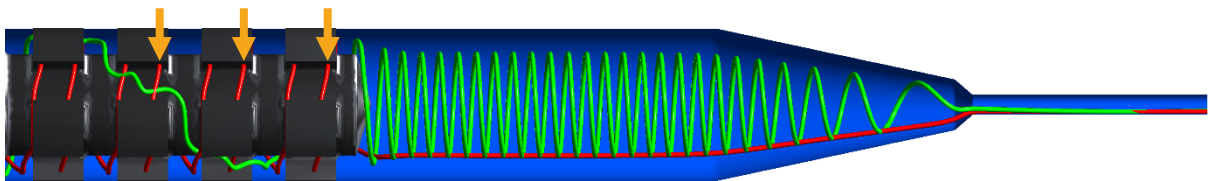


Figure 46. Examples of streamlines in the extrusion simulation with different frame of references. The streamline in a rotating frame of reference (green) flows between the extruder pins. While the streamline in the stationary frame of reference (red) flows through the pins. The orange arrows point to some of the positions where the red particle enters/exits a pin.

The streamline in a rotating frame of reference (green) and stationary frame of reference (red) shows a similar path after the screw and in the die. The streamline in the rotating frame of reference (green) seems to show a spiraling path, but the path is actually the same as with the red streamline (stationary frame of reference). The spiraling representation in Figure 46 is due to rotation of the frame of reference, i.e. the observer rotates around the extruder. After the screw and in the die the radial distance (from the screw axis) is 1.35 mm for both particles and the residence time in the last 100 mm (in the extrusion direction) is 23.8 s for both streamlines. The particle paths are not in agreement near the screw. The streamline in the rotating frame of reference flows between the pins in the mixing sections, while the red streamline flows through the pins, which is obviously not in agreement with the extrusion experiments, see also the orange arrows in Figure 46. Therefore, it is clear that particle tracking had to be done in the rotating frame of reference (green).

The path of each particle is determined by calculating the next particle position with the velocity and trajectory of the fluid at the current particle position. This results in a series of positions of each particle. The green streamline, in the rotating frame of reference, travels through more mesh elements compared to the red streamline. Therefore, the number of positions of the green particle is much larger (905 positions) compared to the green particle (192) for the last 100 mm. Which also results in a longer calculation time.

The streamlines can be exported, as a text file, from Ansys CFD Post. This file contains the position (xyz), particle number and residence time of each position of each particle. More information can be included, for example the shear rate experienced by the particle (for dispersive mixing). This results in large files (~ 14 GB) with a large mesh (i.e. many particle positions) and a relative low number of particles (~0.1 M).

Optimizing calculation time and the number of particles through parallel processing

A method for particle tracking was presented in part 2: Mixing Quantification [5]. This method has since been modified to compute the Shannon entropy multiple times, to present it as a function of residence time mirroring the experiments as presented in paragraph 2.4. As described in paragraph 3.2.3, Shannon entropy in extrusion simulations is calculated by categorizing particles into groups according to their specific residence times. Dividing the particles into groups results in a relatively low number of particles in some groups. A challenge in these calculations is that a decrease in the number of particles per bin increases the uncertainty. To mitigate this issue, the number of particles was increased to over a million tracer particles.

Though particle tracking is inherently computationally expensive and time consuming, especially when handling numerous particles in large meshes, it operates as a single-thread process in Ansys. Therefore, tools in GNU Octave were developed to utilize the multi core (36) processor by parallelizing the particle tracking. Multiple GNU Octave applications ran in parallel, first to calculate the start position of the streams in CFD-Post, other scripts for calculating the particle positions at the die exit. These CFD-Post and GNU Octave scripts ran until enough particles are created. GNU Octave scripts were used to merge all the particle data of different CFD-Post and GNU Octave calculations and subsequently calculate the Shannon entropy as a function of residence time.

3.2.2. Method for residence time distribution calculations in simulations

A method for calculating the RTD in simulations is shown in this paragraph, the results are presented in paragraph 3.3.

With extrusion the RTD is a distribution of wt.% in the extrusion direction. A high distributive mix quality shows a broad distribution, while a narrow RTD is a sign of a low mix quality. This was also explained in more detail in section 2.3.

The RTD and the particle distribution at the die exit was not calculated with Ansys, but in GNU Octave with the data from the Ansys exports, RTD calculations are straightforward. The simulated RTD is a histogram of the probability ($P_{i,tp}$) of a tracer particle to arrive at the die exit at specific residence time interval. The probability is calculated with the number of particles (n_i) in a bin divided by the total number of tracer particles ($N = 1.6$ M particles) in all bins. The bin size was 0.5 s.

$$P_{i,tp} = \frac{n_i}{N} \quad 37$$

Number of tracer particles

Simulating with tracer particles is time-consuming; therefore, to minimize calculation time, as few tracer particles as possible are preferred. However, using an insufficient number of tracer particles may distort the RTD or introduce excessive variability. The simulated RTD underwent multiple calculations, each time with a reduced particle count, to determine the minimum number of particles essential for an accurate RTD simulation.

The mean increase of deviation in the probability ($P_{deviation}$) as a function of total number of particles was calculated.

$$P_{deviation} = \frac{\sum_{k=1}^M |P_k - P_{k-2.6M}|}{M} \quad 38$$



Where $P_{k,1.6M}$ is the probably of a tracer particle residing in time bin k , calculated with $N=1.6 M$. P_k is also the probability in bin k , but calculated with fewer particles.

$P_{deviation}$ serves primarily as a quantitative indicator for assessing random errors in the RTD. As a criterion, a $P_{deviation}$ of less than 10^{-4} is considered adequate, although this threshold is somewhat arbitrarily selected. The relationship between $P_{deviation}$ and the number of particles is presented in paragraph 3.2.1.

3.2.3. Method for Shannon entropy calculations in simulations

The distributive mix quality in the extrudate cross section was determined using microscopic images (see section 2.4). Leading to quantification of the Shannon entropy and image processing in GNU Octave. For the simulations a similar procedure was implemented, but with simulated particle positions instead of distribution of black pixels. The method for calculating the Shannon entropy in simulations is shown in this paragraph, the results are presented in paragraph 3.4.

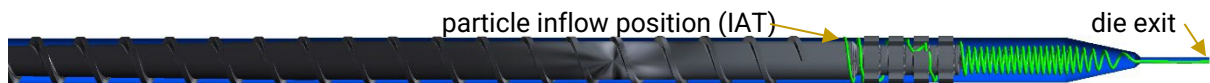


Figure 47. The simulated extruder with 1 streamline (green), the arrows mark the particle inflow position and the die exit. Note: many particles are needed for Shannon entropy calculations, but for clarity only a single streamlines is shown.

In the experiments the masterbatch was injected in a shot of 2 s long. Consequently, the resolution of observation is 2 s in the experiments. The same was achieved with the simulation result by only including particles with the same residence time within a 2 s range. For example, the particle distribution at a 70 s residence time can be determined with all the particles at the die exit between $69 \text{ s} < RT < 71 \text{ s}$.

In the experiments the carbon black masterbatch flows into the extruder with the AIT, which is mounted on the barrel at a position somewhere between the metering zone and the mixing zone, see paragraph 2.2. The same was done in the simulations, with an inflow opening at the AIT position. Tracer particles start at random positions at the AIT opening, see for example the green streamline in the upper Figure 47.

The cross section mix quality was determined in the extrudate for the experiments, while the die exit (last position in the extruder) was used for the simulations. Changes in particle/additive distribution is expected to be limited after the die. Some change will be due to flow rate distribution at the die exit. The velocity in the center of the die is high, while it is low near the wall. This in contrast to the solidified extrudate without a velocity gradient. These differences in distribution is accounted for by adjusting the Shannon entropy bin distribution. The flow rate in each bin is equal in the simulations, while the area of each bin is equal in the experiments.

For the simulations the bin distributions was determined with a GNU Octave script. The script does not assume a circle symmetrical velocity distribution, therefore the script is also applicable to other positions in the extruder (for example in the metering zone) and other dies. The velocity is higher in the center of the die exit compared to near the die wall. Therefore, the area of each bin is larger near the die wall compared to bins in the middle of the die.

Shannon entropy is a single measure to determine a distribution across a number of bins (M). The Shannon entropy (S) is calculated with the probability (p_i) that a particle is found inside a bin.

$$S = \frac{-\sum_{i=1}^M p_i \ln p_i}{\ln M} \quad 39$$

p_i is equal to the number of particles (c_i) in bin i divided by the total number of particles (N). This is the same calculation as with the experiment, but with particles instead of pixels.

For accuracy a high number of particles is preferred, see part 2: *Mixing quantification* [5]. Unfortunately, calculation time increases with the increase of number of particles. Therefore, the Shannon entropy was also calculated with fewer particles. At some point an increase in the number of particles does not result in a significantly different Shannon entropy. To find this point the mean Shannon entropy as a function of number of particles was calculated from 10^4 to $2.6 \cdot 10^6$ particles.

3.3. RTD in extrusion simulations and a comparison to experiments

This section presents the simulated RTD results. First, the results for the minimum number of particles for an RTD calculation are presented in paragraph 3.3.1. Secondly, a comparison between the simulated RTD and experiments is shown in paragraph 3.3.2.

3.3.1. Number of tracer particles

A low particle count may lead to errors in RTD calculations. The number of particles is considered adequate if a significant change in the particle count does not produce a notable change in RTD. Figure 48 shows the RTD calculated with varying particles counts and presents the mean probability deviation as a function of number of particles.

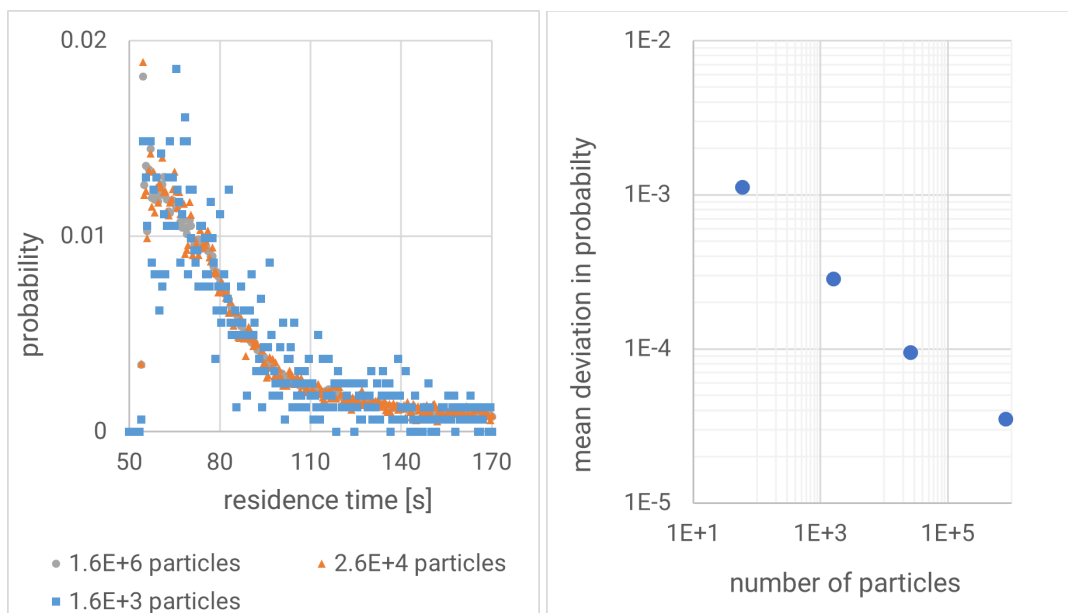


Figure 48. Left: simulated RTD with different numbers of particles for each curve. Note: the vertical axis shows the chance that a particles end up in a bin. Right: Mean deviation as a function of number of particles. Note: both axis are on a logarithmic scale.

With bin size = 0.5 s the simulated RTD remains virtually unchanged between $1.6 \cdot 10^6$ particles and $2.6 \cdot 10^4$ particles, see Figure 48 left. With $2.6 \cdot 10^4$ particles the scatter increases, but the general curve is still clear. The mean deviation in probability shows a power relation between the deviation and number of particles.

It was determined that $2.6 \cdot 10^4$ particles is enough for RTD calculations. When fewer particles are preferred (for calculation time) then the right graph, Figure 57, can be used to estimate the expected mean deviation, optionally a larger bin size could be used.



3.3.2. Simulated RTD compared to the optical RTD

The optical RTD experiments, of HDPE with carbon black masterbatch, and the simulated RTD (with 1.6 M particles) are both shown in Figure 49.

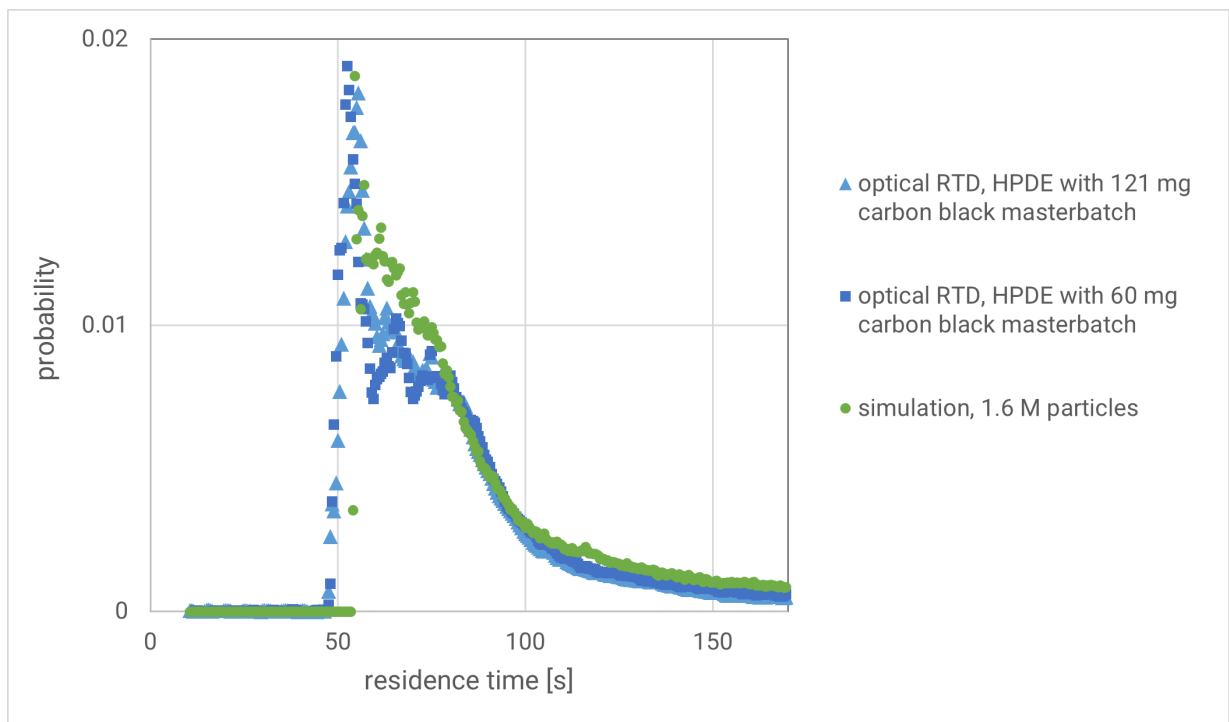


Figure 49. Optical RTD, of HDPE with a carbon black masterbatch, compared to the simulated RTD.

In general, the simulated RTD and the optical RTD are in agreement with each other. The shortest residence time is 47 s with the optical RTD, while the shortest RTD is a bit higher with simulation (54 s).

Because the simulated RTD aligns well with the optical RTD, therefore the simulation setup is deemed suitable for modeling the RTD. Furthermore, this validates that a simulation setup with > 25 k particles and a bin size of 0.5 s are good simulation parameters.

3.4. Mix quality in the cross section of the simulated extrudate

The results concerning the mix quality in the cross section of the simulated extrudate are presented in this section. paragraph 3.4.1 delivers a qualitative comparison between simulated particle distribution and real microscopic images of the extrudate. Paragraph 3.4.2 offers a quantitative comparison between the simulated and experimental mix quality with the Shannon entropy. Paragraph 3.4.3 is focused on the minimum number of particles required in the simulated cross-sectional mix quality to maintain accuracy in the Shannon entropy calculation.

3.4.1. Qualitative comparison between simulated particle distribution and microscopic images

Figure 50 shows both the extrudate cross section from the experiments and the simulated cross section at the die exit.

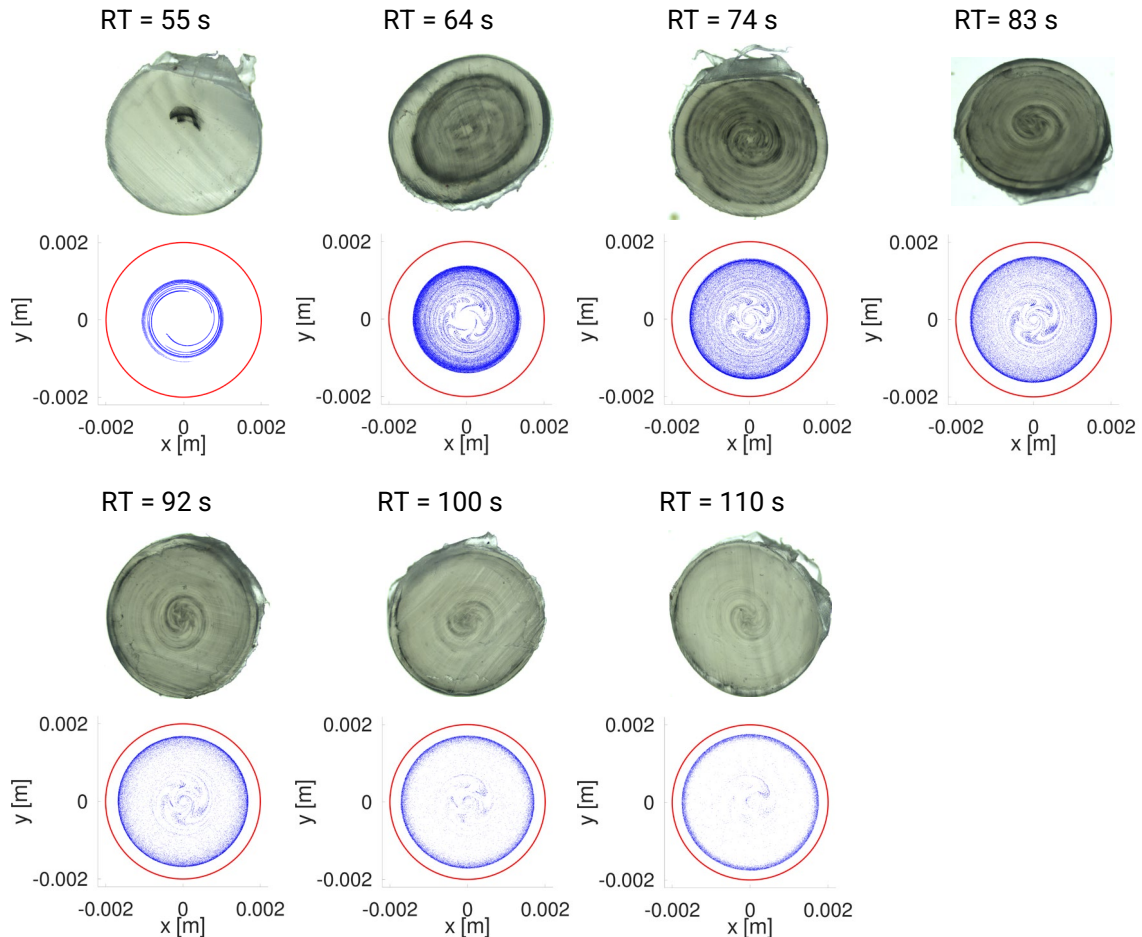


Figure 50. Microscopic images at several residence times (RT) of the carbon black masterbatch. And particle distribution (blue dots) at the extrusion die exit (marked with a red line) at the same residence times as with the microscopic images.

Qualitatively the simulations and experiments are in agreement. Note there is some difference due to the velocity distribution with the simulations (high in the center, low on the sides), while this velocity distribution disappears with solidification of the extrudate. Both in the simulations and experiments most of the additive appearing first center (RT = 55 s), and none at the border. Later on the additive fraction moves to the outside. The additive seems to be relatively homogeneously distributed at RT = 64 s up to RT = 83 s, with both carbon black/particles in the center and near the outside. Therefore, the distributive mix quality is high at this range.

In conclusion visual agreement was found between the simulated and experimental distribution of respectively tracer particles and carbon black.

3.4.2. Quantitative comparison of experimental and simulated cross sectional mix quality

Figure 51 shows the Shannon entropy as a function of residence time for both the simulations and experiments.

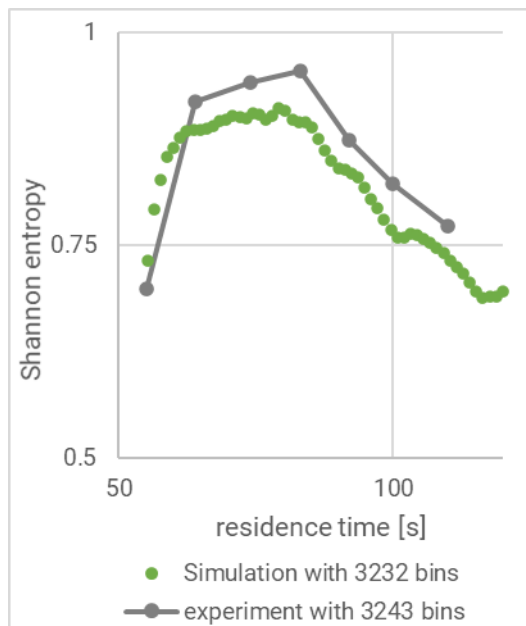


Figure 51. Comparison of the simulated and experimentally found Shannon entropy as a function of residence time.

The simulated Shannon entropy is in agreement with the experimentally found Shannon entropy. Both start at a low value (i.e. low distributive mix quality), and increase to ~ 0.9 at $RT \approx 65$ s (i.e. high distributive mix quality), and start to decrease after $RT \approx 80$ s. The experiment shows a somewhat higher Shannon entropy, this might be due to uncertainty in the experiments as the microscopic images had some imperfections in the roundness of the samples and shadows and streaks due to cutting of the sample, see also 2.4. But the effect on the uncertainty was not studied.

In conclusion, with Shannon entropy agreement was found between simulated and experimental cross sectional mix quality.

3.4.3. Minimum number of particles in simulated cross sectional mix quality

A low number of particles may result in an error in the simulated Shannon entropy. The number of particles is large enough when an increase in the number of particles does not result in a difference in the Shannon entropy.

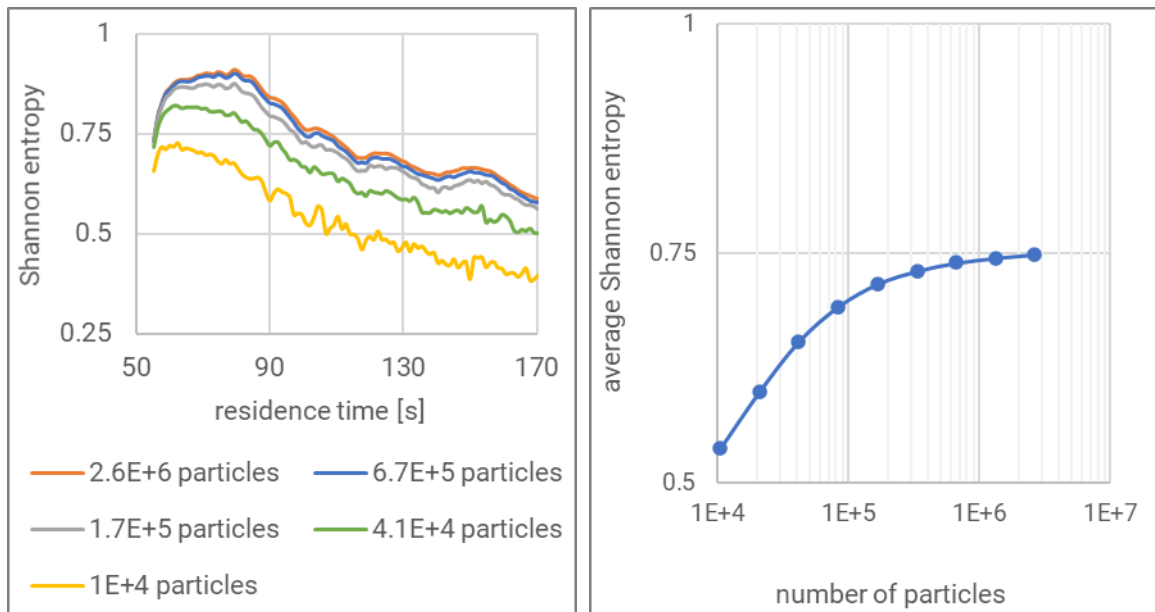


Figure 52. Left: simulated Shannon entropy with different numbers of particles. Right: average Shannon entropy (between RT = 55 s and RT =170 s) as a function of number of particles.

Figure 52 shows the simulated Shannon entropy at different numbers of particles and the average Shannon entropy (between RT = 55 s and RT =170 s) as a function of number of particles. The average Shannon entropy reduces with a decrease in the number of particles. The difference between 2.6 M particles and 1.3 M particles is minor, the difference in average Shannon entropy is only 0.004. Therefore 1.3 M particles is a large enough number of particles of this Shannon entropy calculation. Furthermore, with even fewer particles the difference is still small, for example the average Shannon entropy is only 0.032 less with $1.7 \cdot 10^5$ particles than with 2.6 M particles. But the error in the Shannon entropy rapidly increases if the number of particles is further decreased. In general, most of the curve shape (Shannon entropy as a function of residence time) is still apparent with even a very low number of particles. With all curves the Shannon entropy starts with an increase and reduces after RT \approx 80 s, but it peaks earlier with a lower number of particles.

To summarize: the simulated Shannon entropy as a function of residence time is in agreement with the experimentally found Shannon entropy. The simulated Shannon entropy increases with an increase of number of particles, but is nearly stable at 1.3 M particles.

4. Conclusion

In this study a method to quantify distributive mix quality with CFD simulations was validated with experiments.

Focus limited to the mixing section

The measured and simulated mix quality was limited to the mix section and the extruder die. For the experiments a specialized tool was developed to inject a colorant (masterbatch) into the extruder barrel in between the metering zone and the mixing zone. This allows for mix experiments limited to the mix zone and the extrusion die. This focus on the mixing section is deliberate, given its role in differentiating screw types and its specific function in mixing, unlike other zones like the feed and metering zones.

Measure the distributive mix quality in the extrusion direction

The distributive mix quality in the extrusion direction was expressed with the RTD (residence time distribution). In the experiments the RTD was measured with two methods, an optical method and a burn off method. With the burn off method the wt.% of tracer particles (chalk) was measured. The optical method was indirect, since the light attenuation of the extrudate was measured. Light attenuation is linked to residence time since the naturally translucent extrudate (HDPE or PP) becomes opaque due to tracers (carbon black, chalk, or grey masterbatch). With the Beer-Lambert law the wt.% could be calculated from light attenuation. The optical RTD and the burn off RTD are in agreement with each other. The optical RTD is recommended for measuring distributive mix quality in the extrusion direction due to its quickness, in contrast to the burn off method, which took approximately 50 hours per extrusion experiment.

Measure the distributive mix quality in the extrudate cross section

In the experimental setup, microscopic images capturing carbon black deposition were utilized. These images were subjected to image processing techniques to calculate Shannon entropy. This method served as a reliable metric for assessing the distributive mix quality within the extrudate cross section.

Validation of the simulated distributive mix quality, in the extrusion direction

The distributive mix quality in the simulations was assessed with the RTD using tracer particles. The simulated RTD and the measured optical RTD demonstrate a close agreement with each other. This verifies the simulated mix quality in the extrusion direction.

Validation of the simulated distributive mix quality, in the extrudate cross section

Simulations were conducted to model the distributive mix quality within the extrudate cross section, employing tracer particles to mimic carbon black distribution. Shannon entropy calculations were performed in both the experimental and simulated frameworks. A close agreement between the resulting Shannon entropies from the simulations and experiments validates the simulated distributive mix quality within the extrudate cross section.



5. Future research in simulating extrusion mix quality

A CFD method for simulating mix quality in plastic extrusion has been developed and validated. This chapter sets out future research directions. These include refining how mix quality is measured, studying more types of mixers, and exploring new production techniques.

A single value for mix quality per mixer

The current methods for quantifying mix quality produce different values for mix quality in each dimension ($S(t)$ for the extrudate cross section, RTD over the length of the extrudate), while a single mix quality value per mix element would be preferred when comparing several mixers. Such a value would only be feasible if it encapsulates mix quality across all three spatial dimensions (X, Y, Z) of the extrudate. With the current method the Shannon entropy already determines the mix quality in 3 dimensions, with 2 dimensions in the cross section and time as the third dimension, although the Shannon entropy method currently outputs a curve, the aim is to consolidate this into a single, representative value. The development of the Shannon entropy method is recommended to achieve a single mix quality value that encapsulates all three dimensions (X, Y, Z).

Comparing many different mixers

Only the pin mixer and the spiral Maddock were included in this study, see also part 2: *Mixing quantification* [5]. It is advisable to undertake a comparison of various extruder mixers currently available in the market, such as the pineapple mixer and Dulmage mixers, and to study what features produce a high mix quality, for example the number of pins on a pin mixer, and to use this knowledge to develop a more optimal mixer.

Additive manufacturing for producing more optimal mixers

Extruder screws are produced with conventional methods such as lathe, while CFD simulations are not limited by production methods. Current CFD methods may allow for the design of more optimal screws that may not be achievable through conventional production methods. In additive manufacturing, such as laser powder bed fusion (LPBF), there is greater design flexibility compared to conventional methods. Therefore, it is recommended to investigate whether LPBF is suitable to produce extruder mix elements.

Verifying simulated dispersive mix quality

Current isothermal CFD methods have been experimentally verified for distributive mix quality but not for dispersive mix quality. Hence, the development or adaptation of existing methods for measuring dispersive mix quality is recommended, and to use these methods to verify the extrusion simulations. Shear stress is a driving force for dispersive mix quality, but also for heating (viscous dissipation) the extrudate. Inclusion of thermal effects, particularly viscous dissipation, in the CFD simulation procedure is strongly recommended.



6. Acknowledgements

This research received financial support from Tech For Future (TFF) and Wavin T&I. The Professorship for Polymer Engineering acknowledges the valuable collaboration with Wavin T&I, who provided extrusion materials such as HDPE, PP, grey masterbatch, carbon black masterbatch, and chalk but also invaluable expertise and feedback throughout the study.

Notable contributions to the study came from interns who were instrumental in specific components of the research. Simon Hulshof designed an initial proof-of-principle setup for measuring RTD both optically and through burn-off methods, laying the groundwork for subsequent experiments [20]. Kilian Alderlieste significantly enhanced the reliability and accuracy of these RTD measurements, refining the techniques to yield more trustworthy data. Kilian Alderlieste also carried out the labor-intensive and time-consuming burn-off RTD measurements with great dedication. This substantial effort significantly advanced the research and yielded more reliable data [21]. Joey Veelers developed technique for cutting extrudates that contributed to better sample analysis [22]. Additionally, although working on a different project, Siem van de Wetering offered insightful suggestions and feedback that influenced the RTD measurement setup and the application of the Lambert-Beer law for processing optical measurements.

The study was conducted under the auspices of Windesheim University of Applied Sciences and reflects a collaborative effort that extends beyond the authors listed, and for this, all contributors are gratefully acknowledged.



References

1. Datasheet: Marlex® TRB-432 HDPE.
2. Datasheet: Marlex® M368 black MDPE concentrate.
3. Hostalen PP XN112-I, LyondellBasell.
4. PolyPlast Colour MB PP 7420, Polyplast Müller GmbH.
5. Buist, J., et al., Polymer Mixing in a Single Screw Extruder (Part 2: Mixing Quantification). Windesheim, LKT-DP-106741-2305, 2023.
6. Roussel, M.R., A Life Scientist's Guide to Physical Chemistry. 2012, Cambridge University Press. p. 41-42.
7. Mehta, A. Pharma Xchange - Ultraviolet-Visible (UV-Vis) Spectroscopy – Derivation of Beer-Lambert Law. 2012; Available from: <https://pharmaxchange.info/2012/04/ultraviolet-visible-uv-vis-spectroscopy-%E2%80%93-derivation-of-beer-lambert-law/>
8. P/N1127 with AMS104 light sensor.
9. Wikipedia. Calcium carbonate. Available from: https://en.wikipedia.org/wiki/Calcium_carbonate.
10. Wikipedia. Chalk. Available from: <https://en.wikipedia.org/wiki/Chalk>.
11. Yang, Z., Y. Qi, and J. Zhang, A novel perspective for reflective cooling composites: Influence of the difference between the effective refractive index of polymeric matrix and inorganic functional particles. Construction and Building Materials, 2019. 223: p. 928-938.
12. Kozak, M., et al., Relationship between filler loading and morphology of the interphase in polyethylene chalk composites. Polymers and Polymer Composites, 2004. 12(5): p. 409-416.
13. Liu, Y., et al., A Novel Spectral Matching Approach for Pigment: Spectral Subsection Identification Considering Ion Absorption Characteristics. Remote Sensing, 2020. 12(20): p. 3415.
14. Kamita, G., et al., Biocompatible and Sustainable Optical Strain Sensors for Large-Area Applications. Advanced Optical Materials, 2016. 4(12): p. 1950-1954.
15. Sartorius 1702 specifications.
16. Wikipedia Unsharp Masking.
17. Manas-Zloczower, I., et al., Color Mixing in Extrusion: Simulations and Experimental Validation, in NSF DMII Grantees Conference. 2005: Scottsdale Arizona, USA.
18. Buist, J., et al., Polymer Mixing in a Single Screw Extruder (Part I: Simulation Method). Windesheim, LKT DP-106741-2212, 2022.
19. ANSYS, C., 2019 R2, ANSYS CFX Reference Guide, ANSYS. 2019, Inc.
20. Hulshof, S., Kwantificeren van mengkwaliteit in een enkelschroefextruder. 2021.
21. Alderlieste, K., KWANTIFICEREN VAN DE VERDELINGSGRAAD IN AXIALE RICHTING. 2022.
22. Veelers, J., Ontwikkeling kwantificatiemethode(s) voor verificatie van simulaties van een enkelschroef extruder. 2021.



Appendix 1. Simulation setup and mesh study

This section is focused on finding a proper mesh for the extrusion simulations. A mesh is dense enough when the simulation results (pressure, flow rate and velocity) do not show significant changes when the mesh density is increased. A larger mesh will result in more computational costs, especially memory requirements. The goal of this sub study was to determine the relation between computational costs and mesh independency of the results. This sub study was performed before extrusion experiments were conducted and before a capillary extrusion die was developed. Therefore the simulation uses a similar, but different, extrusion die and material parameters. The simulated screw is the same as the experimental screw. The focus of this study is on the mesh between the barrel and the screw, therefore conclusion do apply to a simulation with a slightly different die and material parameters (as in section 3.1).

Simulations with the different meshes were compared by comparing the pressure and flow rate inside the extruder and the velocity field between the screw and the barrel.

Materials and Methods

The simulation and mesh study setup are shown in this section.

Lab extruder geometry

The lab extruder is a single screw extruder with a 30 mm diameter barrel. The L/D = 30 and the screw consists of 4 zones: the feed zone, the compression zone, the metering zone and a pin mixer.

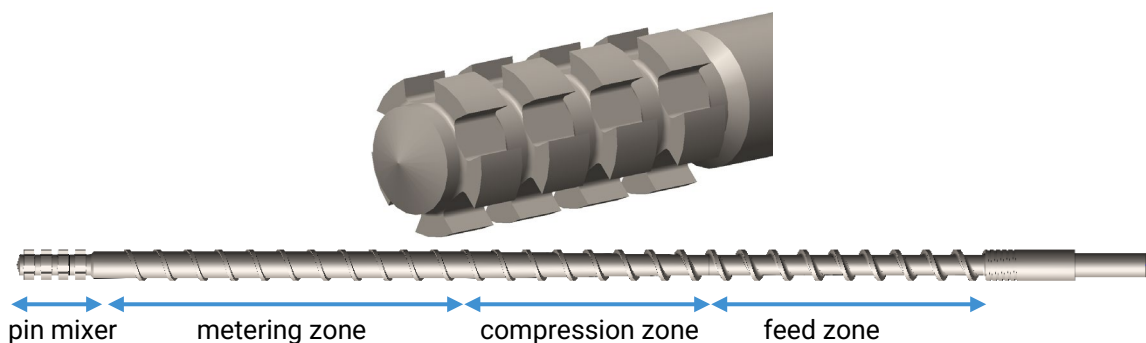


Figure 53. Side view of the screw with pin mixer. This image is a reappearance of Figure 3.

The pitch is 30 mm and continues from the feed zone up to the metering zone.

Table 3. Screw zones.

Zone	Rod diameter	Length
Feed zone	19 mm	270 mm
Compression zone	19 mm – 25.5 mm	225 mm
Metering zone	25.5 mm	383 mm
Pin mixer	20 mm	75 mm

The flight diameter is 29.8 mm, this leaves a gap of 0.1 mm between the barrel and the flight. The flow in this gap is expected to be very small. A gap of 0.1 mm is a small detail compared to the rest of the extruder. Usually at least 4 mesh elements are needed in such a gap for a proper velocity field, this would require elements of 0.025 mm, which would result in an extremely high number of mesh element. Such a mesh is difficult to make and would require very high computational costs when solving the simulation. Larger elements in such a gap might result in numerical instabilities, see also the spiral Maddock mesh as shown in part 1: *Simulation method* [18]. The gap, between the barrel and the screw flight, was removed since it does not have a large contribution to the overall flow behavior of the extruder and since this gap makes meshing difficult. The gap was removed by increasing the flight height to > 30 mm, the same was done with the pins.

A simple round die was used in the simulations. The die is 5 mm in diameter and 40 mm long. This die is similar to the die used for the extrusion experiments, but not the same.

Meshing

The immersed solid method (ISM) was used for the simulations. Separate fluid and solid domains were defined. Both domains were meshed separately. Consideration concerning the ISM are described in more detail in part 1: *Simulation method* [18].

An unstructured mesh, of the screw, was used for each simulation of the mesh study. The element size is 1 mm.

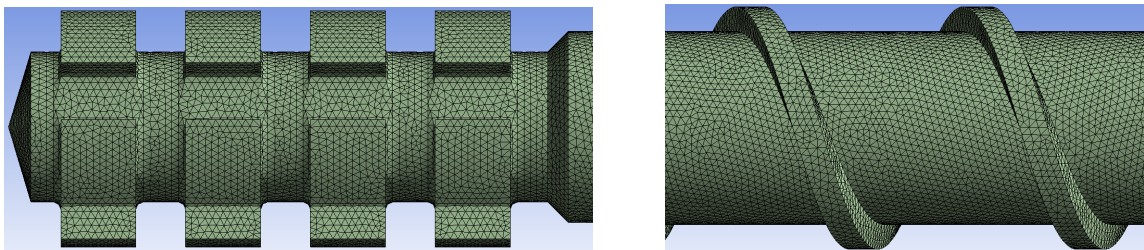


Figure 54. Screw mesh. Left: pin mixer, right metering zone.

The fluid domain fits between the screw rod and the barrel, and is the volume in the die.



Figure 55. Cross section of the fluid domain.

There is never fluid in the volume occupied by the rod of the screw, therefore the fluid domain does not extend to most of the volume of the screw rod. This results in a cylindrical fluid domain for the most part. Only the fluid domain part in the die and after the screw is not cylindrical.

The geometry of the fluid domain is described with a component. A component may consist several bodies, the whole component is meshed as one unit. Meshing of a component is a single thread task, therefore creating a very large mesh (> 100 M elements) is very time consuming. As an alternative multiple components can be meshed simultaneously (multiple threads) with a significant reduction in required time. But the meshes of the components have to be merged to create a single very large mesh. The fluid domain was divided into 41 components. The fluid domain is circle symmetrical therefore 40 of these components are instances of each other. These 40 components are in the cylindrical part of the fluid domain, not in the die. The mesh in each of these instances are identical. The meshes at the interfaces between the components were made identical by using the 'Match control' feature, in Ansys meshing.

A separate component was made for the die and the volume between the screw and the die. The mesh at the interface between this component and the 40 instances were made similar by applying the “Face meshing” feature and forcing the same number of elements on all faces. The meshes, at the interfaces, were made identical by applying “Contact meshing”. The “Contact meshing” feature adapts the mesh, this may result in mesh element with a high aspect ratio. A low aspect ratio is preferred for numerical stability, the Ansys CFX reference guide suggest aspect ratios of less than 50 [19]. Therefore the aspect ratio was reviewed. All the mesh nodes at the interfaces were merged.

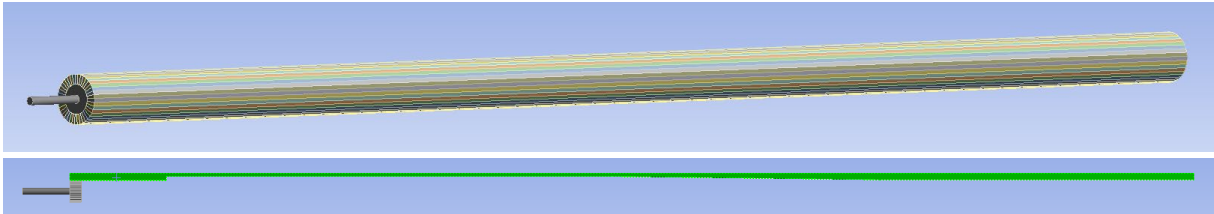


Figure 56. Fluid domain divided into 41 bodies. Upper: all bodies. Lower: a single instance of the 40 instances (green), and the body in de die and the volume between the screw and the die (grey).

All the meshes are unstructured and consist of tetrahedral elements. 4 meshes of different sizes were generated. Each mesh incrementally larger than the previous mesh. Each mesh is characterized with a typical element size from 0.50 mm to 0.20 mm. The typical element size was reduced with $2^{-1/3}$ with each incremental increase of mesh size.

Simulation setup

The simulation setup is similar to setups used in a previous study [18]. The simulations were steady state. The simulation parameters are shown in this section.

Boundary conditions

There is a 0 Pa condition at the inflow and outflow, see Figure 57.

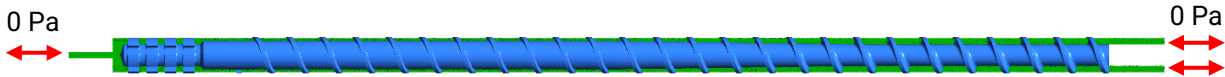


Figure 57. a 0 Pa pressure condition at the inflow opening and at the die opening. The fluid domain is shown in green, the immersed solid domain (i.e. the screw) is shown in blue.

A no wall slip condition at the barrel wall, i.e. the velocity of the fluid at the wall is equal to the velocity of the wall. The screw rotates during extrusion experiments, but with the simulations the screw was kept stationary, while the barrel was rotated with 200 rpm.

Material parameters

The material parameters are identical to the simulations in part 1: *Simulation method* [18]. The fluid model is a Bird-Carrea fluid, see equation 40, with $n = 0.346$, $\lambda = 1000$ s, $\eta_0 = 3.01184$ MPa·s and $\eta_\infty = 1$ Pa·s.

$$\eta = \eta_\infty + (\eta_0 - \eta_\infty) \left(1 + (\lambda \dot{\gamma})^2 \right)^{\frac{n-1}{2}} \quad 40$$

All the simulations were isothermal at 200 °C. Melting of plastic pellets was not included in the simulations.

Mesh study assessment criteria

The results of a simulation with a proper size mesh do not change when the mesh size is increased. 4 parameters were chosen to represent how well the simulation, with a specific mesh, performed.

- Pressure at a point between the screw and the die, see the red dot in Figure 58.
- The maximum pressure inside the extruder.
- The flow rate.
- The number of iterations needed for convergence.
- Velocity profile between the screw and the barrel wall in the metering zone, see Figure 58.

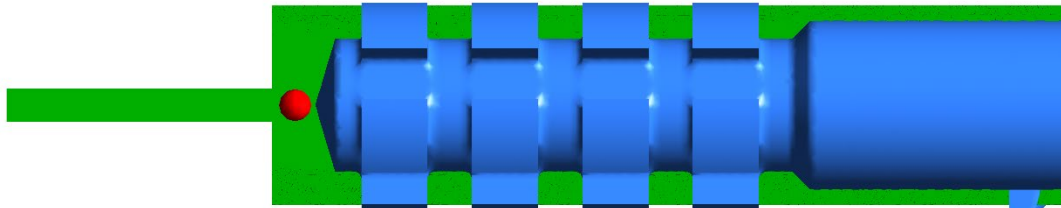


Figure 58. The red sphere indicates a position where the pressure was monitored.

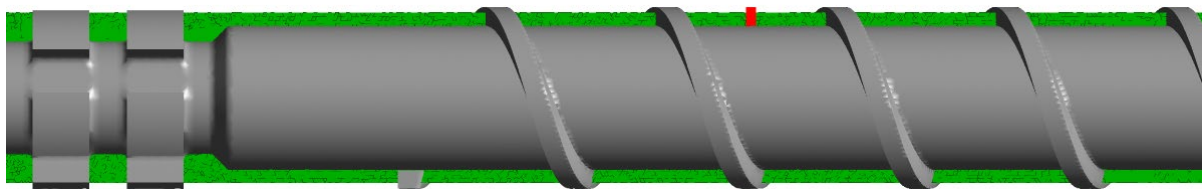


Figure 59. The red line indicates where the velocity profile was determined.

The parameters were monitored during solving. Several iterations were needed to achieve a stable value for the pressure and flow rate. Some preliminary simulations were performed to determine proper convergence criteria. Unfortunately there was not a single convergence criteria adequate for all meshes. With some meshes the equation residuals did not descend below $6 \cdot 10^{-5}$. While equation residual of $6 \cdot 10^{-5}$ where not low enough to reach a stable pressure and flow rate with other meshes. Therefore a second convergence criterium was used. A relative difference (Q_r) of $<10^{-3}$ in flow rate, between the inflow rate (Q_{inflow}) and outflow rate ($Q_{outflow}$), was used as convergence criterium. Furthermore for the equation residuals a criterium of $<10^{-5}$.

$$Q_r = \left| \frac{Q_{inflow}}{Q_{outflow}} - 1 \right|$$

41

Computer and software setup

The simulations were sequential performed with a HP Z840 with Ansys CFX:

Windows 10, 64-bit
2X Intel Xeon CPU E5-2696 v3, 2.3 GHz
512 Gb ram, 2133 MHz
Ansys 2019 R2

The meshes were made with the standard meshing tool. The simulations were performed with CFX. Parameter Set was used to create several simulation setups. With Parameter Set only one mesh, setup, solver and results component are needed in the workbench. Several design points were created, such as the typical element size. The Parameter Set executes meshing and solving for each design point (with a typical elements size). Furthermore results, such as pressure and flow rate, are also design parameters and can therefore be determined as a function of typical mesh element size.

Results

The results of the mesh study are shown in this section.

Mesh size

5 meshes were created. From 23 M element up to 338 M elements. The average element aspect ratio is 1.8 to 1.9 for all meshes. A high aspect ratio (>50) might result in numerical instabilities. The maximum aspect ratio is higher for the smaller meshes compared to the larger meshes. All aspect ratios are below 50, and are therefore acceptable.

Table 4. Mesh parameters.

Typical element size	Number of elements	Average aspect ratio	Standard deviation in the aspect ratio	Maximum aspect ratio
0.50 mm	23 M	1.9	0.5	26
0.40 mm	47 M	1.9	0.5	29
0.31 mm	97 M	1.8	0.5	21
0.25 mm	178 M	1.8	0.4	20
0.20 mm	338 M	1.8	0.5	18

Each simulation is identical to the others, except for the mesh. Therefore the simulations are named after the mesh size. For example '23 M' refers to the simulation with 23 M mesh elements.

Convergence

All simulations converged. The pressure reached a stable values with each mesh. And the difference in inflow and outflow reduced with a higher number of iterations, see for example 23 M and 178 M in Figure 60.

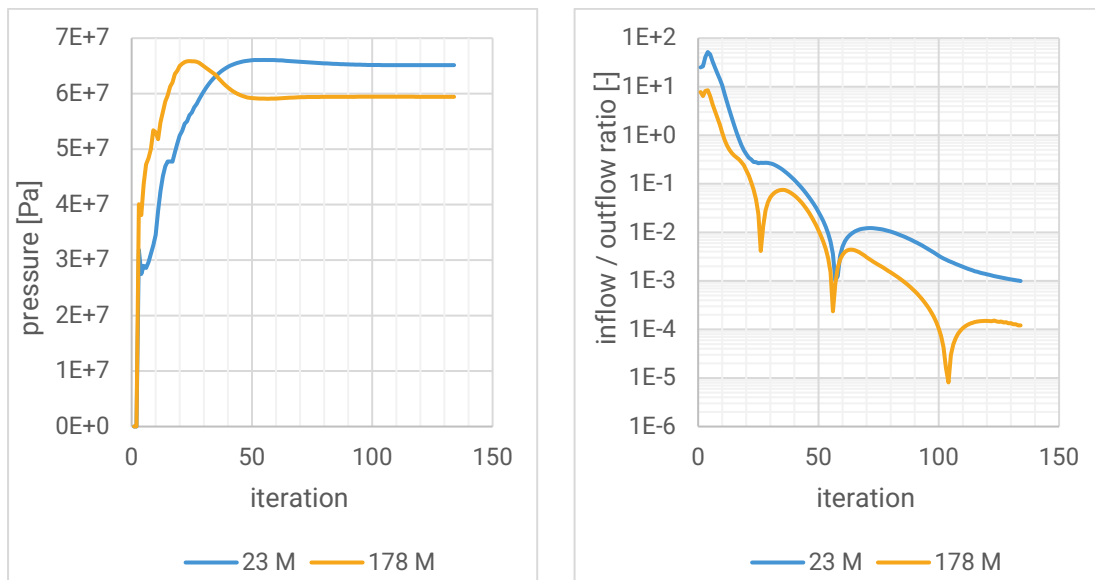


Figure 60. Monitoring points of 23 M and 178 M. Left: maximum pressure as function of iteration number. Right: inflow and outflow ratio as function of iteration number, note the vertical axis is on a logarithmic scale.

The number of iterations needed for convergence reduced with increase of mesh size from 23 M cell up to 97 M cells. The number of iterations is almost mesh independent between 97 M elements and 338 M elements.

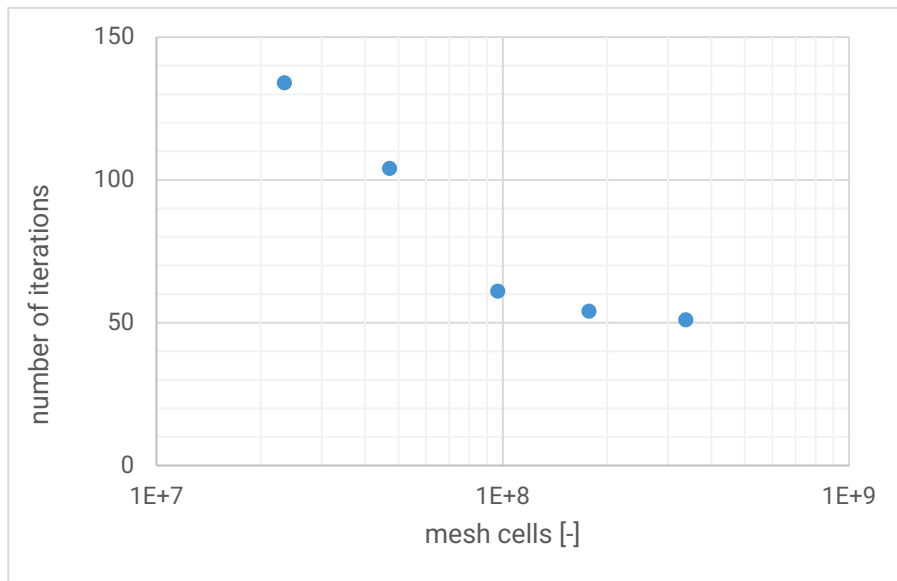


Figure 61. The number of iterations needed for convergence as function of number of elements. Note: the horizontal axis is on a logarithmic scale.

The calculation time per iteration increases with increase with increase of mesh size.

Computational costs

The CPU time and the duration of the simulation are depended on the mesh size and the number of iterations.

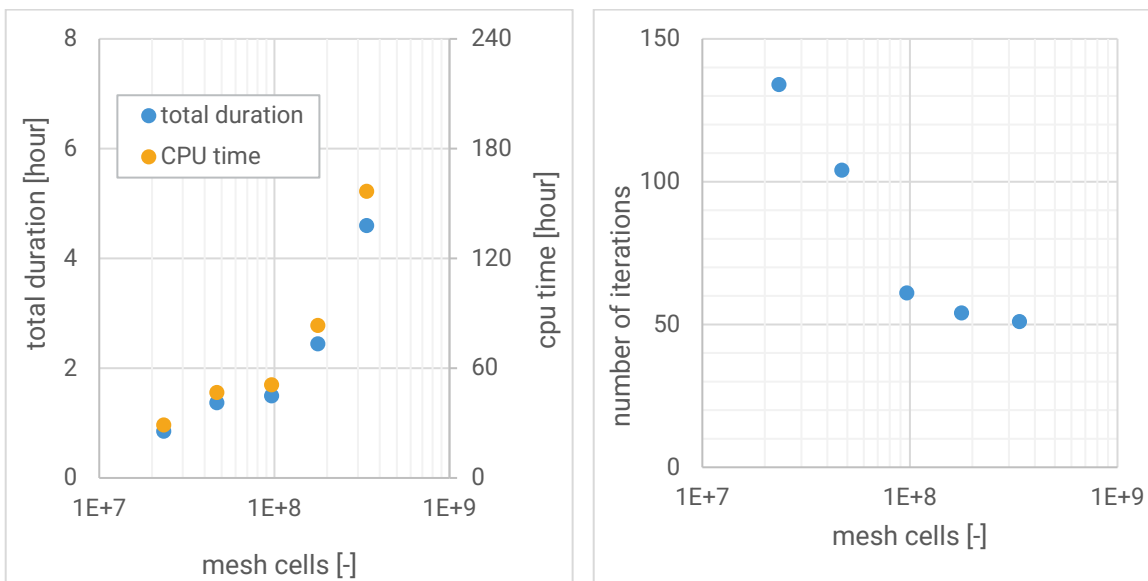


Figure 62. Left: CPU time and total duration of the simulations. Right: The number of iterations needed for convergence as function of number of elements. Note: the horizontal axis is on a logarithmic scale.

CPU time increases with increase of number of mesh elements. But not so much up to a mesh size of 178 M elements. This is due to the number of iterations needed for convergence, the number of iterations reduces with an increase of mesh size from 23 M element up to 97 M elements. The number of iterations is almost mesh independent between 97 M elements and 338 M elements. The lowest total duration is 0.9 hour for 23 M, while the longest total duration of a simulation was 6.4 hours with a mesh of 338 M.

The memory requirements increase linearly with the number of mesh elements, see equation 42.

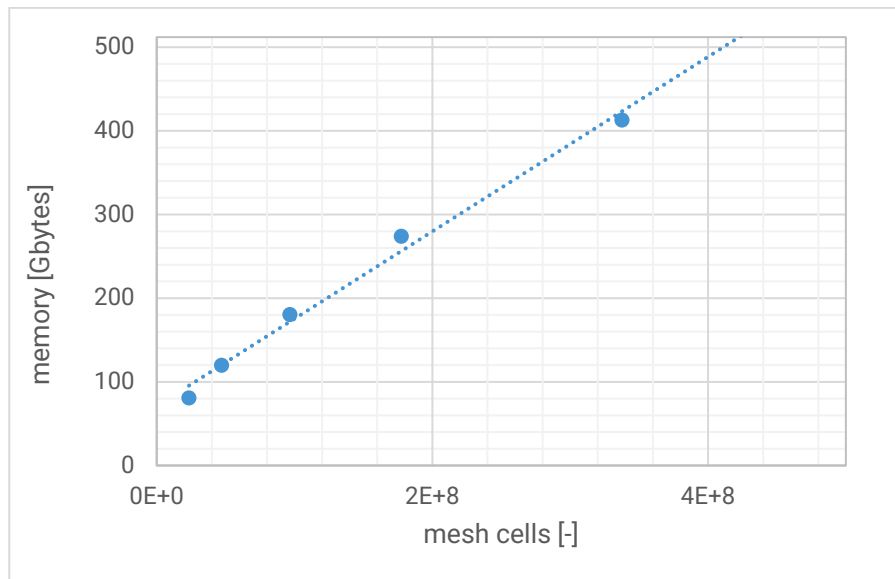


Figure 63. Memory requirements as function of number of mesh elements. The dotted line is a fitted line.

$$\text{memory [Gbytes]} = 1.0 \cdot 10^{-6} [\text{Gbytes}] \cdot N_{\text{elements}} + 71 [\text{Gbytes}] \quad 42$$

A simulation with a mesh of 411 M elements would probably need ~500 GB memory. The used computer has 512 GB memory, therefore it is not recommended to do an extrusion simulation with more than 411 M elements. With 42 a power relation was found between the typical element size and the number of elements (N_{elements}):

$$N_{\text{elements}} = 2.9 \cdot 10^3 (\text{typical element size [m]})^{-3} \quad 43$$

The maximum mesh size, with 411 M elements, would have a typical element size of 0.19 mm.

Pressure

The pressure inside the extruder behaves reasonable. The pressure is lowest at the inflow and outflow, and is highest somewhere in the middle of the axial distance.

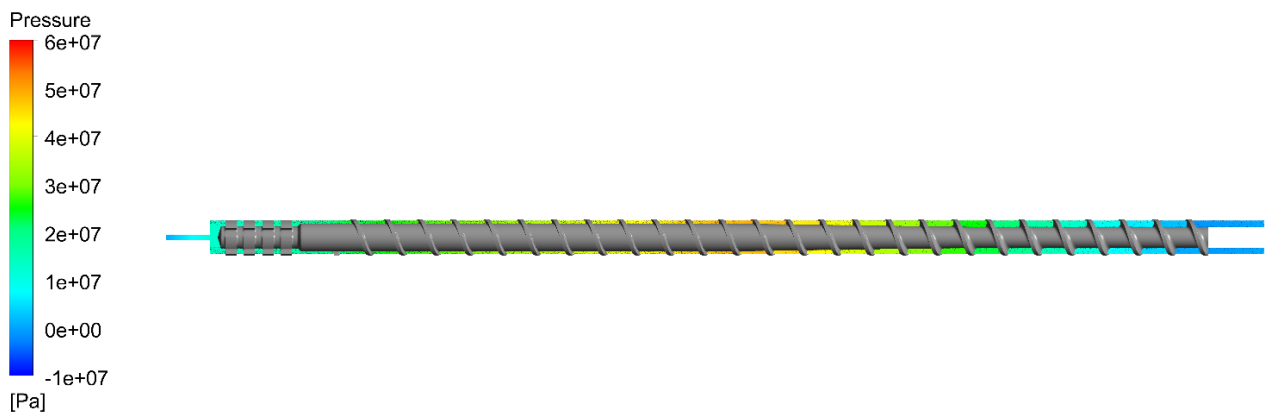


Figure 64. Pressure gradient of 23 M.

The pressure, at the monitoring point between the screw and the die, reduces with increase of mesh size.

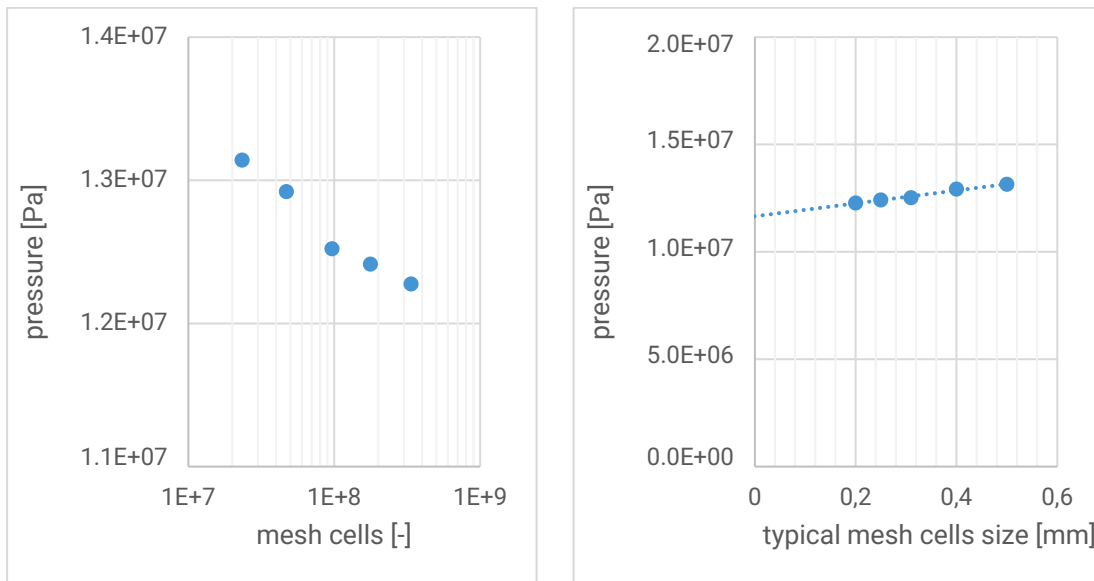


Figure 65. Pressure, between the screw and the die. Left: pressure as function of mesh size, note: the mesh is on a logarithmic scale. Right: pressure as function of typical element size with a fitted line (dotted line).

A linear relation between the typical element size and the pressure was found:

$$P_{screw-die} [\text{Pa}] = 3.0 \cdot 10^9 [\text{Pa} \cdot \text{m}^{-1}] \cdot \text{typical cell size} [\text{m}] + 11.7 \cdot 10^6 [\text{Pa}] \quad 44$$

Pressure between the screw and the die would be approximately 11.7 MPa at a typical element size of 0 mm. a typical element size of 0 mm is of course not reasonable since it would need an infinite number of elements, infinite memory and infinite CPU time per iteration.

A simulation with a mesh of 411 M elements with a typical element size of 0.19 mm would result in a pressure of approximately 12.2 MPa. This is the maximum recommended mesh size. The best achievable results of 12.2 MPa is only 2 % less than the pressure of 97 M simulation.

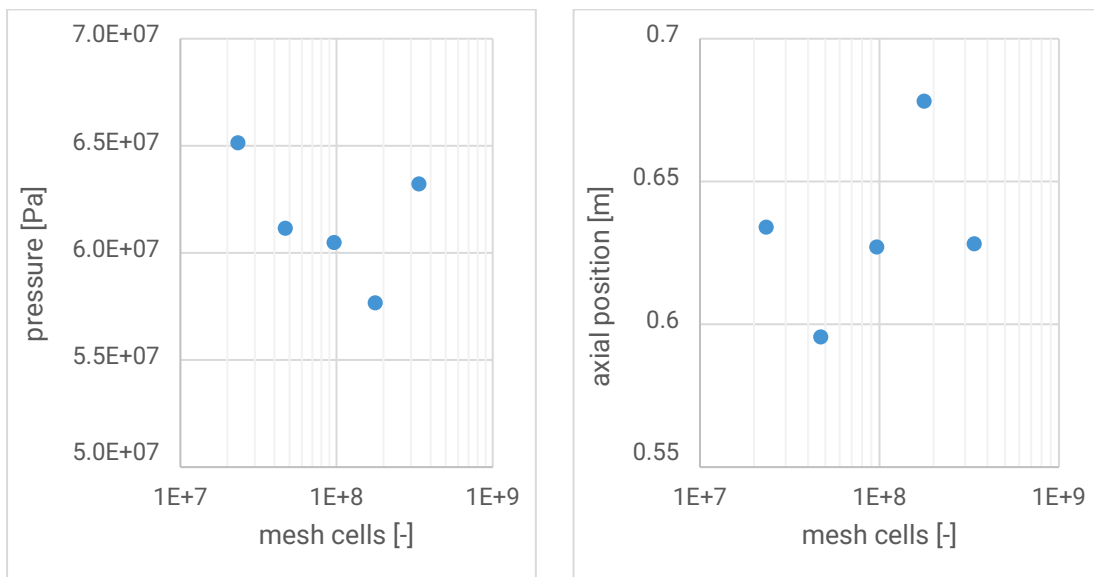


Figure 66. Left: maximum pressure as function of mesh size. Right: axial position of the maximum pressure as function of mesh size. Note: the mesh size is on a logarithmic scale.

The maximum pressure is 0.6 GPa, this pressure was reached near the end of the compression zone. The maximum pressure, and the exact position of the maximum pressure differs per simulation. The maximum pressure and the axial position as function of number of mesh elements are shown in Figure 66.

Flow rate

The flow rate ($\sim 6.3 \cdot 10^{-3}$ kg/s) is nearly mesh size independent, see Figure 67.

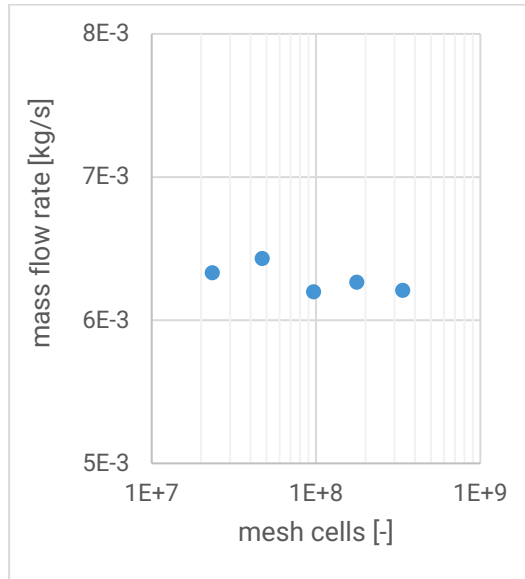


Figure 67. Left: flow rate as function of mesh size, note: the mesh is on a logarithmic scale.

Therefore every mesh meets the flow rate assessment criteria.

Velocity profile

Velocity profile between the screw and the barrel wall was determined, see Figure 68.

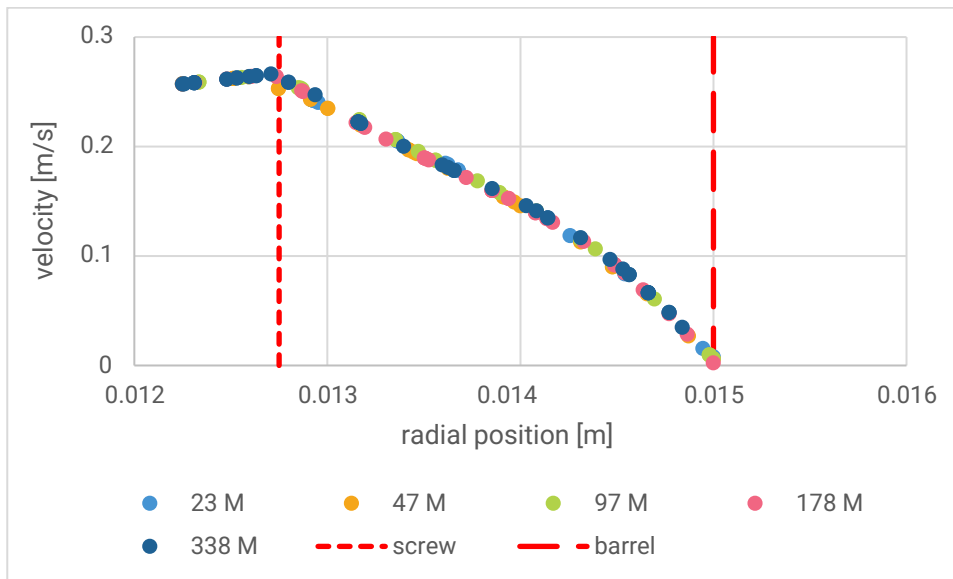


Figure 68. Velocity as function of radial position between the screw and the barrel. The screw and the barrel walls are marked with red striped lines.

Each point, in Figure 68, represents an intersection between a mesh element and a line between the screw and the barrel wall, this line is depicted in Figure 59. The distance between the points is not consistent since unstructured meshes were used.

The velocity profiles are similar to each other, the velocity does not seem mesh dependent in this range of mesh sizes. The velocity profile seems reasonable. A high velocity near the screw due to rotation, and a low velocity near the barrel wall. The velocity profile is for a large part a simple shear flow, therefore the almost linear profile. There is also a pressure flow component, therefore there is a slight curve in the velocity profile. The velocity at a radial position less than the screw (< 0.01275 m) represents movement of the immersed solid body, that is the rotation of the screw.

Conclusion, discussion and recommendations

Meshes were made with typical element sizes from 0.50 mm down to 0.20 mm, with mesh sizes of 23 M elements up to 338 M elements. Simulations with all meshes converged and showed reasonable results.

Increase in mesh size results in a reduction of the pressure between the screw and the die. Mesh independent results were not achieved. But an equation was fitted for pressure as function of typical element size. The mesh dependency can be determined with this equation for a specific elements size and mesh size.

Both the flow rate and the velocity profile were nearly mesh independent.

The memory requirements were 81 GB for 23 M elements up to 412 GB for 338 M elements. The used computer has 512 GB of memory, therefore a mesh of approximately 411 M elements with 500 GB required memory seems feasible. This mesh would have a typical element size of approximately 0.19 mm. Such a mesh might be a good option if accuracy is an absolute priority.

More iterations were needed with the more coarse meshes. While the number of iterations did not reduce much beyond 97 M elements. The least total simulation duration of 0.9 hours with a mesh of 23 M elements, while the longest total duration of a simulation was 6.4 hours with a mesh of 338 M. The 23 M elements mesh might be a good option if calculation time is a priority before accuracy.

The 97 M elements mesh is fairly quick (2.4 hours total duration) since only a few iterations are needed. The 97 M elements mesh results are close to the best achievable results. The 97 M mesh was made with a typical element size of 0.31 mm, a 0.31 mm element size is a good option if both speed and accuracy are priorities. And is therefore recommended for further extrusion simulations.

Several resource consuming activities were not quantified in this study:

- User time to creating a mesh setup and a simulation setup.
- Calculation time consumed for meshing.
- User time for handling of large meshes and simulation results.
- Time for loading and saving large meshes, simulation setups and simulation results.

The consumed time for the above activities was not measured, but it was observed that the activities are time consuming and the consumed time increases significantly with an increase in mesh size.

Design parameters were used to create the different mesh settings and to collect results. User input time reduces with the use of design parameters and are therefore recommended if many simulations are performed.



Professorship for Polymer Engineering

Polymer Mixing in a Single Screw Extruder

Part III: Experimental Validation

About this Professorship

The Professorship for Polymer Engineering of University of Applied Sciences Windesheim was founded in 2009; the group's objective is to improve the knowledge base on sustainable processing of plastics and composites within and through the higher education system. Its primary function is as a research group in Polymer Engineering, delivering output in the field of applied science. The team operates within market based projects and comprises lecturers from Civil Engineering, Industrial Product Design and Mechanical Engineering. The output of the projects is integrated into the curriculum of these study programs.

Summary

In this TechForFuture project 'Polymer Mixing in a Single Screw Extruder' a method to optimize mixing elements is developed based on numerical simulations (Computational Fluid Dynamics, CFD). A numerical procedure is developed to calculate the flow field in the extruder. By tracing particles in this field data is collected to determine distributive and dispersive mixing. Based on these data measuring values, the so called resident time distribution and Shannon entropy, have been used to quantify mixing. This way numerical values can be compared to experimental values such that the developed procedure could be validated with experiment on a single screw extruder on lab scale with different mixing elements. In the end, this numerical procedure can be used to analyze, optimize and judge different mixing elements with respect to their performance. The work has been carried out in close collaboration with Wavin T&I.

University of
Applied Sciences

Windesheim

